SURFACE INTEGRITY EVALUATION AND THE EFFECT OF MACHINING-INDUCED SURFACE INTEGRITY CHARACTERISTICS ON PART'S PERFORMANCE

by

QUANREN ZENG

A thesis presented in fulfilment of the requirements for the degree of

Doctor of Philosophy

Centre for Precision Manufacturing

Department of Design, Manufacture and Engineering Management

University of Strathclyde

Glasgow, Scotland, UK

February 2015

This thesis is the result of the author's original research. It has been composed by the author and has not been previously submitted for examination which has led to the award of a degree.

Signed: 

Date: 25/08/2015

ABSTRACT

Surface integrity (SI) is the integrated surface behavior and condition of a material after being modified by a manufacturing process; it describes the influence of surface properties and characteristics upon material functional performance. As the leading-edge field of manufacturing research, SI finishing/machining and the consequent machining-induced complex combination of surface roughness, residual stress, work-hardening, macro and microstructure transformation, strongly affect the fatigue and stress behavior of machined parts. This kind of influence is particularly sensitive and pronounced in the difficult-to-machine materials, which are typically chosen for the most critical applications in the automobile, aerospace and nuclear industry. Thus, well-designed SI processing requirement and accurate SI evaluation model are essential to control and ensure the surface quality and functional performance for these key parts.

In this thesis, an SI descriptive model for quantitative characterization and evaluation of surface integrity is proposed based on five principal SI characteristics. Considering the nature of surface integrity, a conceptual framework of an SI model for machined parts is established, in which the SI model is constructed based on the correlations between SI manufacturing processes, SI characteristics and final functionality. This model offers a theoretical basis and guideline for controlling SI characteristics and improving fatigue properties for machined parts. An empirical model for estimating the SI-characteristics-caused effective stress concentration factor (SCF) is established with fatigue life as the evaluating indicator. For a typical difficult-to-machine material, GH4169 superalloy, usually used in internal combustion engines, its grindability and the influence of processing parameters on the five principal SI characteristics are investigated in detail. The correlations between the processing parameters and the SI characteristics, between the processing parameters and the fatigue properties, and between the SI characteristics and the fatigue properties, are analyzed based on an orthogonally-designed grinding experiment and corresponding rotary bending fatigue testing for GH4169 samples within the selective range

of grinding processing parameters. The feasibility and effectiveness of the proposed model for estimating the SI effective SCF are also validated by the experimental results, and this has actually offered an equivalent and convenient means for evaluation of SI and fatigue properties. Finally, the conclusions and contribution of the research are discussed, and potential future work to build on this research is identified.

ACKNOWLEDGEMENT

I'd like to say I have been very lucky to start my Phd research in the precision manufacturing field at the Department of Design, Manufacture and Engineering Management, University of Strathclyde. The multiple disciplines involved have enabled me to learn so much out of my original expectation before I began this journey. At the beginning of my odyssey, I was like a piece of "raw material" to be manufactured to some extent. The research process has gradually developed and equipped me with some 'fabricated tools' that have the ability to shape and finish this piece of work. Thanks to all the "craftsmen" who have helped me throughout this process.

The one I should especially thank is my supervisor at the University of Strathclyde, Professor Yi Qin, the chief craftsman who makes me as a competent and independent researcher. Words are not enough to express my appreciation and feeling. I am indebted to his professional supervision, encouragement and patience. What I learned from him will benefit me all my life, especially his attitude and way to manage the academic research activities in everyday life.

My thanks are due to the local supervisor at Northwestern Polytechnical University, Professor Geng Liu, for his persistent support and trust in my research decisions. Thanks to Professor Xiutian Yan and Mrs Youhua Li who helped me to get the chance to start my joint Phd journey at the University of Strathclyde. Thanks to the Asia-link project for funding the first year of my Phd study. It would be impossible for me to finish this work without their support.

I would also like to express my sincere appreciation to Dr Xinchun Huang and Professor Jinxin Ren for their help in experiment design and instructive discussion in my thesis research. Thanks are also extended to emeritus Professor Frank Travis for thesis checking and proofreading.

My thanks are also due to the staff in DMEM. Thanks to the secretaries and IT staff in the Department and all the people that were or are still in the Leonardo Centre, especially

Alasdair Downs, Barry, Dino Bertolaccini and so on. Thanks to my former and current office colleagues Dr Wendan Wang, Dr Wenjuan Wang, Dr Gang Zhang, Dr Jie Zhao and Dr Peipei Wu and so on for helped me to find a pleasant life in Glasgow.

Finally, to my dear mum, Shuiqing Lu, dad, Sanyuan Zeng, sister, Zirong Zeng, and my girlfriend Jinying Sun. Thank you all for your pure-hearted love and unselfish support to me, which had warmed me so much in this cold season in Glasgow.

PUBLICATIONS RELATING TO MY PHD RESEARCH

1. Q. Zeng, et al. Influence of machining-induced 3D surface roughness on component's performance (In preparation and intending to submit to *Wear*).
2. Q. Zeng, et al. Investigation into grindability of a superalloy and effects of grinding parameters on its surface integrity. *Proceedings of the Institution of Mechanical Engineers, Part B: Journal of Engineering Manufacture.* 2015, Vol. 229, pp. 238-250 (first published online on April 29, 2014)
3. Q. Zeng, et al. Characterisation of the relationship between surface texture and surface integrity of superalloy components machined by grinding. *Edited by Essam Shehab, Peter Ball, Benny Tjahjono. Advances in Manufacturing Technology XXVII, Proceedings of the 11th International Conference on Manufacturing Research (ICMR2013), p.239-244. September 19-20, 2013, Cranfield University, UK*
4. Feng, J., Qin, Y., Zeng, Q., et al. Parameterised FE modelling of the surface-systems with coatings which considers the cracking of the coatings and influences of the case-hardening of the substrate, *Journal of Multiscale Modelling,* 2011, Vol. 3, No. 1-2, pp. 1-22
5. Q. Zeng, et al. Surface texture's role in assessing surface integrity of machined parts. *Applied Mechanics and Materials*, 2010, Vols. 34-35, pp. 1145-1148
6. Q. Zeng, et al. Framework of surface integrity model for machined components. *Advanced Materials Research*, 2010, Vols.139-141, pp.167-171

CONTENT

ABSTRACT I

ACKNOWLEDGEMENT III

PUBLICATIONS RELATING TO MY PHD RESEARCH V

CONTENT VI

LIST OF FIGURES X

LIST OF TABLES XIII

NOMENCLATURE XIV

CHAPTER 1 INTRODUCTION 1

1.1 SCOPE OF THE WORK 1

1.2 AIM & OBJECTIVES 3

1.3 ORGANIZATION OF THESIS 4

REFERENCES 7

CHAPTER 2 LITERATURE REVIEW 10

2.1 INTRODUCTION 10

2.2 CHARACTERIZATION AND EVALUATION OF SURFACE INTEGRITY 12

2.3 SURFACE AND SUBSURFACE RESIDUAL STRESS 15

2.4 MICROSTRUCTURE AND MICROHARDNESS 18

2.5 SURFACE TEXTURE AND ROUGHNESS PARAMETERS 21

2.5.1 2D Surface Roughness Characteristic Parameters 27

2.5.1.1 2D surface amplitude parameters 28

2.5.1.2 2D surface amplitude distribution parameters 30

2.5.1.3 2D surface slope parameters 32

2.5.1.4 2D surface spatial parameters 32

2.5.1.5 Other parameters 33

2.5.1.6 2D Surface MOTIF parameters 34

2.5.2 Statistical Functions 35

2.5.3 3D Surface Texture Characteristic Parameters 39
2.6 Surface Integrity for Difficult-to-machine Material 46
2.7 Summary 48
References 49
Chapter 3 Surface Integrity Characteristic Parameters and Its Descriptive Model 60
3.1 Introduction 60
3.2 Descriptive Model for Surface Integrity 62
3.3 Framework of SI Model and The Built-in Correlation 72
3.3.1 The Classification of SI Characteristics for Framework of SI Model 73
3.3.2 The Classification of SI Machining Processes for Framework of SI Model . 74
3.3.3 The Classification of SI Fatigue Performance for Framework of SI Model .. 76
3.4 Summary 78
References 80
Chapter 4 Surface Texture and Its Stress Concentration Effect on Surface Integrity 81
4.1 Introduction 81
4.2 Stress Concentration Evaluation Based on Surface Texture 82
4.2.1 Definition of Stress Concentration Factor (SCF) 82
4.2.2 Stress Concentration Estimations Based on Micro Surface Geometry 87
4.2.3 Measurement of Surface Micro Geometry and Evaluation of Corresponding Stress Concentration 96
4.2.3.1 Measurement of the effect of equivalent root radius on surface texture 96
4.2.3.2 Evaluation of SCFs based on orthogonally-designed external-grinding experiment 98
4.3 Stress Concentration Effect Based on Surface and Subsurface Characteristics 101

4.4 MULTIPLE STRESS CONCENTRATION EFFECT 105
4.5 SUMMARY 111
REFERENCES 112
CHAPTER 5 GRINDING INFLUENCES ON SURFACE INTEGRITY FOR GH4169 SUPERALLOY 115
5.1 INTRODUCTION 115
5.2 GRINDING MATERIAL AND EXPERIMENT ARRANGEMENT 118
5.2.1 Material Properties and Geometry 118
5.2.2 Machining and Measurement Equipment 120
5.2.3 Experimental Design and Procedure 120
5.2.3.1 Grinding arrangement 120
5.2.3.2 Measurement and characterization 122
5.3 EFFECTS OF GRINDING PROCESS ON SURFACE INTEGRITY 124
5.3.1 Surface Roughness and Effects 124
5.3.1.1 Orthogonally designed experiment for external grinding 124
5.3.1.2 Single-factorial experiment for plane grinding 126
5.3.2 Surface and Subsurface Residual Stress and Effects 127
5.3.2.1 Analysis of residual stress distribution below surface 129
5.3.3 Surface and Subsurface Microhardness and Effects 131
5.3.3.1 Effect of grinding parameters on microhardness 134
5.3.4 Subsurface Microstructure and Effects 136
5.3.4.1 Effect of the grinding parameters on microstructure 137
5.4 SUMMARY 140
REFERENCES 142
CHAPTER 6 MACHINING-INDUCED SURFACE INTEGRITY AND ITS EFFECT ON FATIGUE PERFORMANCE FOR GH4169 SUPERALLOY 146
6.1 INTRODUCTION 146
6.2 SURFACE INTEGRITY AND ITS EFFECT ON FATIGUE LIFE FOR GROUND GH1469 PARTS 148

6.2.1 Rotating Bending Fatigue Test for GH4169 Specimens 149
6.2.2 Correlation between Surface Roughness and Fatigue Life 153
6.2.3 Correlation between Surface Microhardness and Fatigue Life 157
6.2.4 Correlation between Surface Residual Stress and Fatigue Life 159
6.2.5 Integrated Effect of Surface Integrity Characteristics on Fatigue Life 163
6.3 Fractographic Analysis for Ground GH4169 Fatigue Specimens 166
6.4 Summary 169
References 170
Chapter 7 Conclusions and Future Work 172
7.1 Conclusions 172
7.1.1 Overall Research Results 172
7.1.2 Discussion and Limitations 173
7.2 Contribution to Knowledge and Practice 174
7.3 Future Work 175
References 177

LIST OF FIGURES

FIGURE 2.1 THE BASIC COMPONENTS OF THE ROUGH SURFACE PROFILE----------22

FIGURE 2.2 SCHEMATIC DIAGRAM OF 2D SURFACE ROUGHNESS HEIGHT PARAMETERS ------30

FIGURE 2.3 MATERIAL LENGTH AND DERIVED BEARING AREA CURVE----------31

FIGURE 2.4 2D SURFACE PROFILE, ADF, BAC FOR A SURFACE AFTER EXTERNAL GRINDING 36

FIGURE 2.5 BAC AND RELATED SURFACE CHARACTERIZATION PARAMETERS REPRESENTING FUNCTIONALITY ----------37

FIGURE 3.1 SCHEMATIC DIAGRAM OF SURFACE/SUBSURFACE INTEGRITY CHARACTERISTICS FOR MACHINED PARTS ----------61

FIGURE 3.2 SI CHARACTERISTIC DESCRIPTIVE MODEL ----------64

FIGURE 3.3 VARIATION OF MICROHARDNESS WITH THE DEPTH BELOW SURFACE ----------70

FIGURE 3.4 VARIATION OF RESIDUAL STRESS WITH THE DEPTH BELOW THE SURFACE --------71

FIGURE 3.5 THE FRAMEWORK OF THE SI MODEL AND ITS BUILT-IN CORRELATION ----------77

FIGURE 3.6 THE "ROADMAP" FOR FOLLOWING CHAPTERS OF THIS RESEARCH----------79

FIGURE 4.1 THE SAW-TOOTH AND SEMI-CIRCLE SURFACE PROFILES FOR MACHINED PARTS.. 88

FIGURE 4.2 STRESS CONCENTRATION OF AN INFINITE PLATE WITH A SINGLE NOTCH AND MULTIPLE NOTCHES 89

FIGURE 4.3 IDEAL SURFACE WITH SINUSOIDAL PROFILE AND ITS INSCRIBED ELLIPSE 92

FIGURE 4.4 EMPIRICAL RELATIONSHIP BETWEEN MATERIAL CONSTANT A AND TENSILE STRENGTH Σ_B 95

FIGURE 4.5 THE MEASURING PROCESS OF THE ROOT RADIUS OF A VALLEY ON THE SURFACE 98

FIGURE 4.6 THE INFLUENCING PROPORTIONS OF SURFACE INTEGRITY CHARACTERISTICS ON FATIGUE STRENGTH DEGRADATION FOR GROUND SUPERALLOY PART ABOVE 800°C).. 103

FIGURE 4.7 MULTIPLE STRESS CONCENTRATION WHEN A SMALL NOTCH OVERLAPPED ON A CENTRAL HOLE 106

FIGURE 4.8 MULTIPLE STRESS CONCENTRATION WHEN MICRO TEXTURE OVERLAPPED ON A MACRO HOLE 108

FIGURE 4.9 MULTIPLE STRESS CONCENTRATION SITUATION FOR THE GRINDING-INDUCED MICRO SURFACE TEXTURE OVERLAPPED ON THE MACRO GEOMETRICAL STRUCTURE OF A FATIGUE TESTING SPECIMEN 109
FIGURE 5.1 3D SURFACE TEXTURE OF EXTERNALLY GROUND COMPONENTS FOR ORTHOGONAL EXPERIMENTS 124
FIGURE 5.2 3D SURFACE TEXTURE OF PLANE GROUND COMPONENTS FOR SINGLE-FACTORIAL EXPERIMENTS 127
FIGURE 5.3 Σ_{RX} DISTRIBUTIONS OVER THE DEPTH BELOW SURFACE FOR DIFFERENT PLANE-GROUND SAMPLES 129
FIGURE 5.4 Σ_{RY} DISTRIBUTIONS OVER THE DEPTH BELOW SURFACE FOR DIFFERENT PLANE-GROUND SAMPLES 130
FIGURE 5.5 THE MECHANISM FOR FORMATION OF MICROHARDNESS OF GROUND SURFACE[29-30] 133
FIGURE 5.6 MICROHARDNESS MEASUREMENT PROCESS 134
FIGURE 5.7 MICROHARDNESS PROFILE VARIES WITH DEPTH BELOW SURFACE FOR PLANE GRINDING TEST 135
FIGURE 5.8 MICROSTRUCTURE OF GH4169 SUPERALLOY 137
FIGURE 5.9 MICROSTRUCTURE METALLOGRAPH OF GH4169 AFTER PLANE GRINDING WITH DIFFERENT A_P 138
FIGURE 5.10 SEM MICROGRAPHS OF THE GH4169 SAMPLES BY PLANE GRINDING WITH DIFFERENT A_P 139
FIGURE 6.1 MACHINING SPECIFICATIONS FOR GH4169 ROTARY BENDING FATIGUE SPECIMENS 150
FIGURE 6.2 3D SURFACE TEXTURES OF THE ROTARY BENDING FATIGUE SPECIMENS 156
FIGURE 6.3 THE CORRELATION BETWEEN THE MICRO SCF K_{ST} AND THE EQUIVALENT ROOT RADIUS ρ 165
FIGURE 6.4 THE CORRELATION BETWEEN THE MICRO SCF K_{ST} AND THE SURFACE ROUGHNESS R_A 165

FIGURE 6.5 THE CORRELATION BETWEEN THE MICRO SCF K_{ST} AND THE FATIGUE LIFE N_F... 166
FIGURE 6.6 MORPHOLOGY OF THE FRACTURED AREAS OF GH4169 FATIGUE SPECIMENS 1# AND 7#..... 167
FIGURE 7.1 SCHEMATIC DIAGRAM OF POSSIBLE STRESS CONCENTRATION FROM THE SURFACE AND SUBSURFACE OF A MACHINED PART 177

LIST OF TABLES

TABLE 2.1 THREE LEVELS OF DATA SETS FOR SI CHARACTERIZATION AND EVALUATION 13

TABLE 2.2 SURFACE INTEGRITY DATA SETS RECOMMENDED BY ANSI B211 14

TABLE 2.3 2D SURFACE ROUGHNESS AMPLITUDE PARAMETERS 29

TABLE 2.4 2D AMPLITUDE DISTRIBUTION PARAMETERS OF ROUGH SURFACE PROFILE 31

TABLE 2.5 2D SLOPE PARAMETERS OF ROUGH SURFACE PROFILE 32

TABLE 2.6 2D SPATIAL PARAMETERS OF ROUGH SURFACE PROFILE 33

TABLE 2.7 OTHER PARAMETERS OF ROUGH SURFACE PROFILE 34

TABLE 2.8 MOTIF PARAMETERS OF ROUGH SURFACE PROFILE 35

TABLE 3.1 DESCRIPTIVE PARAMETERS FOR SURFACE ROUGHNESS CHARACTERISTIC 66

TABLE 3.2 DESCRIPTIVE PARAMETERS FOR MACROSTRUCTURE CHARACTERISTICS 67

TABLE 3.3 DESCRIPTIVE PARAMETERS FOR MICROSTRUCTURE CHARACTERISTIC 68

TABLE 3.4 DESCRIPTIVE PARAMETERS FOR MICROHARDNESS CHARACTERISTICS 70

TABLE 3.5 QUANTITATIVELY DESCRIPTIVE PARAMETERS FOR MICROHARDNESS CHARACTERISTICS 71

TABLE 4.1 THE ORTHOGONALLY-DESIGNED EXTERNAL-GRINDING EXPERIMENT AND THE SCFS EVALUATION FOR THE GROUND GH4169 CYLINDRICAL SPECIMENS 100

TABLE 4.2 THE SCFS MODELS FOR MACHINED PARTS UNDER VARIOUS CONDITIONS 110

TABLE 5.1 THE NOMINAL COMPOSITION OF GH4169 SUPERALLOY (WT. %) [1] 119

TABLE 5.2 THE PHYSICAL AND MECHANICAL PROPERTIES OF GH4169 [1] 119

TABLE 5.3 ORTHOGONALLY-DESIGNED EXTERNAL GRINDING TESTS & SI CHARACTERISTICS MEASUREMENT 121

TABLE 5.4 SINGLE-FACTORIAL TEST OF PLANE GRINDING & SI CHARACTERISTICS MEASUREMENT 122

TABLE 6.1 ORTHOGONALLY-DESIGNED EXTERNAL PLUNGE-GRINDING EXPERIMENTS FOR GH4169 FATIGUE TESTS (GRINDING PARAMETERS ↔ SI ↔ SCF ↔ FATIGUE) 152

NOMENCLATURE

Unless stated explicitly, the following abbreviations and symbols are used in this thesis, with their meaning listed below.

Abbreviations	Meaning
R_a	Arithmetic average roughness or mean-line average roughness (μm)
R_t	maximum peak-to-valley height within the evaluation length (μm)
R_z	ten-point height within the sampling length (μm)
R_q	root mean square (RMS) roughness (μm)
R_p	max peak height (μm)
R_v	max valley depth (μm)
R_{Sm}	average spacing between peaks of a surface profile (mm)
R_{pk}	reduced peak height (μm)
R_k	core roughness depth (μm)
$R_{Mr}(c)$	material ratio at depth 'c' (%)
R_{Mr1}	peak material portion (%)
R_{Mr2}	valley material portion (%)
L_o	actual profile length (mm)
L_{pr}	profile length ratio (%)
L_r	sample length (mm)
R_{sk}	skewness (2D)
R_{ku}	kurtosis (2D)
R_{vk}	reduced valley depth (μm)
R_{vm}	average valley depth (μm)
R_x	largest motif height (μm)
$R_{\Delta q}$	RMS slope
$R_{\Delta a}$	mean-line average slope

$R_{\lambda q}$	RMS average wavelength (mm)
$R_{\lambda a}$	mean-line average wavelength (mm)
S_{al}	fastest decay autocorrelation length (mm)
S_{bi}	surface bearing index (%)
S_c	core valley volume ($\mu m^3/mm^2$)
S_{ci}	core fluid retention index (%)
S_{dr}	developed interfacial area ratio (%)
S_{ds}	density of summits (1/ mm^2)
S_{IMa}	imperfection area (mm^2)
S_{sk}	skewness (3D)
S_{ku}	kurtosis (3D)
S_m	material volume of the surface ($\mu m^3/mm^2$)
S_q	RMS average (3D) (μm)
S_{sc}	mean summit curvature (1/mm)
S_{td}	texture direction
S_{tr}	texture aspect ratio (%)
S_v	valley void volume ($\mu m^3/mm^2$)
S_{vi}	valley fluid retention index (%)
S_z	ten-point height (3D) (μm)
$S_{\Delta q}$	RMS slope (3D)
a	amplitude of a sinusoidal surface profile (mm)
b	spacing of notch (mm)
d	half width of notch (mm)
n	load type
t	depth of notch (mm)
q	notch sensitivity coefficient
$\bar{t}$	equivalent depth of notch (mm)
$\overline{d}$	equivalent half width of notch (mm)

ρ	root radius of a valley for surface profile (mm)
ρ_i	root radius of the i^{th} valley for the surface profile (mm)
$\bar{\rho}$	equivalent root radius of the dominant valleys for the surface profile (mm)
τ	stress of dislocation (MPa)
ρ_d	dislocation density (cm^{-2})
α	material constant
$\sigma_{0.2}$	yield strength (MPa)
σ_b	tensile strength (MPa)
E	modulus of elasticity (GPa)
$\delta_{0.5}$	elongation ratio (%)
γ'	1st strengthening phase, $Ni_3(AlTi)$
γ''	2st strengthening phase, Ni_3Nb
λ_{WL}	wavelength (mm)
λ	ratio of spacing to height of the surface irregularities (%)
K_t	theoretical stress concentration factor (SCF)
K_f	effective stress concentration factor (SCF)
K_{st}	theoretical SCF caused by machining-induced surface texture
K_{t1}	SCF caused by macro pre-designed geometrical structure
K_{EF_NS}	SFC considering material sensitivity caused by micro surface texture
K_{tMG}	Multiple SCF caused by machining-induced micro surface texture overlapped on a macro geometrical notch (multiple stress concentration)
K_{IEF}	fatigue reduce coefficient stress concentration factor (SCF)
K_{ut}	Manufacturing process induced stress concentration factor (SCF) caused by nonuniformity or discontinuity of material properties under the surface (within the material altered layer)
h	depth below the surface (mm)
HV_1	microhardness value on the machined surface (Vickers hardness, HV)
HV_0	microhardness of the bulk material/base material (HV)

$HV(h)$	microhardness distribution along the depth below the surface h (HV)
σ_{R0}	residual stress on machined surface /surface residual stress (MPa)
$\sigma_R(h)$	residual stress distribution along the depth below surface h (MPa)
σ	working load (MPa)
a_p	depth of cut (mm)
v_w	workpiece rotating speed (m/min)
f_a	feed rate (mm/r for external grinding; mm/str for plane grinding)
v_s	grinding wheel cutting speed or grinding wheel linear speed (m/s)
S_e	fatigue strength or fatigue limit (MPa)
N_f	fatigue life (cycle)

CHAPTER 1 INTRODUCTION

1.1 SCOPE OF THE WORK

The demand for high reliability and improved engine performance has led to further research and development of higher temperature and higher strength materials for producing better precision parts [1-6]. However, the high temperature or high strength materials, such as nickel based or titanium alloys, are normally difficult to machine and their surface quality and final functionalities are sensitive to the selected manufacturing processes [7]. Normally, the high-precision or micro-structured parts made of difficult-to-machine materials are more prone to falling short of their required geometry or surface accuracy and this could easily cause the failure of parts in service especially in extreme and complex working environments [8-12]. Thus, it is really important to well control the machining process and surface quality to maintain the service performance. To remain competitive against the global competitors, especially against those from the emerging Far East, the priority for European manufacturers is to improve their product quality by increasing existing technological advantage, as well as to lower the manufacturing costs including both energy consumption and workforce employment [13]. These will demand optimization of existing production processes and the development of innovative manufacturing technologies, both of which could help to control manufacturing accuracy and ensure the surface performance of machined parts suitable for high-temperature, high-strength applications.

For comprehensively and fully characterizing the surface quality and functionality of a

machined part, existing means which only take account of single primary surface/subsurface characteristic, are considered to be inadequate to meet current requirement for accurate assessment of surface quality and integrity. Conventionally, it used to be accepted by engineers that the fatigue properties of a machined part are mainly and directly determined by its surface roughness characteristic if it is processed under gentle machining conditions; and that the fatigue strength will decrease as the value of surface roughness increases. However, now it is well recognized that subsurface characteristics, such as phase transformations, microhardness and residual stress, actually have a more profound influence on the final fatigue property than do surface roughness characteristics, especially when the machining process has massive thermal effects involved. If the machining conditions are abusive to the machined part, the effect of subsurface physical transformation caused by high temperature is likely to override any other influence caused by surface geometrical texture, and the fatigue strength will be consequently impaired. There have already been some catastrophic accidents that originated from the failure of key parts, all of which showed the potential dangers of surface and subsurface material variations caused by excessive heat and force generation during manufacturing processes such as milling, drilling, grinding and electrical discharge machining (EDM). For example, the surface microhardness of a machined part produced under excessive thermal conditions can easily reach five times its bulk hardness, which makes the generated surface layer too brittle to sustain alternating load; Inconel 718 high-temperature alloy normally has a fatigue limit as high as 540 MPa after gentle grinding, but it may drop to as low as 150 MPa after EDM [14]. In a word, the

machining-induced surface texture and subsurface characteristic variations are of vital importance to the mechanical properties and related functional performance of machined parts, especially for critical parts with difficult-to-machine material that are widely used in the aerospace industry.

1.2 AIM & OBJECTIVES

The overall aim of this research is as follows:

To bridge the gap between industry and academia, this research manages to establish a surface integrity (SI) descriptive model which could digitally and quantitatively define the primary surface integrity characteristic parameters for accurately describing their influence on functionality in practice. It could actually be taken as a preliminary standard for the characterization, measurement and evaluation of surface integrity.

And the objectives can be stated as:

(1) Considering the surface and subsurface integrity characteristics interact with each other and jointly determine the functionality of machined surfaces or parts, the research also aims at developing a generalized surface integrity model for better understanding the interactions among the machining processes, surface integrity characteristic parameters and service performance, and effectively evaluating the quality and performance of machined component, especially for difficult-to-machine materials like Ni-based superalloys or Ti-alloys. It is expected that mechanical properties and corresponding performance of machined components could be accurately assessed by applying this method.

(2) In order to accurately evaluate the surface integrity and the consequent functionalities, especially fatigue-related performance for aero-engine-used materials (such as difficult-to-machine Ni-based superalloy GH4169), convenient empirical equations for estimating the effective stress concentration factors (SCFs) of certain machined surface are necessary; the impact of multiple stress concentration, which considers the situation when the machining-induced microscopic surface texture superimposes on its macroscopic pre-designated structural notches or other macro stress raisers, also has to be quantified. The accuracy and feasibility of those empirical equations will be validated by calculating and comparing the SCFs for the externally-ground GH4169 superalloy cylindrical samples with the corresponding experimental measurement.

1.3 ORGANIZATION OF THESIS

The industry used to have limited knowledge about how the manufacturing processes and machining parameters could adversely or favorably affect the surface integrity of machined parts. They are now gradually becoming aware of their impact and know it could be applied to control and improve the surface quality of machined parts in practical production. As a cutting-edge research topic in manufacturing, surface integrity finishing/machining is the key technology which could ensure the required surface/subsurface characteristics and its corresponding functional performance for some critical parts used in automobile, aerospace and nuclear industry. A comprehensive model for surface integrity which could help to conveniently characterize the surface geometrical texture and subsurface mechanical or physical properties of machined parts is indispensable for accurate evaluation of the surface

integrity and functionality of machined parts. In this thesis, a quantitative surface integrity descriptive model is proposed according to the five primary characteristics based on the surface integrity standard data set. An empirical model for estimating the effective stress concentration factor (SCF) is obtained according to specific surface integrity requirements when the fatigue performance of a machined part is taken as the principal evaluating indicator. The influences of machining process and its operational parameters on these primary surface integrity characteristics are studied in detail for the typical engine-used superalloy GH4169 (similar to the material trademarks of Inconel 718 in U.S. and NC19FeNb in France). The correlations between processing parameters and SI characteristics, between processing parameters and fatigue properties, and between SI characteristics and fatigue properties, are derived from the orthogonally-designed grinding experiment and fatigue test for GH4169 specimens. The feasibility and accuracy of the proposed estimating model for the effective stress concentration factor are also validated by the corresponding experimental results, and this has offered a convenient means for the characterization and evaluation of the fatigue properties. The organization and structure of this thesis are as follows:

In Chapter 1, the scope of this research is defined and the research aims are set up.

In Chapter 2, the advances in characterization, measurement and assessment of surface integrity for high standard machined parts are overviewed. The existing researches relating to the primary surface integrity characteristics, such as surface texture and roughness, residual stress, microstructure and microhardness, are reviewed in detail and summarized.

In Chapter 3, according to the high requirement of SI for precision-machined parts, a quantitatively descriptive model of SI, which considers the effects of surface roughness, macrostructure, microstructure, microhardness and residual stress on the functional performance (especially fatigue properties), is established based on the SI standard datasets proposed by Field and Kahles [15-16]. The characteristic parameters within the SI descriptive model are all defined and listed for practical use. Considering the specific parts and corresponding machining process, a conceptual framework of the SI model for machined parts is proposed according to the nature of surface integrity. This SI conceptual model is actually constructed based on the classifications of SI processing parameters, SI characteristics and corresponding functionalities (especially fatigue properties). This model offers a theoretical basis and feasible framework for evaluation of SI characteristics and improvement of fatigue properties for machined parts.

In Chapter 4, the significance of stress concentration factor and its correlation with surface integrity characteristics and fatigue properties are discussed. The empirical equation of stress concentration which is mainly caused by machining-induced micro geometrical topography and texture is deduced; the calculation of multiple stress concentration which considers both macro structural notch and micro surface irregularities is also analyzed. Further, an integrated estimating model for SI effective SCF which is featured by surface roughness, microhardness and residual stress, is proposed according to linear-superposition assumption and existing literature review.

In Chapter 5, the grinding machinability and surface integrity of a typical

difficult-to-machine material, superalloy GH4169, are elaborately studied and evaluated. The formation mechanism of each primary SI characteristic and its relationship with surface quality are investigated. The effects of grinding wheels and processing parameters on each SI characteristic, such as surface roughness, macrostructure, microstructure, microhardness and residual stress, are individually analyzed; and these have provided with a guide for ensuring the desirable machining-induced SI characteristics of ground superalloy GH4169 parts.

In Chapter 6, the correlations between each grinding SI characteristic and its fatigue life are experimentally investigated by rotary bending fatigue testing for the GH4169 specimens, which are ground with the selected grinding parameters range. The applicability and accuracy of the computational equations for micro geometrical caused SCF and the integrated effective SCF are demonstrated by comparing their results with those calculated from Arola's equation [17-21] and validated by the measured fatigue life.

In Chapter 7, the conclusions and contribution of the research are discussed, and potential future work to build on this research is also identified.

REFERENCES

[1] Miller, S. Advanced Materials Means Advanced Engines. Interdisciplinary Science Review, 1996, **21**(2), pp.117-129.

[2] Boyer, R.R. An Overview on the Use of Titanium in Aerospace Industry. Journal of Material Science and Engineering, Part A, 1996, **213**, pp.103-114.

[3] Honnarat, Y. Issues and Breakthrough in the Manufacture of Turboengine Titanium Parts. Material Science Engineering, Part A, 1996, **213**, pp.115-123

[4] Tönshoff, H.K. et. al. Cutting of Hardened Steel. Annals of CIRP, 2000, **49**(2),

pp.547-566

[5] Ulutan, D. and Ozel, T. Machining Induced Surface Integrity in Titanium and Nickel Alloys: A review. International Journal of Machine Tools and Manufacture, 2011, **51**(3), pp.250-280.

[6] Guo, Y.B., Li, W. and Jawahir, I.S. Surface Integrity Characterization and Prediction in Machining of Hardened and Difficult-to-machine Alloys: A State-of-Art Research Review and Analysis. Machining Science and Technology, 2009, **13** (4), pp.437-470.

[7] Brewer, W.D. et. al. Titanium Alloys and Processing for High Speed Aircraft. Material Science Engineering, Part A, 1998, **243**, pp.299-304.

[8] Ezugwu, E.O. and Wang, Z.M. Titanium Alloys and Their Machinability-A Review. Journal of Material Processing Technology, 1997, **68**(3), pp.262-274.

[9] Choudhury, I.A. and El-Baradie, M.A. Machinability of Nickel Base Superalloys: A General Review. Journal of Material Processing Technology, 1998, **77**(1-3), pp.278-284.

[10] Ezugwu, E.O. et. al. The Machinability of Nickel-base Alloys: A Review. Journal of Material Processing Technology, 1999, **86**(1-3), pp.1-16.

[11] Commission Calls for Immediate Action for a European Industrial Renaissance. Brussel: European Commission Press, 2014

[12] DeGarmo, E.P. et. al. Materials and Processes in Manufacturing (11th Edition). New York: John Wiley & Sons, 2011. (ISBN-13: 978-0470924679)

[13] Field, M. and Kahles, J.F. Review of Surface Integrity of Machined Components. CIRP Annals-Manufacturing Technology, 1971, **20**(2), pp.153-162.

[14] Field, M., Kahles, J.F. and Cammett, J.T. A Review of Measuring Methods for Surface Integrity. CIRP Annals-Manufacturing Technology, 1972, **21**(2), pp.219-238.

[15] Arola, D. and Williams, C.L. Estimating the Fatigue Stress Concentration Factor of Machined Surfaces. International Journal of Fatigue, 2002, **24**(9), pp. 923-930.

[16] Arola, D. and McCain, M.L. Surface Texture and the Stress Concentration Factor for

FRP Components with Holes. Journal of Composite Materials, 2003, **37**(16), pp.1439-1460.

[17] Arola, D. and Williams, C.L. Surface Texture, Fatigue, and the Reduction in Stiffness of Fiber Reinforced Plastics. ASME Journal of Engineering Materials and Technology, 2002, **124**(2), pp.160-166.

[18] Arola, D. and McCain, M.L. et. al. Waterjet and Abrasive Waterjet Surface Treatment of Titanium: A Comparison of Surface Texture and Residual Stress, Wear, 2002, **249**(1), pp.943-950.

[19] Arola, D. and McCain, M.L. An Examination of the Effects from Surface Texture on the Strength of Fiber Reinforce Plastics, Journal of Composite Materials, 1999, **33**(2), pp.102-123.

CHAPTER 2 LITERATURE REVIEW

2.1 INTRODUCTION

The ever-increasing demands of precision, performance, reliability and longevity of products require the surface quality of a machined part to satisfy more strict manufacturing standards as well as adopting more advanced materials. Some structures used in critical applications (like aero-engine parts) are being subjected to more severe conditions or extreme environments of stress and temperature. Section size of the parts or structures in aircraft industry are designed to be reduced in order to meet the goal of light weight; in this situation, machined surface conditions or the surface behavior of the part usually have an enhanced and more profound influence on its performance. In view of the above-mentioned demands, there has been a continued development and use of heat resistant, corrosion resistant and high strength alloys in a wide variety of mechanical structural applications, which include stainless steels, high strength steels, titanium alloys, nickel-base high temperature alloys, and so on. The materials used in the aerospace industry are supposed to be with superior properties which also make them really difficult to cut when compared with the normal materials. As a result, the machined surface quality for these materials is sensitive to the employed manufacturing and machining processes.

Dynamic alternating load is also one of the most important concerns in the design of modern mechanical parts and structures in aircraft. The essential design rule for aerospace-used parts is to satisfy both static materials strength and dynamic fatigue life requirement. Fatigue

properties play a leading role in the reliability and lifespan for the aerospace parts in service. The corresponding design objectives are normally dependent on the fatigue properties of the machined parts and structures. Failure analyses of fatigue parts indicate that fatigue cracking and subsequent failures almost always nucleate on and propagate from or near the surface of the machined part. If the structural configurations, dimensional sizes and the material properties are predefined, then the surface quality of a machined part becomes the most important factor that affects performance.

Generally speaking, the global surface quality of a machined part contains two aspects of meanings [1]. The first is the geometrically-related surface texture or topography, which indicates the outermost geometry of the machined part, mainly involves surface roughness parameters and measurement of surface topography; the second is the metallurgical alteration produced in a manufacturing process underneath the subsurface layer. Typical subsurface metallurgical alterations include a series of chemical, physical and mechanical changes such as plastic deformation, microcracks, phase transformations, microhardness, tears and laps related to built-up edge formation, residual stress distribution, etc. The effect of subsurface metallurgical alterations on the functional performance and fatigue life of machined parts is as important as surface texture based on specific applications. To make it more clear, the term *surface integrity* is adopted to describe the machining-induced overall or global features and the built-in correlations between the machining processes, the surface geometrical and subsurface metallurgical features, and the resultant functional performance.

Correspondingly, a manufacturing process will produce a machined surface consisting of

surface geometrical texture and subsurface metallurgical alterations. Both will influence the mechanical behavior and functional performance of the machined part. For example, if the machined surface is of rough irregularities, it is likely that the resultant fatigue performance of the machined part will be poor; whilst if the residual stress is compressive or if the surface layer is work-hardened, the resultant fatigue properties are likely to be good. A well-satisfied surface integrity requirement is indispensable to ensure the functional performance of machined parts.

2.2 CHARACTERIZATION AND EVALUATION OF SURFACE INTEGRITY

Surface integrity was first put forward by Field and Kahles on a technical seminar hold by Defense Metals Information Center in 1964 [1]. It describes surface status in terms of the service performance and was defined as “the unimpaired or enhanced surface condition or properties of a material resulting from a controlled manufacturing process”. Griffiths also later proposed a definition as “the topographical, mechanical, chemical and metallurgical 'worth' of a manufactured surface and its relationship to functional performance from the point of view of surface quality and machining process control”[2-5]. In this research, surface integrity is considered as the integrated surface behavior and condition of a material after being modified by a manufacturing process; it describes and controls the influence of surface properties or characteristics upon part’s functional performance. In 1971, Field and Kahles pointed out in their researches that SI requirement was essential to the surface quality of machined parts and they emphasized the nature of geometrical and metallurgical alterations occurring on the surface and within the subsurface layer for various alloy

materials both from conventional and non-conventional manufacturing processes [6]. Subsequently, Field and Kahles detailedly overviewed the measuring method for SI characteristics at that time, and they ingeniously presented an evaluation model for the characterization and assessment of surface integrity [7-8]. This model indicated that the surface characteristics and functional performance of machined components could be expressed and evaluated both qualitatively and partly quantitatively by three kinds of data sets including different primary SI characteristics, which are minimum SI data set (MSIDS), standard SI data set (SSIDS) and extended SI data set (ESIDS) as shown in Table 2.1.

Table 2.1 Three levels of data sets for SI characterization and evaluation

Minimum SI Data Set (MSIDS)	***Standard SI Data Set (SSIDS)***	***Extended SI Data Set (ESIDS)***
Surface texture (roughness) **Macrostructure (10x or less)** Macrocracks Macroetch indications **Microstructure** Microcracks Plastic deformation Phase transformations Intergranular attack Pits, tears, laps& protrusions Built-up-edge Melted & redeposited layers Selective etch **Microhardness**	Minimum SI Data Set **Residual stress distribution** Fatigue tests (screening) Stress corrosion tests	Standard SI Data Set **Fatigue tests (including fatigue design data)** **Extra mechanical tests:** Tensile test Stress rupture test Creep test Other special tests (e.g., bearing performance, sliding friction evaluation, sealing properties of surfaces)

For the MSIDS, the suggested SI characteristics include surface roughness, macrostructure, microstructure and microhardness. With all of the characteristics in MSIDS covered, the SSIDS provides more extensive and in-depth information, such as residual stress, fatigue and

stress corrosion tests for quite a few critical applications. With all of the characteristics in SSIDS covered, the ESIDS offers more detailed and extended data for the design of the fatigue test and additional mechanical tests. Field's and Kahles's groundbreaking work made it possible to systematically investigate surface integrity, and from then on the significance of surface integrity was gradually recognized both by the industry and academia. Their work also laid the foundation for the establishment and issue of American National Standard of Surface Integrity (ANSI B211.1) in 1986 [9].

Table 2.2 Surface integrity data sets recommended by ANSI B211

Minimum SI Data Set	***Standard SI Data Set***	***Remark***
Material, material hardness and heat treatment or **original metallurgical state** **Process and process intensity level** or the **operating parameters** **Surface roughness** 500-l000x magnification **cross-sectional photomicrograph** of the surface with reference scale and indication whether the view shown is typical or atypical of the entire surface. Include comments about any metallurgical aberration **Microhardness traverse**	Minimum SI Data Set **Residual stress** High-cycle fatigue S-N curve Reference value S-N curve or baseline fatigue endurance strength of material.	More extensive data sets to yield data suitable for more detailed design is beyond the scope of this standard

However, the ANSI B211.1 standard did not completely adopt all of the suggestions proposed by Field and Khales considering the state-of-the-art of manufacturing and measuring technologies at that time. The ANSI B211.1standard suggested and mainly focused on the use of MSIDS and SSIDS; while the ESIDS is only shown and treated as a footnote for engineers' information in this standard. Furthermore, the MSIDS and SSIDS employed in the ANSI B211.1 were simplified to some extent when compared to those

proposed by Field and Khales. Two levels of machining intensity, gentle and abusive machining, are adopted to differentiate practical processing conditions. To some extent, the data sets in the ANSI B211.1 overcome the shortcoming of what Field and Khales originally proposed which were mainly based on experimental measurement rather than characteristic description. Besides, surface roughness, a microhardness trace and a residual stress profile are also explicitly specified and required in this standard [9].

2.3 Surface and Subsurface Residual Stress

Surface residual stress is one of the most important characteristics of surface integrity and has always been the concern of academic research and industrial application. The residual stresses are usually inconvenient to be measured and also difficult to be accurately modelled this phenomenon. The machining-induced surface and subsurface residual stress could be compressive or tensile, which will bring distinct effects on the surface integrity and service performance of the machined parts [10-23]. Initial research on residual stress started in the 1930s. The main means for investigating residual stress was based on experimental measurement; the research concerns mainly focuses on the effect of various manufacturing factors (such as cutting heat, machining parameters) on the direction and magnitude of residual stress [24-29]. Conventional measuring method for residual stress is a kind of mechanical method during which the machining-induced residual stress is released by material removal and is then measured by using a strain gauge to obtain the deformation amount and the corresponding stress [30-35]. Later, McDonach developed an optical interferometry to measure displacement, strain and residual stresses [36]. Li designed a

combination of strain gauges (strain rosette techniques) to measure surface residual stress [37-39]. Gauthier made use of magnetic Barkhausen noise effects to measure surface residual stress on fabricated steels [40]. Nowadays, the main trend of experimental measurements of residual stress includes X-ray diffraction method, indentation method, and ultrasonic method. As for the study of manufacturing factors influence on the residual stress of machined surface, Henriksen firstly investigated formation mechanism of residual stress on and below machined surface [41]; Bailey studied the surface damage induced by excessive residual stress for maragring steel both under the lubricated and unlubricated conditions [42-43]. Liu and Barash studied the surface and subsurface mechanical state during chip-removal process with different shear plane angles which was caused by tool geometry; they also carried out a qualitative discussion about the formation mechanism of residual stress [44-46]. In the 21st century, the means for investigating surface residual stress has been largely enriched and finite element analysis becomes a popular alternative for residual stress studies. Nasr established a finite element model by using the adaptive Lagrange-Euler method and simulated the orthogonal cutting process for AISI 316L stainless steel. The detailed analysis about the impact of the tool geometry on residual stress is also reported [47]. Obikawa proposed a two-phase finite element model for processing alloys. It was evident that the obtained microstructure of the material within the machined surface layer had an important influence on the distribution of residual stress [48].

Machining processes usually leave the machined parts with a surface layer impacted by residual stress. Kong investigated the surface residual stress of workpieces machined with

different turning parameters and different heat treatment using the X-ray diffraction method [49]. It was found that the turning parameters, material types and heat treatment are influential to the final distribution of residual stresses. Wang established an orthogonal cutting model based on the enhanced Lagrange method and normalized chip separation criterion; the relationship between the cutting parameters and the corresponding surface residual stress being analysed [50-51]. Their research result shows that a residual tensile stress is usually produced because of the combination of excessive heat load and mechanical force applied to the workpiece surface. As is well known, surface residual stress has a direct influence on the fatigue life of machined parts and fatigue-related analyses have become an important field for residual stress research. Tensile residual stress on the machined surface is also usually considered as an important factor leading to fatigue crack initiation. When the machined surface has excessive tensile stress, the fatigue life of the machined part tends to be largely lowered when compared with a surface with compressive stress. Guo analyzed the principal causes and factors that may result in the surface residual stress [52]; for different causes, possible means that could be used to control the produced residual stress are suggested, which has actually provided operational guidance for adjusting surface residual stress by manipulating machining processes.

With the development of computer technology, it is becoming more popular to study the surface residual stress and its impact on performance (especially fatigue life) by using both advanced experimental measurement devices and finite element numerical technique which is gradually becoming an important research direction for surface residual stress. Fang and

Zeng had studied a typical orthogonal cutting process by establishing a plane strain FEM model with the help of commercial software DEFORM-2D [53]. The workpiece is modelled as elastic-plastic and the tool is assumed to be rigid. Chip formation, temperature distribution, cutting force variation and residual stress distribution are all investigated by using this FEM model. Li investigated the residual stress in the surface layer for hardened steel SKD11 using the FE method combined with the experimental results for high-speed end milling [54].

2.4 MICROSTRUCTURE AND MICROHARDNESS

The microstructure of a material is usually studied by using metallographic observation methods by which it is possible to qualitatively or semi-quantitatively investigate the changes in the state of the microstructure. Currently, researches on digital characterization of the microstructure and machining-induced material-altered layer for different difficult-to-cut materials are rarely reported. Many researches had mainly focused on the formation of hardened white layer on the surface of steels [55-59]. Chou et al investigated the factors that lead to the formation of white layer by using both theoretical analysis and experimental observation [56]. They concluded that abrupt temperature change, excessive deformation, original grain size and material properties are the key factors for the formation of the white layer. Barry studied the hardened white layer of high-strength steel of the surface and analyzed the reasons for the formation of the white layer [60]. Han made a similar study and proposed the thickness of the white layer as an objective of interest, through which the formation mechanism of the white layer and the corresponding variation in microhardness are clarified [61]. Umbrello proposed an empirical equation for the flow stress for metal

cutting and investigated the performance of the white layer and the grey layer by analyzing the variation of microhardness [62-63]; this laid the foundation for microhardness and microstructure analyses by using the finite element method.

Nowadays, existing studies on material-altered layers are numerous, but they are not systematically organized; some key issues and the correlation between formation mechanism, dislocation and phase transformation within the material-altered layers are still not well identified. Ezugwu compared the surface damage and corresponding subsurface microstructures of G-17 steel and nickel-based high temperature alloy Inconel 718 which are machined with different tools [64]; the result suggests that the tool selection and workpiece material properties are vital to the surface integrity characteristics of machined parts. Zou investigated the machinability of nickel-based superalloy NiCr20TiAl using a Polycrystalline cubic boron nitride (PCBN) cutting tool; the machining-induced surface voids, inclusions and slip-lines being observed in detail [65]. Further, the machining-induced burrs and its chemical composition were analyzed using energy spectral density (ESD). Obikawa [48] investigated the relationship between cutting force, surface residual stress and microstructure for dual-phase steel using finite element numerical simulation. Fox-Rabinovich studied the difference of the microstructure in the material-altered layer of machined parts which are processed using a coated and an uncoated tool respectively [66]. They used an optical microscope, a scanning electron microscope (SEM), an x-ray diffractometer (XRD), an x-ray photoelectron spectroscope (XPS) and a high resolution electron energy loss spectroscope (HREELS) and other advanced measuring instruments to observe and compare the difference

in the subsurface microstructure of parts machined by the two types of tools. Although these were not relating to quantitative analysis of the microstructure, this research could still help to further investigate and characterize the microstructure of the material-altered layer with multiple means of experimental observation.

Lehnert analyzed the changes in the microstructure of aluminum and copper materials processed by hot rolling, but their experimental work was based on light microscopy analysis and was still not concerned with the quantitative description of the microstructure [67]. Tang et al studied and obtained the changes of phase volume fraction in the microstructure using numerical simulation method; the correlation between stress, strain and microstructure are also established based on the different phase volume fraction. However, characterization of microstructure with volume fraction does not apply to the case of single-phase structure [68]. Li proposed and summarized three numerical methods for microstructure simulation: namely the Monte Carlo method, cellular automata method, phase-field method [69]. These numerical methods are implemented in different ways and are mainly used to characterize the grain size of microstructure.

The surface stress state of machined parts will vary when undertaking fatigue loading; the subsurface microstructure will also experience variation due to the dramatic changes in temperature during the machining process. After machining, the rough surface and nonuniform microstructure below the surface will cause uneven distribution of stress within the material. Stress concentration is easily generated at these locations and are the main factors leading to fatigue crack initiation. Lu et al studied crack initiation under fatigue

loading for dual-phase steel [70]. Simultaneously, they also investigated and compared the microstructure of 2Cr13 steel using the transmission electron microscope (TEM) when the samples experienced different cycles of fatigue. The microscopic explanation for damage evolution under low cycle fatigue process is also given.

From the perspective of micromechanics, Yuan studied the relationship between dislocation and the minimum depth of cut when using the rounded cutting tool by using TEM [71]. It is found that the main dislocation density will rise with the increase of tool radius; the larger the tool radius, the more mechanical deformation occurs and the greater the resultant dislocation generates. Yashiro analyzed the dislocation motion at the interface for γ precipitation hardening type nickel-base superalloy; numerical simulation being adopted to study the dislocation accumulation and grain boundary during the nucleation of the γ/γ' interface [72]. Three dislocation motion models are used to reveal the dislocation formation at the γ/γ' interface. Tang studied the properties of silicon by means of molecular dynamics (MD) simulation technology and atomic force microscopy (AFM) [73]. The result showed that the shear strength of the dislocation is much less than the yield strength of the silicon. Dlouh studied the dislocation variation of heat resisting nickel-base alloy 16Cr-10W-4Mo-TiA1 during creep using TEM [74]; the results showed that the dislocation movement could be an alternative to well explain the material deformation and microhardness change.

2.5 SURFACE TEXTURE AND ROUGHNESS PARAMETERS

The actual surfaces of machined workpieces are not completely smooth or flat. They are

essentially composed of many tiny irregular peaks and valleys from the microscopic point of view. As shown in Figure 2.1, the two-dimensional rough surface profile could usually be decomposed into three kinds of components according to the difference in wavelengths, which are surface roughness, surface waviness and error of form [75-76]. Surface roughness, also known as surface finish, could be used to characterize and describe the microscopic geometrical undulations of surface topography. It is generally produced as a result of the plastic deformation; the tool feed marks and the friction between the tool surface and the workpiece surface during the separation of the chip. Surface roughness is superimposed onto the surface waviness. The wavelength of waviness is normally greater than that of surface roughness but shorter than that of error of form. Waviness is considered to be caused by the deflection and vibration of the workpiece or by material strain. It could be the representative of the main direction of the machined surface texture. The error of form defines the deviation of the actual surface shape from the ideal one. It may be caused by errors of the slide way of

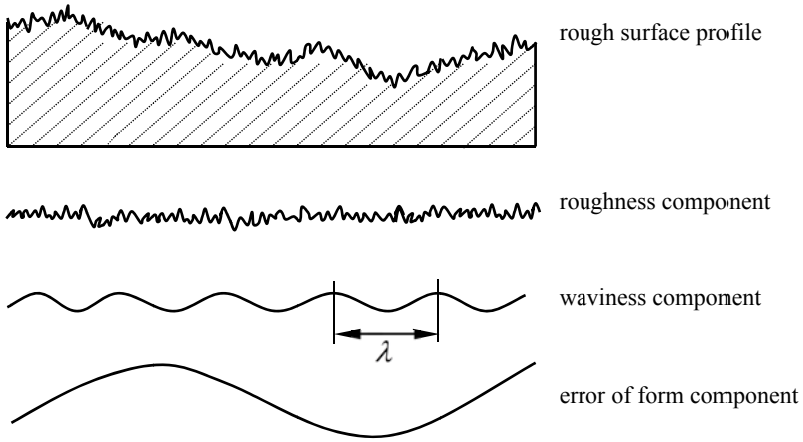

Figure 2.1 The basic components of the rough surface profile

the machine tools or the deflection of the workpiece. In engineering practice, the wavelength

of the surface roughness component is normally considered to be less than 1mm (λ<1mm); the wavelength of surface waviness usually being within in the range of 1mm ~ 10mm; and the wavelength of error of form being greater than 10mm(λ>10mm).It is therefore important to measure the surface microscopic geometrical characteristics in terms of different magnitudes of wavelength. With respect to the measurement of surface roughness, the length over which the identification and assessment of this surface microscopic geometrical characteristic is made is called the sampling length (SL). In ISO 4287 (1997), the sampling length is defined as the length in the direction of the X-axis used for identifying the irregularities and characterizing the profile under evaluation. Normally, 5 sampling lengths are taken in one traverse of a profilometer and they are taken as one evaluation length (EL). The evaluation length is defined as the length in the direction of the X-axis used for assessing the profile under evaluation [77-79].

From the point of view of microscopy, it is really necessary to have an evaluation standard to quantitatively characterize and assess the surface geometrical topography for different machined parts [80-83]. Since the 1920s, manufacturing engineers had already noticed that surface micro geometrical features, such as the surface roughness of machine parts, have a direct impact on the surface performance, especially for parts used in aircraft fuselages or aero-engines. For some critical parts that sustaining complex alternating loads, production engineers also started to pay attention to studying the effects of the machining-induced surface marks or scratches on the reliability and safety. However, limited by the measurement techniques at that time, engineers could not quantitatively measure and

evaluate the microscopic roughness features on machined surfaces, but only could estimate the micro geometrical characteristics visually or by personal experience. In the 1920s and 1930s, many industrial countries used a combination of triangular denotations "▽" to differentiate surfaces of distinct machining precision. In order to quantitatively measure the microscopic surface roughness and accurately study its effect on the performance of machined parts, Germany, the United States and Britain have designed or invented mechanical profile trace recorders or profilometers from the late 1920s to the 1930s. At the same time, the development of the optical microscope, interferometer and other measuring methods or instruments also offered alternative means for theoretical and numerical assessment of microscopic surface topography. In the United States, Abbott proposed the bearing area curve to characterize the surface roughness and its effect on load bearing [84]. In 1936, Schmaltz published his monograph to systematically discuss surface roughness which offered practical recommendations for assessment and standardization of micro surface roughness parameters [85]. Although the emergence of new assessment and computing standards for surface roughness always depended on the actual development level of measurement technology, the systematic study of quantitative characterization and assessment of surface roughness parameters had actually already entered its fast lane.

In the 1940s, many countries had constituted their own standards for surface roughness measurement and characterization. American National Standard ASA B46.1 was released in 1940, and after several amendments it finally evolved into the well-recognized American standard – ANSI/ASME B46.1-1988: "Structure of the Surface Roughness, Surface

Waviness and Processing of Grain". The standard adopted the mean-line system and proposed the arithmetic average roughness R_a as the main parameters for surface roughness evaluation. The former USSR issued a surface roughness standard GOCT2789-1945 as its national standard in 1945, and it finally became its national standards, namely "surface roughness parameters and characteristics" (GOCT2789-1973) after three rounds of amendment. The mean-line system was used and 6 main parameters were suggested for surface roughness evaluation, such as root-mea-square roughness R_q. In 1952, Germany also issued two assessment standards DIN4760 and DIN4762 to regulate surface roughness parameters and terms in its industry. These national standards all adopted the mean-line system and had much in common especially for the calculation of surface roughness parameters such as R_a and R_q, which is why they have also become internationally-recognized and widely-used parameters in the field of manufacturing. With the further development of production and the trend of globalization, ISO sorted out and unified these different standards and developed an series of international standards for the measurement and evaluation of surface roughness, such as ISO 4287 (1997) and ISO 13576-2 (1996). Nearly 20 2D surface roughness characterization parameters are given in the two ISO standards, in which commonly-used parameters such as arithmetic average roughness R_a, root-mean-square roughness R_q and ten point height R_z are all included [77-79]. In addition to the characteristic parameters recommended by the international standards, Taylor Hobson Ltd (THL) in the UK specifically suggested 24 most commonly used surface roughness parameters for industrial application [86]. Apart from parameters identical with

the ISO standard parameters, THL also recommended some parameters which are not covered by the ISO standard but could satisfy some specific applications in practical production. For better understanding and convenience, these 2D surface roughness parameters could be divided into the six categories to characterize and describe different features or functions of the machined surface: (1) amplitude parameters (relating to heights or depths of the surface profile); (2) amplitude distribution parameters (relating to the distribution of heights that feature surface shape); (3) slope parameters (relating to the differential of surface height); (4) Spatial parameters (relating to the vertical and horizontal spacing of surface peaks or valleys); (5) other parameters (combining both amplitude and spacing information); (6) MOTIF parameters (based on the surface characteristic shapes).

In practice, machined surfaces and their related surface quality have been mainly characterized and assessed using 2D surface roughness parameters like R_a and R_q. However, researchers gradually found that surfaces with the same values of R_a or R_q may be obviously different in their micro geometry. This indicates that 2D single-value surface roughness parameters are insufficient to completely characterize and describe surface geometrical and functional features. For a long time, people have been expecting to use 3D characterization and measurement techniques but this required so much processing power and high scanning speed that it was commercially or computationally infeasible at the time. With the development and improvement of metrology and computer technology in the 1990s, there have been significant changes in the way that surface topography can be measured, characterized and described in 3D format. Nowadays, it is well accepted that the features of a

surface can be well described and interpreted with 3D surface texture and related characteristic parameters, considering that important features are likely to be missed out or misinterpreted by only using 2D surface roughness parameters. Pfestorf studied two kinds of textured metal surfaces which are produced by laser and electron beam textured (EBT), and concluded that the common 2D parameters were unsuitable for clearly characterizing and differentiating surfaces with deterministic geometrical features (patterned or structured) [87]. Considering that 2D measurements may restrain the recognition of wear-related surface features, Anamalay adopted a laser scanning confocal microscope instead of a 2D profilometer to observe and measure 3D surface texture although the geometrical features were still calculated and characterized with principal 2D surface roughness parameters [88]. Dong et al also found that 2D characteristic parameters might be misleading when describing a natural 3D surface [89]; therefore, a 3D surface analysis system was adopted to study the surface topography at the estimated contact regions for metal pipe joints. The result shows that 3D characterization is essential for the prediction of joint performance. It has also suggested that the 'parameter rash' that occurred in 2D surface roughness parameters should be avoided by standardizing 3D parameters before this technique became widely used [81]. This reflects that it is necessary to check the functional significance of the newly proposed 3D parameters before they are suggested to industrial production and measurement [90].

2.5.1 2D Surface Roughness Characteristic Parameters

The aforementioned categorized parameters are mostly included in ISO 13565-2 (1996) and ISO 4827 (1997) standards, and are based on the mean-line system [77-78]. When

quantitatively measuring and characterizing a 2D surface profile according to the mean-line system, it is worthy to notice that the measured values of surface roughness parameters not only depend on the positional accuracy of the mean line, but also closely rely on the pre-selected sampling length and evaluation length. Considering this, a reasonable sampling length is specified before measuring surface roughness to avoid and filter the possible effect from waviness that is of longer wavelength. In the International standards, the recommended measurement series of sampling length were 0.08mm, 0.25mm, 0.8mm, 2.5mm, 8mm, 25mm [77-78]. Engineers could choose appropriate sampling length according to the base wavelength of the measured surface or the precision of measurement devices. When the sampling length is determined, the measured values of surface roughness parameters (e.g. R_a or R_z) over one sampling length may be very close to or largely away from that measured over another adjacent sampling length. To ensure the measured values of surface roughness could accurately reflect the measured surface characteristics, the evaluation length is introduced to take account of the effect of undulation of micro asperities over one sampling length, and it usually contains 5 consecutive sampling lengths.

2.5.1.1 2D surface amplitude parameters

Table 2.3 lists 2D surface roughness amplitude parameters with their standard definitions and numerical expressions [5, 77-78, 86]. The mean-line average roughness R_a, also called the arithmetic average roughness parameter, is one of the most commonly-used surface roughness parameters. It is defined as the arithmetic mean deviation of the assessed surface profile over a sampling length according to ISO 4287(1997). The root-mean-square

roughness, denoted by *RMS* or R_q, is an average parameter also, and it is defined as the root mean square deviation of the assessed surface profile. R_q is considered as statistically significant because it also represents the standard deviation of the surface profile height away from the mean line, which means the square of the deviations of the profile height is equal to the variance of random variables from its mean value ($R_q^2 = \sigma^2$).

Table 2.3 2D surface roughness amplitude parameters

2D amplitude parameters		
Denotation	**Name**	**Remark**
R_a	Arithmetic average roughness	$R_a = \frac{1}{SL}\int_0^L \lvert z(x)\rvert \mathrm{d}x = \frac{1}{N}\sum_{i=1}^{N}\lvert z(x_i)\rvert$
R_q	Root-mean-square roughness	$R_q = \sqrt{\frac{1}{SL}\int_0^L [z(x)]^2 \mathrm{d}x} = \sqrt{\frac{1}{n}\sum_{i=1}^{n} z(x_i)^2}$
R_t	Max peak-to-valley height	$R_t = \lvert z(x_i)_{\max} - z(x_j)_{\min}\rvert$
R_z	Ten-points height	$R_z = \frac{1}{5}\left[\sum_{i=1}^{5} z(x_i)_{\max} + \sum_{j=1}^{5}\lvert z(x_j)_{\min}\rvert\right]$
R_p	Max peak height	distance from the highest peak to mean line
R_v	Max valley depth	distance from the deepest valley to mean line

With respect to the parameters that measure extremes rather than averages, R_t measures the vertical distance from the highest peak to the lowest valley within an evaluation length (see Figure 2.2). It is defined in ISO 4287 (1997) as the total height of the profile. The R_t parameter is a kind of extreme parameter of a profile. Therefore, it is especially sensitive to any abnormal perturbation or disturbances on the surface profile. Another comparatively steady parameter which describes the peak-to-valley height is the ten-point height, R_z. It is defined as the average value of the five highest peaks and the five lowest valleys within the

sampling length.

Workpiece material above and below the mean line of the surface profile can be denoted and described by the max peak height and the max valley depth parameters. The max height of peak, R_p, is the vertical distance from the highest peak to the mean line. The max depth of valley, R_v, is the maximum vertical distance between the deepest valley and the mean line. The peak height R_p and the valley depth R_v provide an indication of the spread of the profile above or below the mean line and therefore distinguish between surfaces in a way that the previously-introduced average parameters do not.

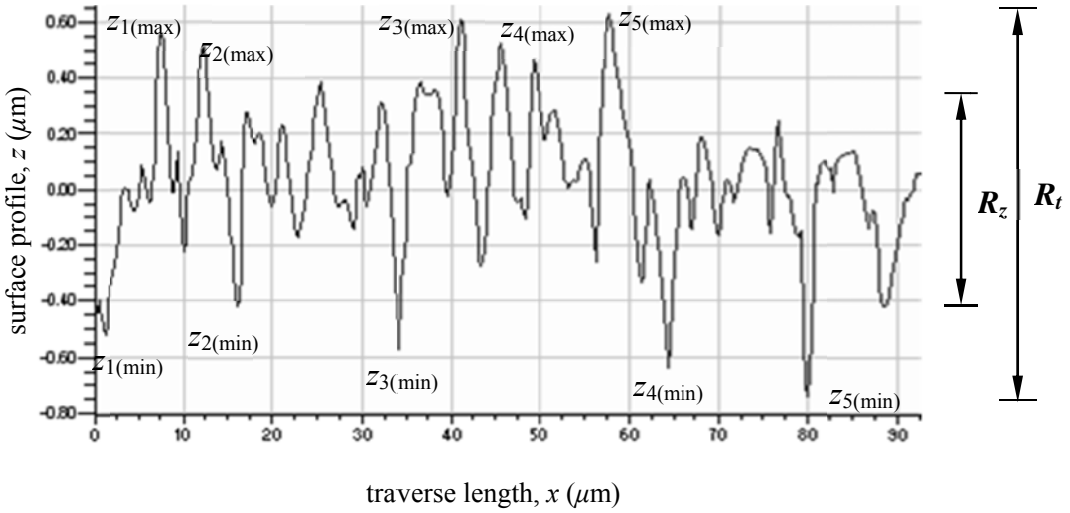

Figure 2.2 Schematic diagram of 2D surface roughness height parameters

2.5.1.2 2D surface amplitude distribution parameters

Table 2.4 introduces the expressions and meanings of the 2D amplitude distribution parameters [5, 77-78, 86]. For a 2D surface profile, the sum of all sectional lengths obtained by a line parallel to the mean line at a given level, c, measured from the highest peak of surface, is defined as the material length at the given level c, $Ml(c)$. If this length is

expressed as a fraction of the measured surface profile, then it could also be called as the material ratio, R_{mr}(c); and it is could be expressed as the ratio of the material length of the surface at the given level *c* to the evaluation length. If the sums of all sectional lengths at different levels are drawn as the right side of Figure 2.3, then the bearing area curve is derived.

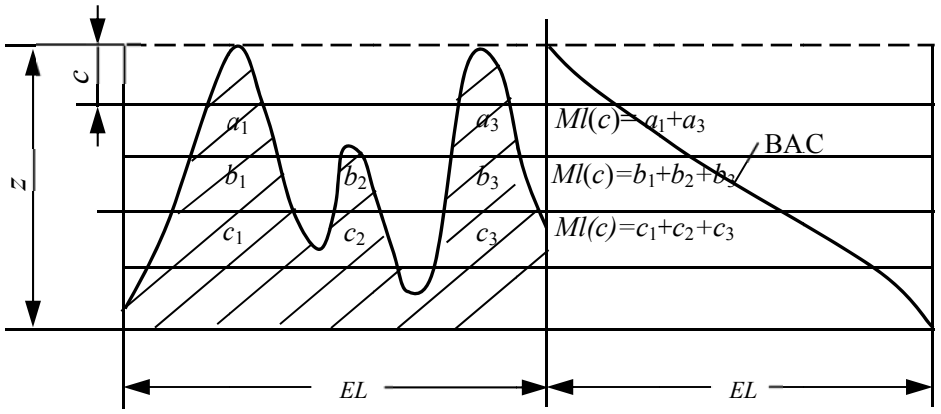

Figure 2.3 Material length and derived bearing area curve

Table 2.4 2D amplitude distribution parameters of rough surface profile

2D amplitude distribution parameters		
Denotation	**Name**	**Remark**
$R_{mr}(c)$	material ratio	$R_{mr}(c)=\frac{1}{EL}\sum_{i=1}^{n}L_i=\frac{Ml(c)}{EL}$
R_{sk}	skewness	$R_{sk}=\frac{1}{R_q^{\,3}}\left[\frac{1}{L_r}\int_0^{L_r}y(x)^3\,\mathrm{d}x\right]=\frac{1}{R_q^{\,3}}\left[\frac{1}{n}\sum_{i=1}^{n}y(x_i)^3\right]$
R_{ku}	kurtosis	$R_{ku}=\frac{1}{R_q^{\,4}}\left[\frac{1}{L_r}\int_0^{L_r}y(x)^4\,\mathrm{d}x\right]=\frac{1}{R_q^{\,4}}\left[\frac{1}{n}\sum_{i=1}^{n}y(x_i)^4\right]$
R_{pk}	reduced peak height	See Figure 2.5
R_k	core height	See Figure 2.5
R_{vk}	reduced valley depth	See Figure 2.5
R_{Mr1}	upper limit of BAC	See Figure 2.5
R_{Mr2}	lower limit of BAC	See Figure 2.5

2.5.1.3 2D surface slope parameters

Table 2.5 gives the definitions of the 2D slope parameters [5, 77-78, 86]. The RMS average parameter $R_{\Delta q}$ is the only slope parameter included in the ISO 4287 (1997) standard. It is defined as the root mean square of the ordinate slopes dz/dx within the sampling length. There will normally be five $R_{\Delta q}$ values: $R_{\Delta q1}$ to $R_{\Delta q5}$. The $R_{\Delta q}$ value is statistically significant because it is the standard deviation of the slope profile about the mean line. Furthermore, the variance of slope is the second moment of the slope's distribution function. The mean-line slope parameter is $R_{\Delta a}$. It is a non-ISO parameter. In theory, this parameter can be just as easily calculated from the differentiated profile as from the original profile.

Table 2.5 2D slope parameters of rough surface profile

2D slope parameters		
Denotation	**Name**	**Remark**
$R_{\Delta q}$	RMS slope	$R_{\Delta q} = \sqrt{\frac{1}{n}\sum_{i=1}^{n}\theta_i^2} = \sqrt{\frac{1}{L_r}\int_0^{L_r}\theta_i^2 dx}$
$R_{\Delta a}$	Mean-line average slope	$R_{\Delta a} = \frac{1}{n}\sum_{i=1}^{n}\lvert\theta_i\rvert = \frac{1}{L_r}\int_0^{L_r}\lvert\theta\rvert dx$

2.5.1.4 2D surface spatial parameters

Obviously, R_a, R_q etc. are average parameters only describing the surface features on the direction of amplitude and they could not differentiate or give more information between a peak and a valley along the spacing direction. Table 2.6 gives the definitions of the 2D spacing parameters [5, 77-78, 86]. The average peak spacing parameter, R_{Sm}, is the spacing between peaks over the sampling length at the mean line. It is defined in ISO 4287 (1997) as

the mean value of the profile element widths within a sampling length. The high spot count parameter, HSC, is the number of peaks that protrude above a section line parallel to the mean line within the evaluation length. The line can be above, below or on the mean line. An alternative method of defining a peak is with two section lines rather than one (a band). This is the case with the peak count parameter, PC, where the profile has to pass above one section line and then below another within the evaluation length. HSC and PC are non-ISO parameters. As with the HSC parameter, the PC parameter will depend upon where the band is placed relative to the mean line.

Table 2.6 2D spatial parameters of rough surface profile

2D spatial parameters		
Denotation	**Name**	**Remarks**
R_{Sm}	Average peak spacing	$R_{Sm} = \frac{1}{n_p}\sum_{i=1}^{n_p} X_{Si}$
HSC	High Spot Count	Number of peaks which protrude above a section line parallel to the mean line
P_c	Peak count	Number of peaks which pass through a band equi-spaced about and parallel to the mean line

2.5.1.5 Other parameters

Other parameters mentioned here are those that are not suitable to be categorized conveniently into the amplitude, distribution, slope or spatial classes given above. Table 2.7 gives the definitions of 2D other parameters. The RMS average wavelength $R_{\lambda q}$ is a measure of peak spacing taking into account relative magnitudes. This is a weighted average and considers a profile as a series of harmonics in which the amplitudes are weighted in

proportion to their frequencies. It should not be confused with any peak spacing parameter because the two are different. The RMS average wavelength is derived from the RMS average roughness and RMS slope, and it is a non-ISO parameter. The mean-line average wavelength $R_{\lambda a}$ parameter is not included in the ISO4287 (1997) standard or the THL booklet, but it could be derived as similar to $R_{\lambda q}$. Actual profile length, L_o, is the total length of the surface. It can be important in things like adhesion. A surface with high peaks and deep valleys would have a higher L_o, than those with low peaks and shallow valleys. It is a non-ISO parameter and is not included in the THL booklet. If the profile length, L_o, is divided by the horizontal component of the profile, the profile length ratio, L_{pr}, is derived. The L_{pr} parameter of most engineering surfaces is close to unity and typically less than 1.01.

Table 2.7 Other parameters of rough surface profile

Other parameters		
Denotation	**Name**	**Remarks**
$R_{\lambda q}$	RMS average wavelength	$R_{\lambda q} = \dfrac{2\pi R_q}{R_{\Delta q}}$
$R_{\lambda a}$	Mean line average wavelength	$R_{\lambda a} = \dfrac{2\pi R_a}{R_{\Delta a}}$
L_o	Actual profile length	$L_o = \int \sqrt{1+\left[\dfrac{dy}{dx}\right]^2}\, dx \approx 1 + \dfrac{[MeanSlope]^2}{2}$
L_{pr}	profile length ratio	$L_{pr} = \dfrac{L_p}{L_n}$ (usually between 1～1.01)

2.5.1.6 2D Surface MOTIF parameters

Motif analysis is an entirely different way of classifying and defining a surface profile based

on experience within the French automotive industry and its suppliers. Its characteristic forms or features of the profile are called 'motifs' [5, 77-78, 86]. Because motif analysis divides a 2D surface profile into characteristic shapes, it is already a form of filtering. So, the advantage of motif analysis is that it needs no sampling length or filtration. The technique is defined in ISO 12085 (1996) and its main parameters are listed in Table 2.8 .

Table 2.8 Motif parameters of rough surface profile

MOTIF **parameters**		
Denotation	**Name**	**Remarks**
R_X	Largest motif height	Maximum value of the profile irregularity *H(j)*
R	Average motif depth	$R = \frac{1}{m}\sum_{j=1}^{m} H(j)$
AR	Average motif spacing	$AR = \frac{1}{n}\sum_{i=1}^{n} AR(i)$

2.5.2 Statistical Functions

A machined surface is usually complex and with random geometrical features at the microscopic scale. This is mainly due to the fact that many machining processes, such as grinding and polishing, are statistical by nature. To accurately describe and measure these surface irregularities, sometimes statistical functions which combine random process theory and time series analysis are needed when compared with the single-value statistical parameters aforementioned. For example, surface roughness parameters like R_a or R_q are the statistical denotations which attempt to quantify one or two aspects of surface geometrical features with a fixed or a single value; while the statistical functions are a more powerful

means that could characterize the related functionalities of machined surfaces as well as geometrical features. Many statistical functions have already been developed or introduced to characterize random surface profiles, the most commonly-used being the amplitude distribution function, bearing area curve, power spectral density function and auto-covariance function. The definitions and applications of these functions are elaborated and illustrated in the literatures or in standards [77-79, 91].

The amplitude distribution function (ADF), also known as the probability distribution or histogram, is the probability density of surface height; its plot showing the distribution of the number of points within different surface height spacings. The bearing area curve (BAC), sometimes called the Abbott-Firestone curve, is defined by the ratio of the sum of the sectional lengths obtained by intersecting a line at a different depth c to that obtained by intersecting a line at the depth R_t. Statistically, the BAC could be derived by the integration of the ADF.

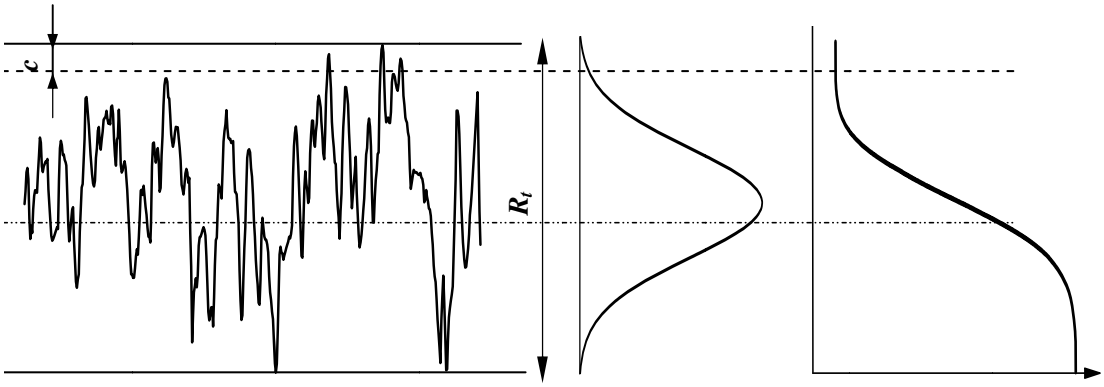

Figure 2.4 2D surface profile, ADF, BAC for a surface after external grinding

Figure 2.4 shows the correlation between a 2D rough surface profile and its ADF and BAC. BAC is normally taken as an indicator in for the assessment of fluid retention properties,

wear resistance and load-bearing capacity of a 2D surface profile. Further, it is well accepted that BAC is particularly suitable for characterizing a surface which is quite flat on the top and with grooves or notches at the bottom.

Five 2D surface characterization parameters, R_{pk}, R_k, R_{vk}, R_{Mr1} and R_{Mr2}, have been introduced to well define the BAC [5, 77, 91]. The method of how to derive these parameters is based on a best fit line over 40% of the BAC central portion, as shown in Figure 2.5. The parameter R_{pk} is the reduced peak height and is defined as the average height of the

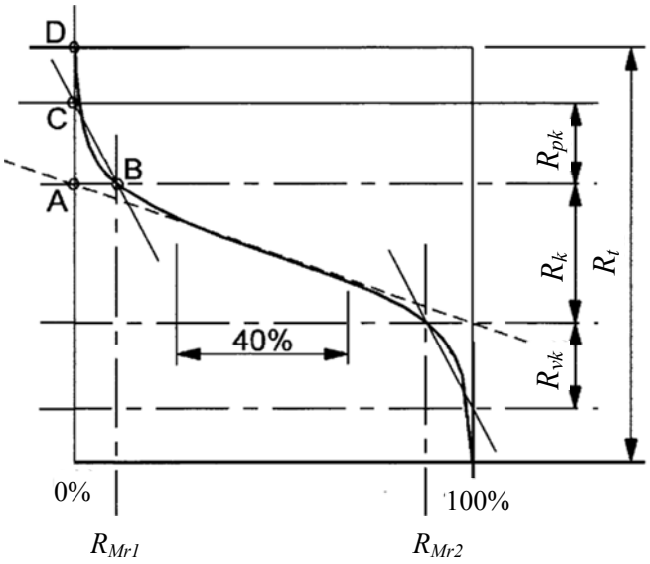

Figure 2.5 BAC and related surface characterization parameters representing functionality

protruding peaks above the roughness core profile. It represents the top portion of the surface that will be worn away quickly when the machined surface is contacting and rubbing with another one for the first time. The parameter R_k is called the core roughness depth and it is defined as the depth of the core profile of surface roughness. It characterizes the long-term running surface that will influence the performance and life of the machined part. The parameter R_{vk} is the reduced valley depth and is defined as the average depth of the profile

valleys below the roughness core profile. It characterizes the oil-retaining capacity provided by the deep valleys of surface profile. The parameters R_{Mr1} and R_{Mr2} are peak and valley material portions. They are respectively defined as the peak material portion determined for the intersection line which separates the protruding peaks from the roughness core profile, and the valley material portion determined for the intersection line which separates the deep valleys from the roughness core profile.

Further, considering that machined surface geometrical features being of random nature, statistical functions, such as power spectral density function (PSD) and auto-covariance function (ACV) methods, will also be necessary to accurately reveal and characterize the surface features relating to certain specific application. PSD analysis is useful for studying the strengths of various periodic components in the surface profile. It decomposes the measured surface geometrical texture/topography into different components of spatial frequencies by using the Fourier transform technique (FTT). By computing the amplitudes of the frequency components that make up the surface texture, it provides more information than single-value parameter such as R_a or R_t do. Mathematically, the PSD is defined as the square of the Fourier transform of the measured height of surface texture and it can be expressed as:

$$PSD(f) = \frac{d_0}{N}\left|\sum_{j=1}^{N} Z_j \cdot \exp[-i \cdot 2\pi f (j-1) \cdot SL]\right|^2 \tag{2.1}$$

where $i = \sqrt{-1}$; SL is the sampling length; Z_j is the surface amplitude function; the spatial frequency f is equal to K/L, and K is an integer that ranges from 1 to N/2.

The ACV is defined as the covariance of the random variable against a shifted version of itself and indicates how well the shifted surface correlates with the original one and gives a measure of the randomness of the surface. In 2D surface profile analysis, ACV is the inverse Fourier transform of the PSD data. The amplitude of ACV is a measure of the degree of similarity of a surface profile or texture at a given distance from the original location. If the shifted surface at a given distance is similar with or identical to the original surface, then the value of ACV is close to1; if all peaks of the shifted surface align with corresponding valleys of the original one, then the value of ACV approaches -1. When the values of ACV fall rapidly to zero along a given direction, the shifted surface profile is different and thus “uncorrelated' with the surface at the original location.

2.5.3 3D Surface Texture Characteristic Parameters

During the practical manufacturing and measurement, it was found that 2D surface roughness parameters and statistical functions could not completely characterize and reflect the practical surface geometrical features and behavior of machined parts for some specific application. 3D surface texture parameters normally have better statistical property than that of 2D surface roughness parameters. For example, some important functionality features relating to surface friction, wear and sealing, are closely interlinked with 3D surface characterization parameters. In order to achieve reproducible measurement results, the metrology requires a series of widely recognized and standardized 3D parameters to characterize the surface texture and topography. Although there were no well-recognized uniform 3D surface measurement and characterization standards, Stout et al proposed a

characterization system containing 14 3D surface texture parameters in the early 1990s [89, 92]. Later, Stoutfurther revised this 3D parameter system and made it finally become a recognized characterization standard which is often called the “Birmingham 14” (B14) parameters [93]. Due to the cost and practical technology level at that time, 3D surface texture characterization and relating measurement techniques had not been widely accepted and adopted in actual industry except for being researched in the academic and certain professional field (e.g. sheet-metal forming for automobile bodies). Nevertheless, some academic institutions have always been trying to improve and enrich the 3D surface texture parameters characterization system for the establishment of more effective and practical 3D surface characterization standards. In the early 2000s, there were two well-known research projects funded by the EU on the standardization of 3D surface characterization parameters, which were Autosurf coordinated by Brunel University, UK and SurfStand coordinated by University of Huddersfield, UK. Autosurf established customized correlations between the 3D surface geometrical characterization parameters and the coating performance of autobody from draw forming [94]. SurfStand verified the actual functionalities of 3D surface topography parameters and revised the meaning of 3D surface topography through a series of case studies, which laid the foundation for the establishment of a new ISO standard for 3D surface topography. SurfStand also proposed and added another three 3D parameters to the original B14 parameter system, and finally extended the “Birmingham 14” 3D surface texture parameters characterization system to “Huddersfield 17” (H17) system [95]. In the H17 parameters characterization system, there are 2 height parameters, 2 height distribution

parameters, 4 spatial parameters, 3 hybrid parameters and 6 functionality parameters. The majority of 3D surface characterization parameters in the H17 system parameters have been adopted by the latest international standard for 3D surface texture characterization [96-98].

Considering the 3D nature and related functional requirement of the machined surface, reasonable use of 3D measurement and characterization techniques can give a comprehensive understanding of the processes by which surfaces are machined. Generally, some of the commonly-used 2D surface roughness parameters are suitable and easy to be extended to the corresponding 3D surface texture parameters. However, for some specific particular functional properties of a machined surface, new 3D surface parameters are also needed to be developed. Compared with 2D surface roughness parameters denoted with a letter "R", the 3D surface texture parameters start with a letter "S". For example, S_q, the root mean square deviation of the surface, is an extension of 2D surface roughness parameter R_q. It is a dispersion parameter defined as the root mean square value of the surface height deflection off mean plane within the sampling area [5, 92-93, 95-98]. Statistically, it is the standard deviation of the height distribution and can be expressed as:

$$S_q = \sqrt{\frac{1}{MN}\sum_{j=1}^{N}\sum_{i=1}^{M}[z(x_i, y_j)]^2} \tag{2.2}$$

S_a, the arithmetic mean deviation of the surface, is an extension of 2D surface roughness parameter R_a [5, 92-93, 95-98]. It is a dispersion parameter defined as the average value of the surface departures within the sampling area and can be expressed as:

$$S_a = \frac{1}{MN}\sum_{j=1}^{N}\sum_{i=1}^{M}|\, z(x_i, y_j)\,| \tag{2.3}$$

S_z is the ten-point height over the complete 3D surface and it is also an extension of 2D surface roughness parameter R_z [5, 92-93, 95-98]. It is an extreme parameter defined as the average value of the absolute heights of the five highest peaks and the depths of five deepest valleys within the sampling area, and it can be expressed as:

$$S_z = \frac{1}{5}[\sum_{i=1}^{5} z_{pi} + \sum_{i=1}^{5} z_{vi}] \tag{2.4}$$

When a surface is modified by different production processes or wear mechanisms, S_z may demonstrate a change sooner than S_a or S_q.

S_{sk}, the skewness of surface topography height distribution, is the measure of the asymmetry of surface deviations about the mean plane [5, 92-93, 95-98]. Like its 2D counterpart R_{sk}, this parameter can be used effectively to describe the shape of the topography height distribution and its expression is:

$$S_{sk} = \frac{1}{MNS_q^{\ 3}} \sum_{j=1}^{N} \sum_{i=1}^{M} z^3(x_i, y_j) \tag{2.5}$$

For a Gaussian surface which has a symmetrical shape for the surface height distribution, (the value of) $S_{Sk} = 0$. This parameter will give some indication of the existence of spike-like features.

S_{ku}, the kurtosis of surface topography height distribution, is the measure of the peakedness of the surface height distribution and it characterizes the spread of the height distribution [5, 92-93, 95-98]. S_{ku} is an extension of two-dimensional surface roughness parameter R_{ku} and its expression is:

$$S_{ku} = \frac{1}{MNS_q^{\ 4}} \sum_{j=1}^{N} \sum_{i=1}^{M} z^4(x_i, y_j) \tag{2.6}$$

A Gaussian surface has a kurtosis value of 3. A centrally distributed surface has a kurtosis value larger than 3 whereas the kurtosis of a well-spread distribution is smaller than 3. By a combination use of the S_{sk} and the S_{ku}, (together with other parameters), it is possible to identify and differentiate surfaces which have a relatively flat top and deep valleys.

S_{al}, the fastest decay autocorrelation length, is a parameter in length dimension used to describe the autocorrelation characteristic of the areal auto-correlation function (AACF). It is defined as the horizontal distance of the AACF which has the fastest decay to 0.2 [5, 92-93, 95-98]. In other word, S_{al} is the shortest autocorrelation length where the AACF decays to 0.2 in any possible direction. For an anisotropic surface, S_{al} is in a direction perpendicular to the surface lay. A large value of S_{al} denotes that the surface is dominated by low frequency (or long wavelength) components, while a small value of S_{al} denotes the opposite situation. S_{al} can be express as

$$S_{al} = \min(\sqrt{\tau_x^2 + \tau_y^2}), \quad \text{in which } \widetilde{R}(\tau_x, \tau_y) \le 0.2 \tag{2.7}$$

S_{tr}, texture aspect ratio or isotropy index of the surface, is a spacing parameter and is used to identify texture strength, e.g. uniformity of texture aspect [5, 68-69]. Mathematically, it is defined as the ratio of the fastest to slowest decay to 20% of the correlation length of the AACF. In principle, S_{tr} has a value of between 0 and unity. Large values of the ratio indicate uniform texture in all directions, i.e. no defined or clear lay. Smaller values (S_{tr}<0.3) indicate an increasingly strong directional structure or lay. It can be express as:

$$S_{tr} = \left. \frac{\min(\sqrt{\tau_x^2 + \tau_y^2})}{\max(\sqrt{\tau_x^2 + \tau_y^2})} \right|_{R(\tau_x, \tau_y) \le 0.2} \tag{2.8}$$

in which $R(\tau_x, \tau_y) = \frac{1}{(M-1)(N-1)} \sum\sum \eta(x_k, y_l)\eta(x_{k+i}, y_{l+j})$, and $i = 0,\ 1,\ ..., m < M$

$j = 0,\ 1,\ ..., n < N$, $\tau_i = i \cdot \Delta x,\ \ \tau_j = j \cdot \Delta y$.

S_{td}, the texture direction of surface, is a spacing parameter and is not an extension of any 2D surface roughness parameter. This parameter is used to determine the most pronounced direction of the surface texture with respect to the Y axis within the frequency domain, i.e. it gives the lay direction of the surface. Thus, a surface with a lay along the Y axis will have S_{td} = 0 degree.

$S_{\Delta q}$ is a hybrid parameter and is the root-mean-square value of the surface slope within the sampling area [5, 92-93, 95-98]. It is expressed as:

$$S_{\Delta q} = \sqrt{\frac{1}{(M-1)(N-1)} \sum_{j=1}^{N} \sum_{i=1}^{M} \rho_{i,j}} \tag{2.9}$$

in which:

$$\rho_{i,j} = \left[\left(\frac{\partial \eta(x,y)}{\partial x} \right)^2 + \left(\frac{\partial \eta(x,y)}{\partial y} \right)^2 \right]^{0.5}_{x=x_i, y=y_j}$$

$$\approx \left(\frac{\eta(x_i, y_j) - \eta(x_{i-1}, y_j)}{\Delta x} + \frac{\eta(x_i, y_j) - \eta(x_{i-1}, y_{j-1})}{\Delta x} \right)^{0.5}$$

S_{sc} is the arithmetic mean summit curvature of the surface [5, 92-93, 95-98]. It is defined as the average of the principle curvatures of the summits within the sampling area. It can be expressed as:

$$S_{sc} = -\frac{1}{2} \frac{1}{n} \sum_{k=1}^{n} \left[\frac{\partial \eta^2(x,y)}{\partial x^2} + \frac{\partial \eta^2(x,y)}{\partial y^2} \right] \tag{2.10}$$

S_{dr}, the developed interfacial area ratio, is also a hybrid parameter and is defined as the ratio of the increment of the interfacial area of a surface over the sampling area [5, 92-93, 95-98].

S_{dr} reflects the hybrid property of surfaces. A large value of this parameter indicates the significance of either the amplitude or the spacing or both, and it can be expressed as:

$$S_{dr} = \frac{\sum_{j=1}^{N-1}\sum_{i=1}^{M-1} A_{i,j} - (M-1)(N-1)\Delta x\Delta y}{(M-1)(N-1)\Delta x\Delta y} \cdot 100\% \tag{2.11}$$

in which the area of an element is

$$d\mathrm{A}_{i,j} = \sqrt{1 + \left(\frac{\partial z(x,y)}{\partial x}\right)^2 + \left(\frac{\partial z(x,y)}{\partial y}\right)^2}\, d\mathrm{x}d\mathrm{y} \tag{2.12}$$

S_{bi}, the surface bearing index, is a functional parameter and is defined as the ratio of the S_q parameter over the surface height at 5% bearing area [5, 92-93, 95-98]. It can be expressed as: $S_{bi} = \frac{S_q}{\eta_{0.05}} = \frac{1}{h_{0.05}}$. A large value of the parameter indicates a good bearing property.

S_{ci}, the core fluid retention index, is a functional parameter and is defined as the ratio of the void volume of the unit sampling area at the core zone (5-80% bearing area) over the S_q parameter [5, 92-93, 95-98]. It can be expressed as:

$$S_{ci} = \frac{V_c}{S_q} = \left[\frac{V_v(h_{0.05}) - V_v(h_{0.80})}{(M-1)(N-1)\Delta x\Delta y}\right] / S_q \tag{2.13}$$

A large S_{ci} parameter indicates good fluid retention (in the core zone). For a Gaussian surface, this index is about 1.56.

S_{vi}, is a functional parameter and is the valley fluid retention index. This is the ratio of the void volume of the unit sampling area at the valley zone (80-100% bearing area) over the S_q parameter. A large S_{vi} indicates good fluid retention in the valley zone:

$$S_{vi} = \frac{V_v}{S_q} = \left[\frac{V_v(h_{0.80})}{(M-1)(N-1)\Delta x\Delta y}\right] / S_q \tag{2.14}$$

in which, $z(x_i, y_j)$ is the surface height at coordinate (x_i, y_i) on the sampling area; M is the

number of sampling points along x direction within the sampling area; N is the number of sampling points along the y direction within the sampling area.

2.6 SURFACE INTEGRITY FOR DIFFICULT-TO-MACHINE MATERIAL

The main research scope and application of surface integrity focuses on the systematic analysis of the effects of different machining processes or processing chains on the final surface properties and consequent part performance, especially for the difficult-to-machine material widely adopted in the automotive and aerospace industries [99-102]. By implementing and analyzing a large number of single-factor or multi-factor orthogonally-designed machining experiments with different machining parameters, the surface integrity characteristics (such as surface geometrical texture, microstructure, residual stress, microhardness) and their impact on parts' service performance (especially fatigue properties) are investigated. This procedure also can determine the manufacturing sensitivity to the machining process and condition for certain difficult-to-machine material. If the state of the surface layer or the magnitudes of the surface integrity characteristics vary slightly with the corresponding change of machining process parameters or conditions, then this material is considered as insensitive to the machining process and condition. Accordingly, the corresponding machining processes or process chains for this kind of material could be more efficient by improving the material removal rate or by adopting highly-effective machining methods to reduce the cost of machining time.

By applying surface integrity requirements, design and production engineers could effectively ensure the surface quality and final performance of machined parts by earlier and

better control of the corresponding processing parameters or machining conditions. However, implementation of surface integrity requirements and relating machining process control needs to accurately measure a large number of surface integrity characteristics from a series of single-factor or multi-factor orthogonally designed machining experiments, which will undoubtedly increase measuring costs and lower production efficiency. Therefore, the surface integrity requirements are normally compulsory to some key parts demanding high performance or only applied to the critical locations affecting the functionality of key parts; for ordinary parts without any specific demands, it is usually unnecessary to adopt the surface integrity machining and measurement standard due to the unwanted time and measurement cost. From an overall optimal perspective in manufacturing, if the manufacturer could manage to ensure the high surface integrity of key parts or at their critical locations and relax the processing requirement for the rest of majority of non-critical parts or locations, then the reliability of and the global production cost for manufacturing this kind of product are likely to be controlled and lowered. For example, the surface roughness requirement for different kinds of linking rods used in aero-engine is within a comparatively large range (such as 0.32~6.1μm); but their concerned fatigue strengths are sometimes found to be insensitive to their processing condition and working environment. According to economical and reliable surface integrity requirement, the manufacturer may relax the surface roughness requirement for many rods from the originally designed R_a= 0.8μm to more easy-to-achieve R_a=1.6~3.2μm or ever larger (as long as it won't affect its functionality and could keep working safely), and only apply high-standard machining process to some

key rods. Due to less restriction in processing control, the overall machining cost could be reduced by approximately 10% as well as keeping good functionality for the engine. Generally, the global production cost could be effectively controlled or lowered without compromising the functional performance of the machined products if the surface integrity requirement and evaluation are well applied.

2.7 SUMMARY

The advance in characterization, measurement and assessment of surface integrity for high standard machined parts are overviewed. The existing researches relating to the primary surface integrity characteristics, such as residual stress, microstructure and microhardness, surface texture and roughness, are reviewed and summarized. Although the concept of surface integrity has been proposed for quite some time, there has always been lack of effective and convenient quantification means for accurately evaluating surface service performance; the previous researches mainly focused on the effect of single or two to three kinds of SI characteristics on the mechanical properties or surface performance of the machined parts; there is still no systematic research into an integrated model which could actually cover 5 primary SI characteristics and evaluates their overall effect on the performance of machined parts, especially for some difficult-to-machine materials used in extreme environment such as aero-engine-used high-temperature alloys. Besides, the industry had actually realized that the manufacturing processes and machining parameters could adversely or favorably affect the surface integrity of machined parts, but they don't know how the rationale rules. To fill the gap in the field of global surface integrity

evaluation based on primary characteristics and to bridge the connection between industry and academia, a surface integrity (SI) descriptive model which could digitally and quantitatively define the primary surface integrity characteristic parameters for accurately describing their influence on functionality is needed. Considering the surface and subsurface integrity characteristics interact with each other and jointly determine the functionality of machined surfaces or parts, a generalized surface integrity model or framework for better understanding the interactions among the machining processes, surface integrity characteristic parameters and service performance, and effectively evaluating the quality and performance of machined component, is also expected. This research will manage to achieve these demands based on theoretical analysis and validated by grinding and fatigue experiment of GH4169 superalloy.

REFERENCES

[1] Field, M. and Kahles, J.F. The Surface Integrity of Machined and Ground High Strength Steels. DMIC Report, 1964, **210**, pp.54-77.

[2] Griffiths, B.J. Manufacturing Surface Design and Monitoring for Performance. Surface Topography, 1988, **1**, pp.61-69.

[3] Griffiths, B.J. Manufacturing Measurement, Part 2, Advanced Manufacturing Systems MSc Programme Distance Learning Book, Brunel University, Manufacturing and Engineering Systems Department, 1989.

[4] Sacerdotti, F., Griffiths, B.J., Butler, C. and Benati, F. Surface Topography in Autobody Manufacture-The State of the Art. Proceedings of the Institution of Mechanical Engineers, Part B: Journal of Engineering Manufacture, 2000, **214**,

pp.811-822.

[5] Griffiths, B.J. Manufacturing Surface Technology-Surface Integrity and Functional Performance. London: Penton Press, 2001(ISBN 1-8571-8029-1).

[6] Field, M. and Kahles, J.F. Review of Surface Integrity of Machined Components. CIRP Annals-Manufacturing Technology, 1971, **20**(2), pp.153-162.

[7] Field, M., Kahles, J.F. and Cammett, J.T. A Review of Measuring Methods for Surface Integrity. CIRP Annals-Manufacturing Technology, 1972, **21**(2), pp.219-238.

[8] Field, M. Surface Integrity-A New Requirement for Improving Reliability of Aerospace Hardware. Proceedings of 18th Annual National SAMPE Symposium, April 3-5, 1973, Los Angeles, California, USA.

[9] ANSI B211.1, American National Standards on Surface Integrity. Society of Manufacturing Engineers (SME),1986

[10] Arunachalam, R.M. et. al. Surface Integrity When Machining Age Hardened Inconel 718 with Coated Carbide Cutting Tools. International Journal of Machine Tools and Manufacture, 2004, **44**(14), pp.1481-1491.

[11] Arunachalam, R.M. et. al. Residual Stress and Surface Roughness When Facing Age Hardened Inconel 718 with CBN and Ceramic Cutting Tools. International Journal of Machine Tools and Manufacture, 2004, **44(**9), pp.879-887.

[12] Sharman, A.R. et .al. An Analysis of the Residual Stresses Generated in Inconel 718 When Turning. Journal of Materials Processing Technology, 2006, **173**(3), pp.359-367.

[13] Axinte, D.A. et. al. Turning of Advanced Ni Based Alloys Obtained via Powder Metallurgy Route. Annals of the CIRP, 2006,**55**(1), pp.117-120.88

[14] Chevrier, P. et. al. Investigation of Surface Integrity in High Speed End Milling of A Low Alloyed Steel. International Journal of Machine Tools and Manufacture, 2003, **43**(12), pp.1135–1142.

[15] Ulutan, D. et. al. Analytical Modeling Of Residual Stresses In Machining. Journal of Materials Processing Technology, 2006, **183**(1), pp.77-87.

[16] Özel, T. and Zeren, E. Finite Element Modeling the Influence of Edge Roundness on the Stress and Temperature Fields Induced by High-Speed Machining. International Journal of Advanced Manufacturing Technology, 2007, **35**(2), pp. 255-267.

[17] Hua, J. et. al. Effect of Feed Rate, Workpiece Hardness and Cutting Edge on Subsurface Residual Stress in the Hard Turning of Bearing Steel Using Chamfer+Hone Cutting Edge Geometry. Materials Science and Engineering A, 2005, **394**(1-2), pp.238-248

[18] Hua, D. et. al. Investigation of Cutting Conditions and Cutting Edge Preparations for Enhanced Compressive Subsurface Residual Stress in the Hard Turning of Bearing Steel. Journal of Materials Processing Technology, 2006, **171**(2), pp.180-187.

[19] M'Saoubi, R. et. al. Residual Stress Analysis in Orthogonal Machining of Standard and Resulfurized AISI 316L Steels. Journal of Materials Processing Technology, 1999, **96**(3), pp.225-233.

[20] Dahlman, P. et. al. The Influence of Rake Angle, Cutting Speed and Cutting Depth on Residual Stresses in Hard Turning. Journal of Materials Processing Technology, 2004, **147**(2), pp.181-184.

[21] Capello, E. Residual Stresses in Turning Part I: Influence of Process Parameters. Journal of Materials Processing Technology, 2005, **160**(4), pp.221-228.

[22] Outeiro, J.C. Umbrello, D. and M'Saoubi, R. Experimental and Numerical Modeling of Residual Stresses Induced in Orthogonal Cutting of AISI 316L Steel. International Journal of Machine Tools and Manufacture, 2006, **46**(14), pp.1786-1794.

[23] Nasr, M.N.A., Ng, E.-G. and Elbestawi, M.A. Effects of Workpiece Thermal Properties on Machining-Induced Residual Stresses-Thermal Softening and Conductivity. P IMechE Part B: Journal of Engineering Manufacture, 2007, 221, pp.1387-1400.

[24] Abukhshim, N.A., Mativenga P.T. and Tsheikh, M.A. Heat Generation and Temperature Prediction in Metal Cutting: A Review and Implications for High Speed Machining. International Journal of Machine Tools and Manufacture, 2006, **46**(7-8), pp.782-800.

[25] Sutter, G., Faure, L., Molinari, A. et. al. An Experimental Technique for the Measurement of Temperature Fields for the Orthogonal Cutting in High Speed Machining. International Journal of Machine Tools and Manufacture, 2003, **43**(7), pp.43-46.

[26] Majumdar, P., Jayaramachandran, R. and Ganesan S. Finite Element Analysis of Temperature Rise in Metal Cutting Processes. Applied Thermal Engineering, 2005, **25**(14-15), pp.2152-2168.

[27] Lu, J. and Flavenot, J.F. Application of the Incremental Hole-Drilling Method for Measurement of Residual-Stress Distribution. Experimental Techniques, 1989, **13**(11), pp.18-24.

[28] Schajer, G.S. and Tootoonian, M.A New Rosette Design for More Reliable Hole-Drilling Residual Stress Measurements. Experimental Mechanics, 1997, **37**(3) pp.299-306.

[29] Ee, K.C., Dillonjr, O.W. and Jawahir, I.S. Finite Element Modeling of Residual Stresses in Machining Induced by Cutting using a Tool with Finite Edge Radius. International Journal of Mechanical Sciences, 2005, **47**(10), pp.1611–1628.

[30] Prime, M.B. Residual Stress Measurement by Successive Extension of a Slot: The Crack Compliance Method. Applied Mechanics Review, 1999, **52**(2), pp.75-96.

[31] Schajer, G.S. and Steinzig, M. Full-Field Calculation of Hole-Drilling Residual Stresses from ESPI Data. Experimental Mechanics, 2005, **45**(6), pp.526-532.

[32] Schajer, G.S. and Prime, M.B. Use of Inverse Solutions for Residual Stress Measurements. ASME Journal of Engineering Materials and Technology, 2006, **128** (3), pp.375-382.

[33] Schajer, G.S. Hole-Drilling Residual Stress Profiling with Automated Smoothing. Journal of Engineering Materials and Technology, 2007, **129**(3), pp.440-445.

[34] Schajer, G.S. Advances in Hole-Drilling Residual Stress Measurements. Proceedings of the XIth International Congress and Exposition, June 2-5, 2008, Orlando, Florida, USA.

[35] Baldi, A. A New Analytical Approach for Hole Drilling Residual Stress Analysis by Full Field Method. Journal of Engineering Materials and Technology, 2005, **127**(2), pp.165-169.

[36] McDonach, A. et. al. Improved Moire Interferometry and Applications in Fracture Mechanics, Residual Stress and Damaged Composites. Experimental Techniques, 1983, **7**(6), pp.20-24.

[37] Li, K. Application of Interferometric Strain Rosette to Residual Stress Measurements. Journal of Optics and Lasers in Engineering, Special Issue on Optical Methods for Residual strain Measurement, 1997, **27**, pp.125-136.

[38] Li, K. Interferometric Strain/slope Rosette for Static and Dynamic Measurements. Experimental Mechanics, 1997, **37**, pp.111–118.

[39] Li, K. Residual Stress Measurement with Optical Strain Rosettes. Solid Mechanics and its Applications, 2002, 82, pp.145-152.

[40] Gauthier, J. et. al. Measurement of Residual Stress in Steel Using the Magnetic Barkhausen Noise Technique. NDT&E International, 1998, **31**(1), pp.23-31.

[41] Henriksen, E.K. Residual Stresses in Machined Surfaces. Transactions of the ASME Journal of Engineering for Industry, 1951, **73**, pp.69-76.

[42] Bailey, J.A. Surface Damage During Machining of Annealed 18% Nickel Maraging Steel, Part 1 - Unlubricated Conditions. Wear, 1977, **42**, pp. 277-296.

[43] Bailey, J.A. Surface Damage During Machining of Annealed 18% Nickel Maraging Steel, Part 2 - Lubricated Conditions. Wear, 1977, **42**, pp. 297-303.

[44] Liu, C.R. and Barash, M.M. The Mechanical State of the Sublayer of a Surface

Generated by Chip-Removal Process, Part 1: Cutting with a sharp Tool. ASME Journal of Manufacturing Science and Engineering, 1976, **98**(4), pp.1192-1199.

[45] Liu, C.R. and Barash, M.M. The Mechanical State of the Sublayer of a Surface Generated by Chip-Removal Process, Part 2: Cutting with a Tool With Flank Wear. ASME Journal of Manufacturing Science and Engineering, 1976, **98**(4), pp.1202-1208.

[46] Liu, C.R., Barash, M.M. Variables Governing Patterns of Mechanical Residual Stress in a Machined Surface. ASME Journal of Engineering for Industry, 1982, **104**(3), pp.257-264.

[47] Nasr, M.N.A., Ng, E.-G. and Elbestawi, M.A. Modelling the Effects of Tool-edge Radius on Residual Stresses When Orthogonal Cutting AISI 316L. International Journal of Machine Tools & Manufacture, 2007, **47**(2), pp. 401-411.

[48] Obikawa T. et. al. Microscopic Phase-dependent Residual Stresses in the Machined Surface Layer of Two-phase Alloy, Journal of Materials Processing Technology, 2009, **209**(9), pp.4496-4501.

[49] Kong, Q.H. and Yu Y.H. Research on Turning Residual Stress. Journal of Tongji University. 1999, **27**(5), pp.550-552.

[50] Wang, S.Y. et. al. Effect of Cutting Speed on Residual Stress of Workpiece by using FE. Tool Engineering, 2005, **39**(9), pp.33-36.

[51] Wang, S.Y. Research on the Machined Surface Quality for High-speed Milling. Ph.D. thesis, Shandong University, 2006.

[52] Guo, P.Y. and Wang S.Y. et. al. Results and Controlling Techniques of Residual Stress in Machined Layer for High-speed Machining. Tool Engineering. 2007, **41**(3), pp.46-48.

[53] Fang, G. and Zeng P. FEM Simulation of Orthogonal Metal Cutting Process. Mechanical Science and Technology, 2003, 22(1), pp. 641-645.

[54] Li, J.L., Jing, L.L. and Chen, M. An FEM Study on Residual Stresses Induced by

High-speed End-milling of Hardened Steel SKD11. Journal of Materials Processing Technology, 2009, **209**(9), pp.4515-4520.

[55] König, W. and Tönshoff, H.K. Machining of Hard Materials. Annals of the CIRP, 1984, **33**(2), pp.417-427.

[56] Chou, Y.K. and Evans, C.J. White Layers and Thermal Modeling of Hard Turned Surfaces. International Journal of Machine Tools and Manufacture, 1999, **39**, pp.1863-1881.

[57] Sauvage, X. et. al. Phase Transformations in Surface Layers of Machined Steels Investigated by X-ray Diffraction and Mössbauer Spectrometry. Materials Science and Engineering A, 2003, **362**, pp.181-186.

[58] Hashimoto, F. et. al. Surface Integrity Difference between Hard Turned and Ground Surfaces and Its Impact on Fatigue Life. Annals of the CIRP, 2006, **55**(1), pp.81-84.

[59] Ramesh, A. et. al. Analysis of White Layers Formed in Hard Turning of AISI 52100 Steel. Materials Science and Engineering A, 2005, **390**, pp.88-97

[60] Barry, J. and Byrne, G. TEM Study on the Surface White Layer in Two Turned Hardened Steels. Materials Science and Engineering: A, 2002, **325**(1-2), pp.356-364.

[61] Han, S. et. al. White Layer Formation due to Phase Transformation in Orthogonal Machining of AISI 1045 Annealed Steel. Materials Science and Engineering A, 2008, **488**, pp.195-204.

[62] Umbrello, D. and Filice, L. Improving Surface Integrity in Orthogonal Machining of Hardened AISI 52100 Steel by Modeling White and Dark Layers Formation. CIRP Annals - Manufacturing Technology, 2009, **58**(1), pp.73-76.

[63] Umbrello, D. Influence of material microstructure changes on surface integrity in hard machining of AISI 52100 steel. The International Journal of Advanced Manufacturing Technology, 2011, **54**(9-12), pp.887-898.

[64] Ezugwu, E.O. and Tang, S.H. Surface Abuse When Machining Cast Iron (G-17) and

Nickel-base Superalloy (Inconel 718) with Ceramic Tools. Journal of Materials Processing Technology, 1995, **55**(2), pp.63-69.

[65] Zou, B. et. al. Study on Surface Damages Caused by Turning NiCr20TiAl Nickel-based Alloy. Journal of Materials Processing Technology, 2009, **209**(17), pp.5802-5809.

[66] Fox-Rabinovich, G.S. et. al. Impact of Annealing on Microstructure, Properties and Cutting Performance of an AlTiN Coating. Surface and Coatings Technology, 2006, **201**(6), pp.3524-3529.

[67] Lehnert, W. and Cuong, N.D. Experimental and Mathematical Simulation of Microstructural Evolution during Hot Rolling of Al and Cu Material. Journal of Materials Processing Technology, 1996, **60**(1-4), pp.567-574.

[68] Tang, Z. et. al. Microstructure Evolution and Numerical Simulation of TAl5 Titanium Alloy during Hot Compressive Deformation. The Chinese Journal of Nonferrou Metals, 2008, **18**(4), pp.722-727.

[69] Li, J.H. The Microstructure Evolution and Its Simulation for the TC21 Titanium Alloy during Hot-working Process. Master thesis, Nanjing University of Aeronautics and Astronautics, 2007.

[70] Lu, T. et. al. Low Cycle Fatigue Damage Evolution Law of 2Cr13 Steel. Journal of Mechanical Strength, 1999, **21**(2), pp.118-121.

[71] Yuan, Z.J., Zhou, M. and Dong, S. Effect of Diamond Tool Sharpness on Minimum Cutting Thickness and Cutting Surface Integrity in Ultra-precision Machining. Journal of Materials Processing Technology, 1996, **62**(4), pp.327-330.

[72] Yashiro, K. et. al. Discrete Dislocation Dynamics Simulation of Cutting of γ Precipitate and Interfacial Dislocation Network in Ni-based Superalloys. International Journal of Plasticity, 2006, **22**(4), pp.713-723.

[73] Tang, Q.H. MD Simulation of Dislocation Mobility during Cutting with Diamond Tip on Silicon. Materials Science in Semiconductor Processing, 2007, 10(6),

pp.270-275.

[74] Dlouhý, A. et. al. Monotonous and Cyclic Creep in a Heat-resistant 16Cr-10W-4Mo-TiA1 Nickel-based Alloy Transmission Electron Microscopy Study of Microstructure. Materials Science and Engineering: A, 1996, **205**(1-2), pp.40-49.

[75] British Standard, BS 1134-1, Assessment of Surface Texture. Part 1: Methods and Instrumentation, 1988

[76] British Standard, BS 1134-2, Assessment of Surface Texture. Part 2: Guidance and General Information, 1990 (and 2010)

[77] International Organization for Standardization, ISO 4287, Geometrical Product Specifications—Surface Texture: Profile Method-Terms, Definitions and Surface Texture Parameters, Switzerland, 1997(E/F)

[78] International Organization for Standardization, ISO 13565-2, Surface Texture: Profile Method—Surfaces Having Stratifying Functional Properties, Part 2: Height Characterisation using the Linear Material Ratio Curve, Switzerland, 1996.

[79] International Organization for Standardization, ISO 12085, Surface Texture: Profile Method—Motif Parameters, Switzerland, 1996

[80] Thomas, T.R. Roughness Surfaces. London: Longman, 1982.

[81] Whitehouse, D.J. The Parameter Rash-is there a Cure?. Wear, 1982, **83**(1), pp.75-78.

[82] Whitehouse, D.J. Surface Metrology Instrumentation. Journal of Physics E: Scientific Instruments, 1987, **20**(10), pp.1145-1155

[83] Whitehouse, D.J. Surfaces and Their Measurement. London: Hermes Penton Science, 2002(ISBN 1-9039-9601-5)

[84] Abbott, E.J. and Firestone, F.A. Specifying Surface Quality: A Method Based on Accurate Measurement and Comparison. Journal of Mechanical Engineering, 1933, **55**, pp.569-572.

[85] Schmaltz, G. Technische Oberflächenkunde. Berlin: Springer Verlag, 1936.

[86] Taylor Hobson Ltd (THL), Surface Texture Parameters. Leicester: THL, 1998. (THL

Booklet Number 800-304/897)

[87] Pfestorf, M., Engel, U. and Geiger, M. 3D-surface Parameters and Their Application on Deterministic Textured Metal Sheets. International Journal of Machine Tools and Manufacture, 1998, **38**(5-6), pp.607-614.

[88] Anamalay, R.V., Kirk, T.B. and Panzera, D. Numerical Descriptors for the Analysis of Wear Surfaces using Laser Scanning Confocal Microscopy. Wear, 1995,**181-183**(part 2), pp.771-776,

[89] Dong, W.P. et. al. Instruments and Measurement Techniques of Three-Dimensional Surface Topography. *In* Stout, K.J. and Blunt, L. *Three Dimensional Surface Topography, Measurement, Interpretation and Applications: A Survey and Bibliography*. London: Penton Press, 1994, pp.19-94.

[90] Peters, J. et. al. Contribution of CIRP to the Development of Metrology and Surface Quality Evaluation during the Last Fifty Years. CIRP Annals-Manufacturing Technology, 2001, **50**(2), pp.471-488.

[91] WYKO Surface Profilers Technical Reference Manual(P/N 980-085), Veeco Metrology Group,1999

[92] Stout, K.J. et. al. Development of Methods for the Characterisation of Roughness in Three Dimensions, Report EUR 15178 EN, Commission of the European Communities, Brussels, 1993, ISBN 0-7044-1313-2

[93] Stout, K. J. and Blunt, L. Three-Dimensional Surface Topography (2nd Edition). London: Penton Press, 2000 (ISBN 1857180267)

[94] Sacerdotti, F. and Griffiths B.J. et. al. Surface Topography in Autobody Manufacture -The State of the Art. Proceedings of the Institution of Mechanical Engineers, Part B: Journal of Engineering Manufacture, 2000, **214**, pp.811-822.

[95] Blunt, L., Jiang, X. and Stout, K.J. Developments in 3D Surface Metrology. *In* Chiles, V. and Jenkinson, D. *Proceedings of the 4th International Conference on Laser Metrology and Machine Performance*. Southampton: WIT Press, 1999,

pp.255-263.

[96] http://en.wikipedia.org/wiki/ISO_25178

[97] http://www.iso.org/iso/iso_catalogue/catalogue_tc/catalogue_detail.htm?csnumber=42785#

[98] ISO/TS 25178-2: 2006 Geometrical product specification (GPS)—surface texture: areal—part 2: terms, definitions and surface texture parameters.

[99] Ezugwu, E.O., Bonney, J. and Yamane, Y. An Overview of the Machinability of Aeroengine Alloys. Journal of Materials Processing Technology, 2003, **134**(2), pp.233-253.

[100] Ezugwu E.O. Key Improvements in the Machining of Difficult-to-cut Aerospace Superalloys. International Journal of Machine Tools and Manufacture, 2005, 45(12-13), pp.1353–1367.

[101] Jawahir, I.S. et. al. Surface Integrity in Material Removal Processes: Recent Advances. CIRP Annals-Manufacturing Technology, 2011, **60**(2), pp. 603-626.

[102] DeGarmo, E.P. et. al. Materials and Processes in Manufacturing (11th Edition). New York: John Wiley & Sons, 2011. (ISBN-13: 978-0470924679)

CHAPTER 3 SURFACE INTEGRITY CHARACTERISTIC PARAMETERS AND ITS DESCRIPTIVE MODEL

3.1 INTRODUCTION

The primary concern for the machined parts used in aerospace is to achieve the desirable strength and reliability requirements. Machined surfaces along with their relating geometrical, mechanical and physical characteristics usually play a leading role in determining the reliability and fatigue life of the practical parts in service. Sometimes, people may wonder why researchers and investigators have paid so much attention to the surface of a machined part but not the bulk sections. The answer to this question is actually obvious in that most machined parts fail starting from just the surface of the parts and finally result in malfunction in practice. The modes of failure may be shown as excessive plastic deformation or adhesive wear, surface cracks initiation, cracks growth, and final fracture [1]. Usually, once the overall structural configuration, geometrical size and material types are selected and fixed, the machining-induced global surface quality, which is also referred to as surface integrity (SI), will become the most important factor that affects the functionality and fatigue performance of a machined part.

Generally speaking, surface integrity includes at least two levels of content [1-2]. The first level is mainly the surface geometrically-related information which indicates the outermost geometrical features of the machined part and mainly covers surface roughness and texture; another is principally the physical, chemical or mechanical-related properties and

metallurgical transformation within the shallow subsurface layer caused by excessive force and heat during machining process, as shown in Figure 3.1. [1-5]

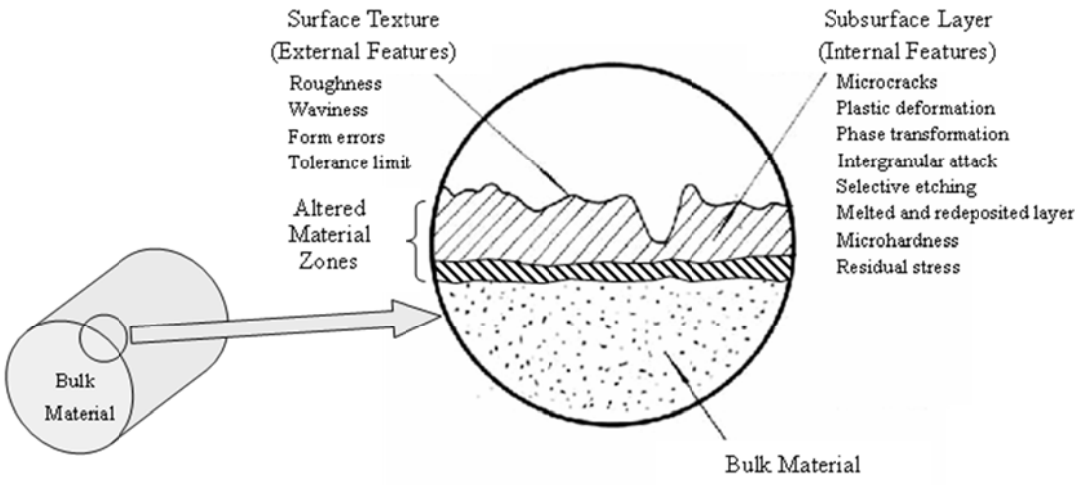

Figure 3.1 Schematic diagram of surface/subsurface integrity characteristics for machined parts

Typical subsurface metallurgical alterations include a series of physical or mechanical alterations such as plastic deformation, microcracks, phase transformations, microhardness and residual stress distribution. Depending on the specific application, the effect of subsurface alterations (such as residual stress or microhardness distribution) on the functional performance of a machined part is sometime more profound than that caused by surface geometrical changes [5]. However, the subsurface alterations are more difficult to be discerned when compared with the surface-geometrical-related information. Accurate characterization and good control of SI, both for surface geometrical and subsurface mechanical/physical characteristics, are indispensable to ensure the functional performance (especially the fatigue property) of machined parts.

3.2 DESCRIPTIVE MODEL FOR SURFACE INTEGRITY

With the development of modern manufacturing industry, quite a few advanced manufacturing and machining technologies for complex surface generation are proposed; many new metrological apparatuses and measuring methods are also correspondingly developed. As is well known, most of the traditional 2D surface roughness parameters only emphasize the geometrical information of a surface profile in the vertical direction but neglect some main features on the horizontal directions, which makes them cannot fully reflect micro geometrical characteristics and corresponding functional properties of real surface texture. Some of the surface roughness parameters defined in the previous standards may have been found obsolete and incompetent to the needs of modern metrological technology and surface characterization requirements. Although 2D surface roughness parameters are already amongst the most important indexes for evaluating the surface integrity of machined components, they are not the only ones and it is still necessary to develop more functionally-oriented parameters to comprehensively and quantitatively describe SI characteristics within the subsurface layer.

Surface integrity usually provides the link to the service environment in which a part will have to function. It was proposed to underline the link between processing and performance and furthermore to give an indication of the likely genuineness and reliability of all aspects of a manufactured surface. It is generally recognized that SI characteristics have a direct influence on the functional performance of machined parts, especially for some key parts used in the field of automotive and aerospace industry. The concept of surface integrity has

been proposed for quite some time; however, there has always been lack of effective and convenient quantification means for accurately evaluating surface service performance. Manufacturers are always looking forward to establishing the direct and accurate links between the surface integrity characteristics and the functional performance of components in service.

With the progress of modern measurement technology, surface integrity characteristics parameters are constantly being enriched and developed. The surface roughness is surely still one of the most important indexes for the evaluation of the surface functional performance of machined parts. The ever-developing technologies, such us interferometry, SEM and AFM, have also enriched the surface roughness characterization parameters and embrace them to the industrial-level application along the existing surface roughness standards. Macro- and micro-structure within the subsurface layer of machined parts has been reckoned to reflect the effects of grain size, plastic deformation, phase transformation, and melt and redeposited layer after material-removing processes; both of them are essential to predict the surface integrity. The microhardness values on the machined surface and within the subsurface indicate the physical and mechanical properties of machined parts after different kinds of processing; it is a commonly-used indicator for comprehensive evaluation of surface integrity. Residual stress on the surface or within the subsurface will have direct influence on the functional performance, especially the fatigue properties of machined parts; it is indispensable index for evaluating the surface integrity of some key components used in aerospace industry. Based on above-mentioned considerations and combined with the real

demand and practical manufacturing condition in specific applications in industry (especially the fatigue performance of machined parts in aerospace industry), a surface integrity descriptive model, which covers the specific descriptions and detailed definitions for the primary SI characteristics, such as surface roughness, macro and microstructure, microchardness and residual stress, is proposed, as shown in Figure 3.2, based on the surface integrity datasets proposed by Field and Kahles and ANSI B.211 standard [6-10].

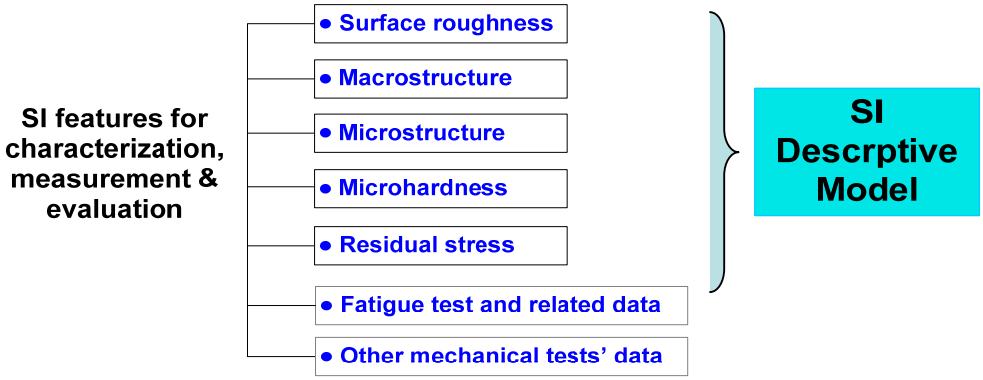

(a) The primary characteristics within SI descriptive model

Surface roughness	Macrostructure	Microstructure	Microhardness	Residual Stress
average roughness, R_a	crack length, l	microcrack depth, h_{MC}	surface microhardness, HV_1	surface RS, σ_{R0}
RMS roughness, R_q	crack width, d	thickness of MAL, h_B	microhardness of bulk material, HV_0	peak tensile RS, σ_{TMax}
ten-point height, R_z	inclusion diameter, d_{XI}	dislocation density, ρ_d	thickness of hardened layer, h_{HV}	peak compressive RS, σ_{CMax}
skewness, R_{sk}	dispersion density, ρ_{XI}	grain deflection, θ_{gd}	distribution of microhardness, $\Delta HV(h)$	thickness of RS layer, h_R
kurtosis, R_{ku}	metallograph	SEM/TEM picture	...	distribution of RS, $\Delta\sigma_R(h)$
...	...	...	...	...

(b) Specific parameters of each primary SI characteristic

Figure 3.2 SI characteristic descriptive model

The proposed SI descriptive model not only includes the specific quantitative parameters of

the primary SI characteristics (e.g. the surface roughness characteristics will include surface roughness standard parameters such as R_a, R_y, R_z and R_{sk} as shown in Figure 3.2(b)), but also cover the typical characteristics measurement methods, the information of measured data format and digital denotations which will make them easy to derive and follow. The SI characteristics' parameters in the descriptive model are defined to digitally denote or quantitatively represent their physical and geometrical features. With this model, any SI characteristic data from different machined materials could be collected, analyzed and saved for further exploiting and data- mining.

As above-mentioned, surface roughness characteristic parameters have always been one of the most important and widely-used methods for quantitatively describing and evaluating surface integrity of some key parts. With the ever-developing of surface generating and measuring technology, numerous 2D surface roughness characteristic parameters with different application-oriented functionalities have been proposed and adopted during the last 60 years. In view of both specific and general requirements of surface integrity evaluation, the digital representations and the measurement means for the descriptive parameters of surface roughness characteristics within the surface integrity descriptive model are listed in Table 3.1. Both 3D and 2D surface topographical parameters can be measured by using a 3D optical interferometer (Veeco NT1100) in one step. Considering that the measurement area of 3D optical interferometer is quite limited and the cleanness requirement for the specimen surface is demanding, 2D surface measurement with a surface profilometer (such as TR240 profilometer) is also an alternative for surface profile parameters.

Table 3.1 Descriptive parameters for surface roughness characteristic

SI Characteristics	Specific descriptive parameters		Measurement
surface roughness	**2D parameters** (a) amplitude parameters ①average roughness R_a ②RMS roughness R_q ③ten-point height R_z ④max peak height R_p ⑤max valley depth R_v ⑥max peak-to-valley R_t (b) functional parameters ①skewness R_{sk} ②kurtosis R_{ku} (c) Slope parameters ①RMS slope $R_{\Delta q}$ (d) Spacing parameters ①average spacing on mean line R_{Sm} ②high spot count HSC	**3D parameters** (a) amplitude parameters ①RMS roughness S_q ②ten-point height S_z ③max peak height S_p ④max valley depth S_v (b) functional parameters ①3D skewness S_{sk} ②3D kurtosis S_{ku} (c) spacing ①surface texture aspect ratio S_{tr} ②surface texture direction S_{td} ③Fastest decay length of ACF S_{al} (d) Hybrid ①3D RMS slope $S_{\Delta q}$	Using stylus profiler, optical profilometer or SEM to scan and measure the sample surface. e.g. Veeco NT1100 3D optical profilometer is adopted to measure multiple 2D and 3D surface roughness parameters

The machining-induced high temperature usually leads to microstructural or metallurgical transformations at the surface layer or within the subsurface during the cutting process. This alteration may affect some functional performances (such as fatigue life) of the machined components. Therefore, it is extremely necessary to accurately measure, characterize and analyze the microstructure both on the surface and within the subsurface for the surface integrity of machined components. The main means for the microstructure and metallurgical research are qualitative observation and comparative analysis using metallograph, SEM pictures and other non-quantitative descriptive methods. In the proposed surface integrity descriptive model, digitalized expressions are adopted to denote and characterize the physics

characteristics related to SI microstructure analysis. This actually offers at least a kind of quasi-quantitative method to investigate microstructural characteristic and give more accurate prediction or evaluation of the functional performance of the machined components. Within the surface integrity descriptive model, the detailed quantitative characterization parameters and measurement methods for macro and microstructure are as shown in Table 3.2 and Table 3.3.

Table 3.2 Descriptive parameters for macrostructure characteristics

Characteristics	Specific descriptive parameters	Measurement
Macrostructure (<10X) (a)macro crack (b)inclusion	(a) macro crack ①crack length l ②crack width d ③ metallograph (b) inclusion ①diameter d_{Xl} ②dispersion density ρ_{Xl}	Magnifying the sample to 5-10X with metallographic microscope or optical microscope. Observe and calculate surface characteristic parameters with low-magnification microscope and image processing technology

Table 3.3 gives microstructure characteristic parameters for quantitative characterization of surface integrity. Surface microstructural changes can be measured by metallographic optical microscopy, scanning electron microscopy (SEM) and transmission electron microscopy (TEM). It is worthy to be noted that the microstructure characteristics may not be present simultaneously in certain particular processing conditions. For example, it is impossible to quantitatively characterize built-up-edge (BUE) relevant characteristic parameters for electron-discharge-machined (EDM) surface, because there will be no built-up-edge (BUE) occurring during the EDM process; while it is unnecessary to care about intergranular-attack-related characteristic parameters for a mechanically-cut surface because

there is rarely intergranular attack occurring during non-chemical cutting [11].

Table 3.3 Descriptive parameters for microstructure characteristic

Characteristics	Specific descriptive parameters		Measurement
Microstructure (a)microcrack (b)plastic deformation (c)phase transformation (d)intergranular attack (e)pits, tears, laps protrusions (f)built-up edge (g)melted and redeposited layers (h)material-altered layer	(a) microcrack ① metallograph ②depth of microcrack h_{MC} ③width of microcrack d_{MC} (b)plastic deformation ①distorted thickness of grain d_{Tor} ②grain aspect ratio after distorted k ③metal streamline direction f ④dislocation density ρ_d (c)phase transformation ①volume fraction of phases φ ②TEM pictures (d)intergranular attack ①length of eroded grain boundary l_{EGB} ②depth of eroded grain boundary h_{EGB} (e)pits, tears, laps protrusions	①pit depth h_{Pi} ②surface area of pit s_{Pi} ③ tearing-off length l_T ④ tearing-off angle θ_T ⑤lap length l_L ⑥protrusion height h_{Pr} (f) built-up edge ①BUE angle θ_{BUE} ②BUE height h_{BUE} ②BUE area s_{BUE} (g)melted & redeposited layers ①melted grain diameter l_{Xd} ②area of redeposition s_{RD} ③height of redeposition h_{RD} (h)Material-altered layer ①thickness of MAL h_B ②deflection angle of grain θ_{GD}	Magnifying the metallograph to 500-1000X and observing various potential SI microstructure characteristics preparing TEM sample and finding dislocation and calculating dislocation density, estimating the composition of phase and its fraction proportion

Hardness is an important performance-related index/indication for assessing the abilities of material that resists plastic deformation or fracture damage. Hardness is not a simple physical quantity but an integrated indicator representing the material plasticity, strength, toughness and even other mechanical properties. For a freshly machined component, its surface or subsurface microhardness may vary due to factors such as surface humidity,

chemical changes and mechanical deformation happening during cutting. At the same time, the magnitude of surface microhardness will directly affect some mechanical properties of machined components, including friction and wear resistance, fatigue resistance and so on. Quantitative study of the effect of surface microhardness change could guide the parts machining processes and finally help to achieve the desirable surface integrity requirements. The microhardness of a machined surface could usually be tested by using a microhardness tester (such as an EverOne sclerometer). The basic procedure for microhardness (Vicker Hardness, HV) measurement could be as follows:

1) apply the normal load to the rectangular pyramid diamond indenter (cone angle of 136°) and press it into the surface to be measured;

2) calculate the sample's Vickers hardness HV_1 according to the indentation area left on the surface of the sample;

3) use inclined plane method or chemical etching method to measure the microhardness over the depth direction and underneath the surface of sample with a specific distance; repeat this step until reach to the depth of bulk material;

4) draw the distribution curve of microhardness with the increase of depth under the sample surface

Table 3.4 gives the typical characteristic parameters for microhardness. By measuring 4 key points as shown in Figure 3.3, it is possible to describe how the microhardness varies with the change of depth below the machined surface. The key points on the curve represent the SI characteristic parameters for microhardness.

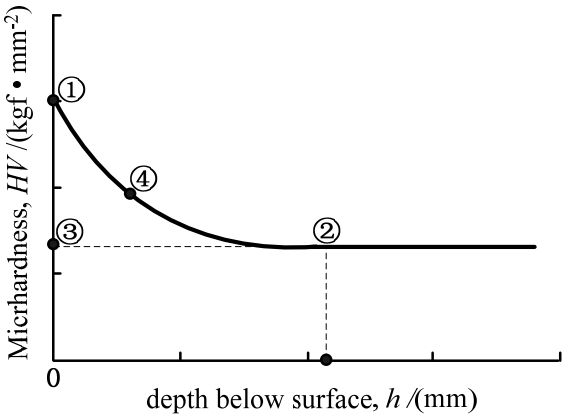

Figure 3.3 Variation of microhardness with the depth below surface

Table 3.4 Descriptive parameters for microhardness characteristics

Characteristics	Specific descriptive parameters	Measurement
Microhardness	① microhardness at surface HV_1 ② thickness of hardened layer h_{HV} ③microhardness of bulk material HV_0 ④distribution of microhardness *vs* depth (micro hardness profile) *HV-h*	Microhardness could be measured by applying Vicker indentation on the sectional area of metallurgical sample

Residual stress is the remaining effect of stress in the solid body of machined parts after removing all the external loading such as mechanical load, temperature change or thermal load caused by energy radiation. In addition to affecting the basic size and shape, the presence of residual stress will also have a direct impact on the fatigue performance of the machined parts. A typical distribution curve of surface residual stress varying with the depth below the surface is shown in Figure 3.4. By measuring the key points on the distribution curve, the basic properties of the produced surface residual stress are derived. The magnitude of surface residual stress in the depth direction is usually measured using an X-ray diffractometer combined with a chemical-etching peeling method, removing the material

from the machined surface layer-by-layer. The key points on the residual stress distribution curve are illustrated in Table 3. 5.

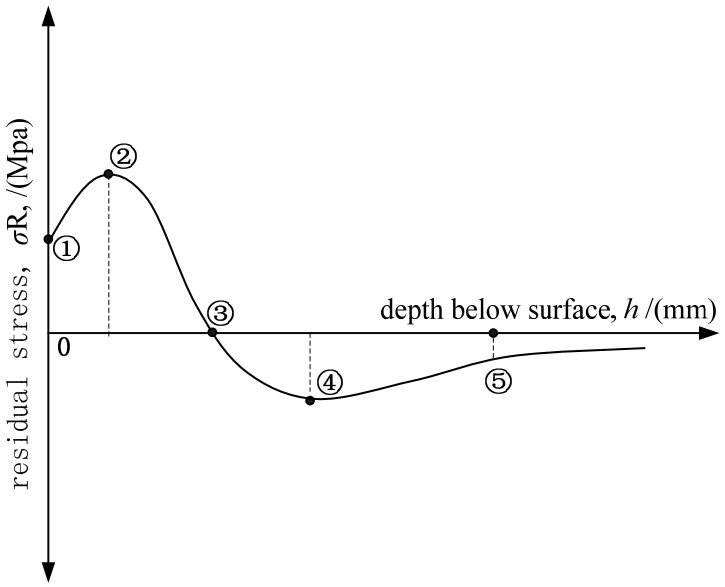

Figure 3.4 Variation of residual stress with the depth below the surface

Table 3.5 Quantitatively descriptive parameters for microhardness characteristics

Characteristic	Specific descriptive parameters		Measurement
residual stress (RS)	①surface RS	σ_{R0}	XRD and surface chemical etching peeling method are used to measure RS
	②peak tensile RS	σ_{TMax}	
	③depth of reverse RS	h_{r0}	
	④peak compressive RS	σ_{CMax}	
	⑤ thickness of RS layer	h_R	
	⑥distribution of RS vs depth (RS profile)	σ_R-h	

Unfortunately, the presence of surface residual stress generally goes unrecognized until a malfunction or failure occurs. The influence of surface residual stress on part's performance may be either beneficial or detrimental, depending upon its magnitude, pattern and distribution. Normally, compressive residual stress is beneficial to fatigue life, creep life and resistance to stress corrosion cracking, whereas tensile residual stress is usually detrimental to these same properties.

From Table 3.2 to Table 3.5, the most concerned and important surface integrity characteristic parameters are listed along with their commonly-used measurement methods, data formats and denotation. Although the proposed SI descriptive model does not cover all of the characterization parameters for each primary SI characteristic considering the actual measurement conditions and cost in practical production, it is believed that engineers could more easily and efficiently characterize, inspect and evaluate the surface integrity and performance by adopting a tabular-form, customized SI descriptive model for a specified machining process and material. It is also worthy to notice that in many situations of functional evaluation, the subsurface physical characteristics usually have a more profound effect on the final performance than that of surface geometrical features such as surface roughness.

3.3 Framework of SI Model and The Built-in Correlation

The concept of surface integrity actually contains not only related primary SI characteristics and corresponding characterization parameters, but also their correlations and mutual effects. These require the surface integrity model to be a complex system which involves many aspects and various factors interacting and influencing with each other. To fully and accurately establish the characterization and evaluation framework of a surface integrity model, many influencing factors which define and constitute a SI model system are categorized into different sets or classes according to their nature of functionality. These classes actually construct the characterization and evaluation framework/system of a surface integrity model from bottom to top and from local to global.

3.3.1 The Classification of SI Characteristics for Framework of SI Model

As aforementioned, the SI model is complicated and involves many influencing factors which even interact with each other. To establish an integrated and effective architecture for the description and evaluation of SI, qualitative classification and quantitative definition of these abstract factors, which finally construct the framework of SI model from the local to global and from the bottom up, are indispensable. The detailed classification and defined data sets are discussed as follows.

Assuming all of the SI characteristic parameters belong to a data set called *SI characteristic class* and denoted as *SIC,* then it could be expressed as

$$SIC=SIC\ (SIC_1,\ldots,\ SIC_j) \tag{3.1}$$

where SIC_j represents the jth characteristic of SI. Based on above-mentioned research and standard of the SI, j=1, …, 5 and $SIC_1,\ldots,\ SIC_5$ are representatives of surface roughness, macrostructure, microstructure, microhardness and surface residual stress respectively.

As one of the primary SI characteristics, surface roughness SIC_1 is represented and described by numerous 2D and 3D surface parameters such as average roughness R_a, peak-to-valley height roughness R_t, 10-ponit roughness R and so on. However, it is impossible to cover all of these 2D and 3D description parameters in a practical model. Thus, it is better to preferentially choose some of the parameters which are usually considered to have a direct effect on the final fatigue performance of parts or other kinds of application, so that:

$$SIC_1\ =\ SIC_1(R_1,\ldots,\ R_i) \tag{3.2}$$

where i=1, …, 17 and $R_{1,...,}\ R_{17}$ are the selected 2D and 3D surface roughnessparameters. They are sequently R_a, R_q, R_z, R_p, R_v, R_t, R_{sk}, R_{ku}, $R_{\Delta q}$, R_{Sm} for 2D description and S_q, S_z, S_p, S_v, S_{sk}, S_{ku}, S_{Sm} for 3D description [4].

If the correlation between different characteristic parameters is considered, then there would be a *SI characteristic domain* which is composed of two levels of content: one is the set containing all of the values of SI characteristic parameters belonging to the *SI characteristics class* which meet the specific requirement of fatigue performance; another is a set in which the networking and relationship among different characteristic parameters are included.

3.3.2 The Classification of SI Machining Processes for Framework of SI Model

Assuming the employed manufacturing process parameters for SI machining are all included in a set called *SI process conditions clas*s, *P,* then it could be expressed as:

$$P=P(P_1,\ldots,\ P_j) \tag{3.3}$$

in which P_j represents the j^{th} machining process condition adopted and j=1, …, n. For conventional cutting process schemes, $P_{1,...,}\ P_4$ stand for turning, milling, grounding and drilling respectively.

For each of the cutting process P_j, it also contains specific influencing factors such as the tool's type and geometry, cutting control parameters, coolant and lubricant and so on, all of which have a direct effect on the SI characteristics and fatigue performance of machined parts. Taking turning process as an example, then all the factors affected could be categorized and defined separately.

Assuming the tool's type and geometry for turning constitute a date set denoted by D, then:

$$D=D(D_1,\ldots,\ D_i) \tag{3.4}$$

where D_i represents the ith tool parameters. For turning, i=1, 2, …, 4 and D_1, …, D_4 represent tool geometrical parameters: tool's type, tool nose radius, tool rake angle, clearance angle respectively.

Assuming all of the cutting control parameters for turning constitute a data set denoted by C, then:

$$C=\ C(C_1,\ldots,\ C_i) \tag{3.5}$$

where C_i represents the change of ith cutting control parameters. For turning, usually i=1, 2, 3 and C_1, C_2, C_3 stands for the cutting speed v_c, feed rate f_z and cutting depth a_p respectively.

Assuming the cutting coolants and lubricating means for turning constitute a data set denoted as L, then

$$L=L\ (L_1,\ldots,\ L_i) \tag{3.6}$$

L_i indicates the ith specific methodemployed for cooling or lubrication. Usually, L_1,..., L_i stands for dry turning, oil fog cooling and lubrication, fluid nitrogen cooling, water cooling and lubrication, etc.

After all of the preparation for definition and classification, the *SI process conditions class* for turning process could be further expressed as

$$P_{\text{Turning}}=P\ \{P_1\ [D(D_1,\ldots,\ D_4),\ C(C_1,\ldots,\ C_3),\ L(L_1,\ldots,\ L_i)\ ]\ \} \tag{3.7}$$

Assuming there is a corresponding *SI process conditions domain*, then it would be composed of two parts: one is the set in which all of the processing conditions and cutting parameters belonging to the *SI process conditions class* and meeting final criterion of fatigue

performance; another is a set in which the correlation between different processing conditions and cutting parameters are included.

3.3.3 The Classification of SI Fatigue Performance for Framework of SI Model

Assuming the functionalities of the final machined parts constitute a data set called *SI functional performance class* and denoted as F, then

$$F=F\ (F_1,\ldots,\ F_i) \tag{3.8}$$

where F_i represents the ith fatigue property parameter. Generally, i=1, 2 and F_1, F_2 represent the fatigue limit of material and the corresponding number of stress cycle to fatigue failure.

The qualitative classification and digital definition of these abstract factors that affect the SI requirement of machined parts make the framework of the SI model be much clearer as shown in Figure 3.5. In this architecture, the *SI process conditions domain* is made up of the *SI process conditions class* and its correlations inside. *SI characteristic domain* is composed by the *SI characteristic class* and the correlation among the characteristics. The final SI model could be taken as a top element constituted by the *SI process conditions domain* and *SI characteristic domain* together with their accumulated database of processing parameters and evaluation standard based on SI characteristics.

After defining and classifying all of the abstract factors that affect the SI requirement of machined components, the image of the SI model is going to be clear as shown in Figure 3.5. In this architecture, the *SI Process Conditions Domain* is made up of the *SI process conditions class* and its internal correlation. The *SI Characteristic Domain* is composed of the *SI characteristic class* and the correlation among the characteristics. The final SI model

could be taken as a top constituted by the SI process conditions domain and *SI characteristic domain* together with their accumulated database of processing and evaluation system.

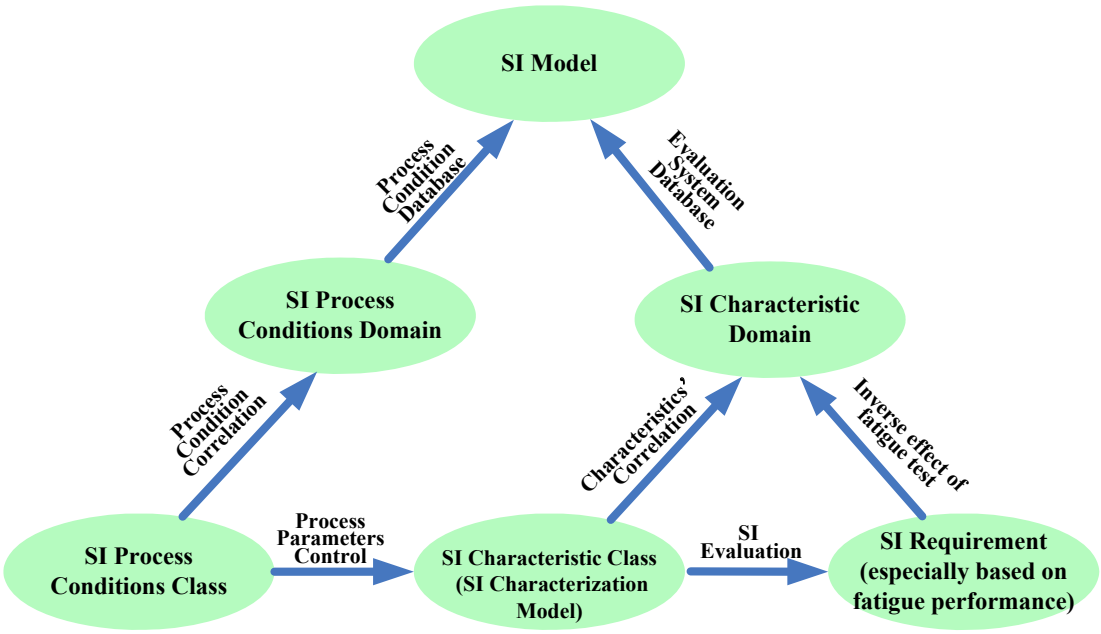

Figure 3.5 The framework of the SI model and its built-in correlation

Different manufacturing processes and corresponding machining parameters will produce different SI characteristics on the surface and within the subsurface of the machined parts. Obviously, the SI characteristics produced in a machining process will have a direct influence on its subsequent fatigue properties of the parts. According to Figure 3.5, reasonable control of process conditions and cutting parameters will result in high quality of SI and consequently better reliability and functional performance of the machined components. This is an especially important consideration for the machining of key aerospace components. This framework of the SI model offers a theoretical basis and some feasible approaches for the control of the surface integrity and functional performance of machined parts.

3.4 SUMMARY

The SI descriptive model which covers the primary SI characteristic parameters and the appropriate measurement selections is established based on the relevant surface integrity and functional performance requirement in practice, which also make the desired and accurate assessment of surface quality achievable. The surface integrity descriptive model not only digitally and quantitatively defines the primary SI characteristics, but also accurately describes and characterizes the surface geometrical feature and physical functionality. It is actually an integrated framework for the measuring, characterizing and assessing of surface integrity. In this model, surface and subsurface characteristics will interact with each other and finally determine the functionality of the machined surfaces or parts. The proposed framework of the surface integrity model enables a better understanding of interactions among the machining processes, surface integrity characteristic parameters and service performance, which will finally help to control and avoid detrimental influences on the machined surface.

In the following of the thesis, the significance of stress concentration factor (SCF) and its correlation with surface integrity characteristics and fatigue properties will be discussed in Chapter 4. The computational equation of SCF which is mainly caused by machining-induced micro geometrical topography and texture, the calculation of multiple stress concentration which considers both macro structural notch and micro surface irregularities, and the integrated estimating model for SI effective SCF which is featured by surface roughness, microhardness and residual stress, are proposed to evaluate the partial or

overall effect of SI characteristics on the SI and relating performance of machined parts. In Chapter 5, a typical difficult-to-machine material GH4169 superalloy is selected to investigate its grinding process influence on surface integrity. The effects of grinding wheels and processing parameters on each SI characteristic, such as surface roughness, macrostructure, microstructure, microhardness and residual stress, are individually analyzed. Finally in Chapter 6, the correlations between each grinding SI characteristics and its fatigue life (N_f) are experimentally investigated by rotary bending fatigue testing for the GH4169 specimens, which are ground with the selected grinding parameters range. The applicability and accuracy of the computational equations for micro geometrical caused SCF and the integrated effective SCF are demonstrated by comparing their results with those calculated from Arola's equation and validated by the measured fatigue life. Figure 3.6 gives a "roadmap" for the thesis arrangement and global thinking flow.

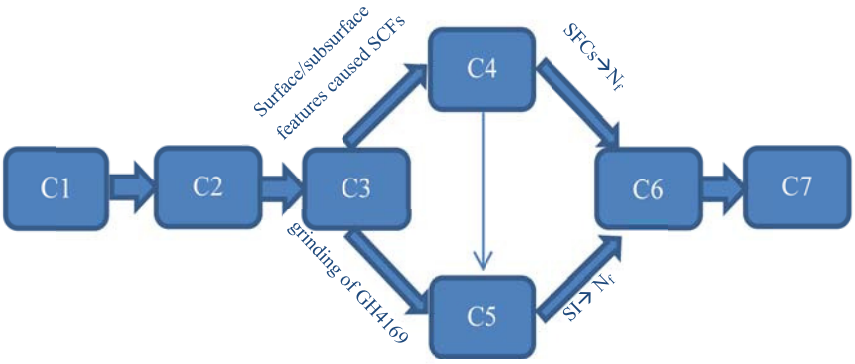

C1: (Chapter 1) Introduction to SI research; C2: (Chapter 2) Literature review of SI
C3: (Chapter 3) SI characteristics & models; C4: (Chapter 4) Stress concentration effect on SI
C5: (Chapter 5) Grinding effect on SI for GH4169
C6: (Chapter 6) Machining-induced SI effects on fatigue performance for GH4169
C7: (Chapter 7) Research contribution & future work

Figure 3.6 The "roadmap" for following chapters of this research

REFERENCES

[1] Bellows, G. and Tishler, D.N. Introduction to Surface Integrity, Pamphlet 1 in Series of 4, TM70-974, Aircraft Engine Group(AEG), GE Co., Cincinnati Ohio, October 1970

[2] Davim, J. P. Surface Integrity in Machining. London:Springer-Verlag, 2010

[3] Jawahir, I.S. et. al. Surface Integrity in Material Removal Processes: Recent advances. CIRP Annals-Manufacturing Technology, 2011, **60** (2), pp.603-626.

[4] Griffiths, B.J. Manufacturing Surface Technology-Surface Integrity and Functional Performance. London: Penton Press, 2001(ISBN 1-8571-8029-1).

[5] M'Saoubi, R. et. al. A Review of Surface Integrity in Machining and Its Impact on Functional Performance and Life of Machined Products. International Journal of Sustainable Manufacturing, 2008, **1**(1/2), pp.203-236.

[6] Field, M. and Kahles J.F. Review of Surface Integrity of Machined Components. CIRP Annals-Manufacturing Technology, 1971, **20**(2), pp.153-162.

[7] Field, M., Kahles J.F. and Cammett, J.T. A Review of Measuring Methods for Surface Integrity. CIRP Annals-Manufacturing Technology, 1972, **21**(2), pp.219-238.

[8] Field, M. Surface Integrity-A New Requirement for Improving Reliability of Aerospace Hardware. Proceedings of 18th Annual National SAMPE Symposium, April 3-5, 1973, Los Angeles, California, USA.

[9] Field M., Kahles J. F., Review of Surface Integrity of Machined Components, CIRP Annals-Manufacturing Technology, 1971, **20**(2): 153-162

[10] ANSI B211.1, American National Standards on Surface Integrity. Society of Manufacturing Engineers (SME),1986

[11] Metcut Research Associates, Machining Data Handbook (3rd Edition). Institute of Advanced Manufacturing Sciences, Inc., Cincinnati, USA.

CHAPTER 4 SURFACE TEXTURE AND ITS STRESS CONCENTRATION EFFECT ON SURFACE INTEGRITY

4.1 INTRODUCTION

Surface texture, sometimes also known as surface roughness or surface topography, has been considered as one of most important indexes for assessing the surface quality of machined parts. Surface roughness and its relevant parameters also belong to the five primary characteristics which are defined in SI descriptive model for comprehensive evaluation and assessment of surface integrity of machined parts. For a long time, surface roughness requirement (for example R_a) has always been taken as the most convenient and imperative means for quality control of machined parts in practical production. This is because the surface roughness parameters not only have been well defined in terms of uniform ISO standard and are equipped with relatively mature measurement devices, but also they could be used to conveniently reflect the effect of stress concentration caused by the variation of surface micro geometrical texture on surface properties, especially the fatigue performance of the machined parts. Existing standards for characterizing and measuring the surface topographical features of machined parts are mostly based on the 2D quantitative surface roughness parameters.

As is well known, a machined surface is not completely smooth even if it is machined by the most advanced ultra-precision machining methods. There is a variety of microscopic asperities and defects which actually constitute the real surface texture or topography on the

machined surface. All of these microscopic surface geometrical features, such as machined marks, lays, peaks and valleys, will directly affect contact bearing properties, interfacial friction and lubrication properties and the fatigue performance of the machined parts [1]. For some critical parts used in extreme applications, e.g. the key parts used in automobile or aero engines which need to withstand high temperature and alternating loads, the machining-induced surface marks, or micro grooves, are a kind of stress raisers and will reduce the fatigue strength of machined parts in service. Many previous researches have already shown that machined surfaces with larger values of surface arithmetic average roughness, R_a, normally have much severer stress concentration and the corresponding fatigue life of the parts is usually much shorter than those of a smoother machined surface [2-8]. However, some other researchers have found that the surface roughness parameters is not the only principal factor that affects the surface stress concentration and fatigue propertied of machined parts [9-11]. Obviously, there are other aspects strongly influencing the physical and mechanical properties of machined parts. Therefore, systematic analysis and study of stress concentration caused by micro-surface-topography and its effect on the eventual fatigue performance is imperative to the secure application of critical parts.

4.2 STRESS CONCENTRATION EVALUATION BASED ON SURFACE TEXTURE

4.2.1 Definition of Stress Concentration Factor (SCF)

During the machining process, the cross-sectional area of the machined part will vary

slightly with the moving of the cutting tool and the corresponding machining marks, such as micro notches or lays, will be finally left on the machined surface. If a machined part is in service and undertaking external loading, the local stress at the locations with macroscopic cross-section change or even microscopic notches, will increase abruptly. This factor is especially prominent for some high strength metals [9, 11]. The phenomenon that produces a higher working stress than the nominal stress due to the local geometrical size change is called stress concentration. Locations with geometrical size change or discontinuities, such as pre-designated macroscopic structural shoulders, holes or notches for specific parts, and machining-induced microscopic grooves for the machined surface, are also referred as to stress risers in structural stress analysis. Generally speaking, stress concentration may occur in any structure or machined parts and the surface stress risers are often the locations of the initiation of material damage or cracking. This damage will ultimately propagate to fracture failure under the practical load. For brittle materials, their static strength is slightly larger than the ratio of the maximum working stress to the value of stress concentration factor at the pre-designated notch where brittle fracture occurs. For ductile materials, the stress concentration has no effect on its static strength due to the plastic flow and the redistribution of stress inside the material. Considering that many materials used in the actual engineering structures are ductile and elastic-plastic, the effect of stress concentration weakening the static strength is normally not taken into account. However, if the external load applied is cyclic or alternating, the weakening effect of stress concentration on the fatigue properties of a machined part becomes very important. In practical application, the nominal stress value of

the alternating load applied on a machined part is usually less than the yield strength of the material and the global structure is in the elastic state on the whole. However, the material at the locations near the micro notches or grooves actually has already entered into a plastic state due to the presence of stress concentration which enormously increases the actual stress value at the stress raiser locations. At the same time, the fatigue strength of a machined part will mainly depend on its local stress-strain state at the weakest locations. Usually, the stress concentration raiser is the weakest link or the location undertaking the largest load, and it in fact determines the final fatigue life of a machined part [12-14]. Considering all of these factors, it is important to realize the ubiquity of stress concentration and is necessary to quantitatively analyze the overall and local stress behavior of critical parts, especially those for some extreme applications, such as the rotor blades or vanes used in aero-engine under high pressure, high temperature and even with chemical corrosion.

Stress concentration factor (SCF) is mathematically defined as the ratio of local maximum stress to the average or nominal stress, and is conventionally denoted by K [8, 12-14]. Usually, the extent of stress concentration at the locations with micro or macro notches could be expressed by using the theoretical stress concentration factor K_t or K_{ts} as follows:

$$K_t = \frac{\text{local max tensile stress } \sigma_{\max}}{\text{nominal stress } \sigma_{\text{nom}}} \quad \text{for tensile or bending} \qquad (4.1)$$

$$K_{ts} = \frac{\text{local max shear stress } \tau_{\max}}{\text{nominal shear stress } \tau_{\text{nom}}} \quad \text{for torsion} \qquad (4.2)$$

where the stress $\sigma_{\max}$ and $\tau_{\max}$ represent the maximum tensile and shear stresses at the local notches or grooves when the actual load is applied on the sample part; while σ_{nom} and τ_{nom} are

reference normal and shear stresses. It is noted that the theoretical stress concentration factor K_t is actually defined in terms of the practical condition of working stress. The value of K_t represents the ratio of the actual working stress at the specific location to the nominal stress and it is notable that it does not exactly mean the reduction extent of fatigue strength of a machined part. Although theoretical stress concentration factor K_t may have influence on the final fatigue property of the machined parts, it is insufficient to fully describe and calculate the degree of reduction on the fatigue strength due to stress concentration effect. Hence, the effective stress concentration factor K_f, also known as the fatigue strength reduction coefficient, is introduced. The effective stress concentration factor K_f is defined in terms of the fatigue strength of a machined part as follows:

$$K_f = \frac{S_e}{S_{notch}} \qquad \text{for tensile or bending} \tag{4.3}$$

$$K_{fs} = \frac{\tau_e}{\tau_{notch}} \qquad \text{for torsion shear} \tag{4.4}$$

in which S_e is the tensile fatigue strength of the smooth specimen without any obvious notches or geometrical discontinuity; S_{notch} is the tensile fatigue strength of the specimen with designed notches or geometrical discontinuity; τ_e is the shear fatigue strength of the smooth specimen without any obvious notches or geometrical discontinuity and τ_{notch} is the shear fatigue strength of the specimen with designed notches or geometrical discontinuity. These equations represent the degree of reduction of the fatigue strength of the machined part due to geometrical discontinuities no matter if it is caused by the pre-designed macro structural size change or by the machining-induced micro notches or surface texture.

In general, there is a greater difference between the theoretical stress concentration factor K_t and the effective stress concentration factor K_f, both in terms of their basic definitions or in the ways of acquisition. Theoretical stress concentration factor K_t is based on elasticity theory and was originally derived by the experimental measurement with the photo-elasticity method, or by using the finite element method. Theoretically speaking, it only depends on the surface geometry of the machined part and has nothing to do with materials or working conditions. That is why K_t is also known as the shape factor, which represents the increased times/folds of actual working stress at the locations with abrupt geometrical size change. The effective stress concentration factor K_f represents the reduced times/folds of fatigue strength which has been weakened under specific operating conditions such as torsion or bending load, high temperature or high strain rate and so on. K_f depends on many factors such as surface status, material metallurgy, internal defects, chemical composition, specimen size, load property and working environment as well as theoretical stress concentration factor K_t. Obviously, the most direct and reliable method that determines K_f is to carry out fatigue test for the machined specimens, but the costs of the fatigue test are quite high and it is sometimes impractical. Further, the experimentally-derived K_f is size-dependant and it could not be directly applied to a specimen of the same material but with different size or shape. Even if the size and shape for different materials specimen are the same, the actual K_f will be distinct because of diverse material sensitivity to the stress concentration effect. Considering all these limitations, it is more common in engineering practice to use an empirical equation method to firstly determine K_f, and then to estimate the fatigue strength or life based on K_f.

4.2.2 Stress Concentration Estimations Based on Micro Surface Geometry

It is now well accepted that the surface micro geometrical feature of a machined part will profoundly affect its fatigue performance especially for some hard-to-machine materials. Different kinds of stress concentration factors, which are dependent on the surface roughness parameters measured and acquired from the surface texture, are also proposed to assess the effects of micro surface topographical geometry and subsurface mechanical status on the fatigue properties. From the point view of surface integrity requirement and assessment, the fatigue properties of a machined part are actually influenced by the machining-induced surface integrity characteristics as well as by the fatigue limit of the material itself. In engineering practice, an appropriate correction coefficient, which could both take account of the effects of machining-induced surface geometrical texture and subsurface physic/mechanical properties, is employed to estimate the actual fatigue limit of the machined parts. As seen in Figure 2.2, standard surface roughness amplitude parameters (e.g. arithmetic average roughness R_a, maximum peak-to-valley height R_t and ten-point height R_z) could be used as correction coefficients to account for the effect caused by micro surface geometrical topography.

However, only using these surface roughness height parameters is insufficient to overall characterize and calculate the effect of surface texture features on the fatigue properties of the machined parts in some situations. For example, if two 2D surface profiles, a saw-tooth surface A and a semi-circle surface B, are of the same height amplitude as shown in Figure 4.1, then they will have the same values of the corresponding surface roughness height

parameters (such as R_a, R_t and R_z) in terms of the height their definitions. However, they have different root radius of profile valley, ρ. The saw-tooth surface A with smaller root radii of valleys (here ρ=0) obviously causes much severer stress concentration than does the semi-circle surface B (here ρ=c). Also, this geometrical difference may give the two machined surfaces different functional performance when they are undertaking load bearing or fatigue test.

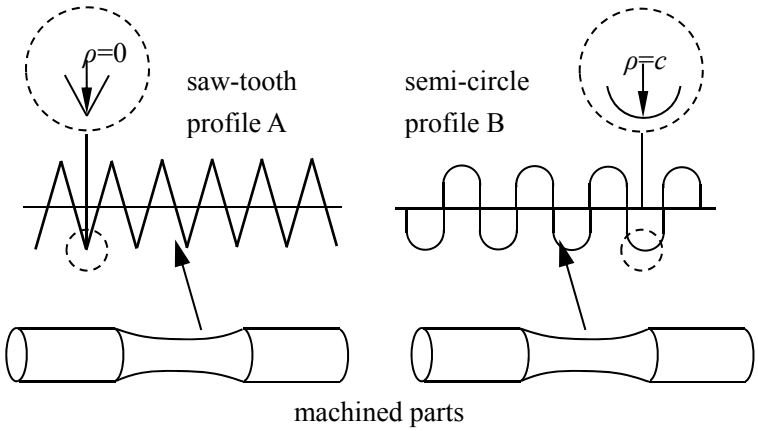

Figure 4.1 The saw-tooth and semi-circle surface profiles for machined parts

Although the standard surface roughness parameters provide a simple and convenient way for the quantitative characterization of some specific surface profiles, it is still not accurate enough to evaluate the degree of stress concentration and assess the consequent fatigue property of the machined surface by means of these height parameters only. In practical application, the effect of pre-designated macro geometrical discontinuities on the local stress state and fatigue property of a mechanical part could usually be represented based on the stress concentration factor such as K_t and K_f. Therefore, it is analogous and feasible to quantitatively estimate the influence of machining-induced micro surface texture on fatigue property of a machined part based on specialized surface micro stress concentration factors.

For an infinite rectangular plate with single shallow semi-elliptical notch subjected to axial tensile load as shown in Figure 4.2(a), its theoretical stress concentration factor at the local notch could be express as

$$K_t = 1 + 2\sqrt{\frac{t}{\rho}} \tag{4.5a}$$

in which t is the depth of the notch and ρ is the root radius of the notch [13-14].

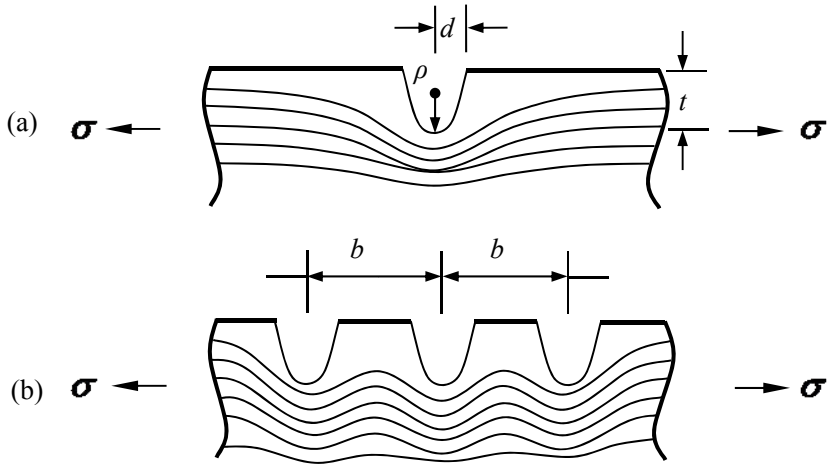

Figure 4.2 Stress concentration of an infinite plate with a single notch and multiple notches

If there are multiple semi-elliptical notches on this plate as shown in Figure 4.2(b), then all these successively neighboring notches will produce a comparatively weakened overall degree of stress concentration than the single notch does at the bottom of the notches. Hence, its theoretical stress concentration factor K_t for the infinite plate could be expressed as:

$$K_t = 1 + 2\sqrt{\lambda \cdot \frac{t}{\rho}} \tag{4.5b}$$

in which λ is the ratio of spacing to height of the surface irregularities or notches. As shown in Figure 4.2, $\lambda = b/t$.

As abovementioned, for a mechanically machined part, its machining-induced micro surface

geometrical texture is analogous with or could be compared to a miniaturized surface profile which is composed of a series of small successive notches as shown in Figure 4.2(b). Considering that the average height t of the micro notches from the machining-induced surface texture are hardly accurately measured in practice, Neuber proposed a semi-empirical equation for evaluating the micro surface stress concentration factor for the machined surface by using standard surface roughness height parameters [15]. The relationship between empirical stress concentration factor and surface geometrical parameters of the micro notches or grooves are expressed as follows:

$$K_{t,N} = 1 + n\sqrt{\lambda \frac{R_z}{\rho}} \tag{4.6}$$

in which R_z is the ten-point height of the machined surface; ρ is the root radius at the valley of the surface; λ refers to the ratio of spacing to the height of surface irregularities; n represents different load types or stress states: n=1 represents shear load, while n=2 represents tensile or bending load. This empirical equation could be analogously used to evaluate the extent of stress concentration caused by the micro surface topographical features produced in machining processes. However, it is still difficult to accurately determine the value of λ for a surface with random texture or topography. For a mechanically machined surfaces, λ=1 is suggested for a secure engineering calculation.

Arola studied the micro surface texture effect on the stress concentration and consequent fatigue strength for fibre-reinforced plastics (FRPs) composite and titanium alloy, and suggested an alternative equation for stress concentration factor evaluation [16-20]. Inspired by this equation, an empirical equation for equivalent stress concentration factor caused by

the micro surface texture (in terms of surface roughness parameters) is proposed. In order to mathematically establish the empirical equation for evaluation of the equivalent stress concentration factor, the machined surface is assumed to be an ideal sinusoidal curve as shown in Figure 4.3(a). Its amplitude is denoted by a and the wavelength is denoted by $2\pi \cdot l$. According to the knowledge of plane geometry, if the root radius of the notch at the valley of surface profile happens to be equal to the curvature radius of the dashed ellipse at the vertex of its major axis, the equivalent root radius of the notch could be calculated as $\bar{\rho} = \bar{d}^2 / a = \bar{d}^2 / \bar{t}$. As shown in Figure 4.3, $\bar{t}$ equals to the length of major axis of the ellipse, a; $\bar{d}$ is the equivalent half width of notch and equals to the length of minor axis of the ellipse. Substituting it into Eq. (4.5a), the theoretical stress concentration factor for the specific elliptical notch could be expressed as:

$$K_{st,\ nor} = 1 + 2\frac{\bar{t}}{\bar{d}} \quad \text{(for single notch)} \tag{4.7a}$$

Considering the different extent of stress concentration for the surface with multiple and successive micro notches, the nominal stress concentration factor of the ideal sinusoidal surface profile could be derived by substituting it into Eq. (4.5b):

$$K_{st,\ nor} = 1 + 2 \cdot \sqrt{\lambda \cdot \frac{\bar{t}}{\bar{\rho}}} = 1 + 2 \cdot \sqrt{\lambda} \cdot \frac{\bar{t}}{\bar{d}} \quad \text{(for multiple notches)} \tag{4.7b}$$

If this ideal sinusoidal surface profile is subjected to different types of stress loads (such as shear load and tensile load), then its equivalent notch height $\bar{t}$ can be assumed and expressed as na, in which n=1 means the ideal sinusoidal surface subjects to shear stress from torsion loads; n=2 represents the ideal sinusoidal surface subjects to normal stress from tensile or bending loads. The equivalent notch half width $\bar{d}$ could be approximately equal to the

length of semi-circular arc, $\pi \cdot \bar{\rho}$, which is inscribed to the bottom of the notch, as

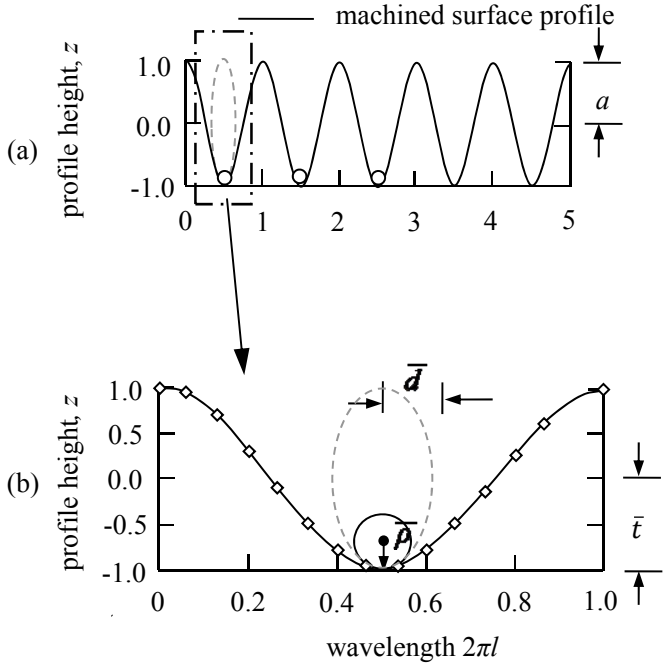

Figure 4.3 Ideal surface with sinusoidal profile and its inscribed ellipse

shown in Figure 4.3(b). Based on these assumptions and approximation, the micro surface stress concentration factor caused by the tiny valleys or notches can be expressed as:

$$K_{st} = 1 + 2\sqrt{\lambda \cdot \frac{na}{\bar{\rho}\pi}} \quad \text{(for micro valleys and notches)} \tag{4.8}$$

If a surface profile meets the sinusoidal function distribution of $z=a\cdot\cos(x/l)$ as shown in Figure 4.3(a), then its average roughness equals to $R_a = \frac{1}{L}\int_0^L |z|dx = 2a/\pi$. Therefore, Eq. (4.8) will reduce to:

$$K_{st} = 1 + n \cdot \sqrt{\lambda} \cdot \frac{R_a}{\bar{\rho}} \tag{4.9a}$$

Eq.(4.9a) is suitable for evaluating the micro geometrical texture caused stress concentration factor for a surface which is overall parallel to the profile mean line within its evaluation

length. To estimate the SCF for a random surface geometrical texture, a correction coefficient needs to be introduced to ensure that both surface roughness and waviness information are all included. For the situation that the surface contains superimposed roughness on the waviness, the ratio of max peak-to-valley height R_t to ten-point height roughness R_z is introduced to rectify the corresponding evaluation of the micro geometrically caused SCF. For an ideal sinusoidal surface profile, the ratio of R_t/R_z is equal to 1 as shown in Figure 4.3(a). Similarly, for the surface profile of a periodic waveform, e.g. a triangular wave or a square wave, R_t/R_z will also approximate to 1 if there is no large waviness over the measurement length. However, for the surface profiles of large waviness and roughness as shown in Figure 2.2, R_t and R_z values will deviate with each other and the ratio of R_t/R_z will precisely reflect this surface amplitude variation along the height direction. Therefore, the theoretical stress concentration factor K_{st} caused by machining-induced micro surface texture change can be expressed with standard surface roughness parameters as:

$$K_{st} = 1 + n \cdot \sqrt{\lambda} \cdot (\frac{R_a}{\bar{\rho}})(\frac{R_t}{R_z}) \tag{4.9b}$$

Accordingly, the K_{st} caused by the machining-induced micro surface texture could also be further deduced based on Eq.(4.8) and it is obviously sensitive and largely dependent on the values of machining-induced surface roughness parameters. Compared to the regular shapes, the average spacing parameter R_{Sm} of the surface texture could be approximately equivalent to the micro notch width b for the machining-induced random surface texture; the ten-point height parameter R_z of surface texture is approximately equivalent to the notch height t of the machining-induced random surface topographical feature. Thus, the ratio $\lambda=b/t$ approximates

to the value of R_{Sm}/R_z, that is $\lambda=b/t \approx R_{Sm}/R_z$. Substituting it into Eq. (4.9), the theoretical stress concentration factor for the machining-induced random surface texture, K_{st}, can be expressed as

$$K_{st} = 1 + A_K \cdot (\frac{R_a}{\overline{\rho}})(\frac{R_t}{R_z}) \approx 1 + n \cdot (\frac{R_{Sm}}{R_z})^{0.5} (\frac{R_a}{\overline{\rho}})(\frac{R_t}{R_z}) \tag{4.10}$$

$\overline{\rho}$ is the equivalent root radius of valleys and represents the average value of root radii measured from several prominent profile valleys; R_{Sm} is the average spacing of the micro surface asperities or peaks. Assuming $A_K = n \cdot \sqrt{\lambda}$, it actually has already considered the effect of load types on surface stress concentration. It is noted that the surface stress concentration factor calculated from Eq.(4.10) totally includes the average spacing of the micro asperities R_{Sm}, equivalent root radius of valleys $\overline{\rho}$, arithmetic average roughness parameters R_a, ten-point height parameter R_z, and max peak-valley height parameters R_t. It actually means that the effect of surface geometrical topography, both in the horizontal direction and the height direction, are counted in the evaluation of micro surface stress concentration factor. It is also worthy to mention that all of the needed surface roughness parameters can be conveniently obtained by using white light interferometry (WLI) and it will definitely facilitate the evaluation of the stress concentration factor in industrial practice. In view of different materials and geometries having a distinct degree/extent of sensitivity to stress concentration and fatigue strength, the effective fatigue stress concentration factor K_{EF_NS} could be estimated by using theoretical stress concentration factor K_t and notch sensitivity coefficient q as follow:

$$K_{EF\_NS} = 1 + q(K_{st} - 1) \tag{4.11}$$

in which q represents the severity extent of stress concentration and $0<q<1$. It is related to material properties as well as notch geometry:

$$q = \frac{1}{(1+\alpha/\overline{\rho})} \tag{4.12}$$

in which α is a material constant. Normally, for Al alloy, α = 0.51mm; for steel, α could be approximated in terms of ultimate tensile strength σ_b as follow: [7, 9]

$$\alpha = 0.025 \left(\frac{2070 \quad \text{Mpa}}{\sigma_b} \right)^{1.8} \tag{4.13}$$

Further, material constant α could also be attained by using the chart below proposed by Peterson [8, 13-14]

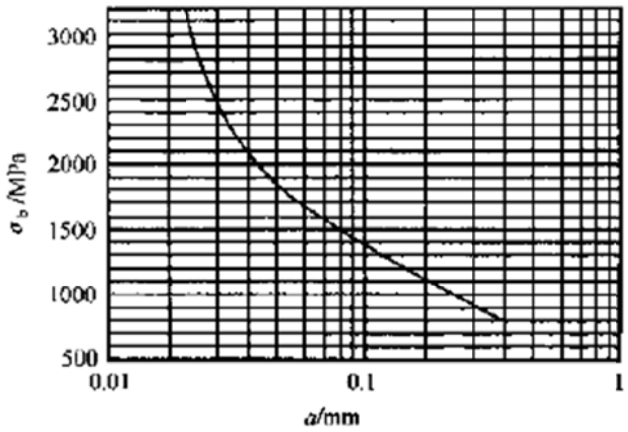

Figure 4.4 Empirical relationship between material constant α and tensile strength σ_b

Although the value calculated by Eq.(4.11) is considered to be conservative to some extent, it is widely accepted and used in practice because of its conciseness and effectiveness. It is notable that material property is one of the key factors that affect the value of the effective fatigue stress concentration factor K_{EF_NS}. If the material is ductile, the value of q will be small and the K_{EF_NS} will be far lower than the K_{st}, which means this kind of material is insensitive to stress concentration caused by micro surface geometrical texture. For some

materials which are brittle or of high-strength, the value of q is large and K_{EF_NS} approaches K_{st}, which means this kind of material is sensitive to stress concentration by micro surface geometrical texture. Normally, for a material of good plasticity and ductility, the value of K_{EF_NS} is from 1.05 to 1.3; for steels and superalloys, their values of notch sensitivity coefficient q are normally higher because these kinds of materials are more sensitive to the stress concentration, and their effective fatigue stress concentration factor K_{EF_NS} is consequently larger than that of materials of good ductility [8].

When it comes to assessment of surface integrity and relating performance of precision-machined parts, the stress concentration caused by surface micro texture will have a profound influence on the ultimate fatigue property for notch-sensitive materials. Good control of the machining parameters and conditions could effectively reduce the effect of the surface stress concentration factor on fatigue property of the machined parts.

4.2.3 Measurement of Surface Micro Geometry and Evaluation of Corresponding Stress Concentration

4.2.3.1 Measurement of the effect of equivalent root radius on surface texture

Reasonable and precise measurement of machining-induced micro geometrical features, which could help to accurately estimate the real stress concentration factor, is extremely important for the evaluation of surface integrity and fatigue performance.

For a surface profile which is expressed by a continuum function $z=f(x)$, its curvature radius at the lowest valley is the inverse of the curvature K_{curve}

$$\rho = 1/K_{curve} = (1+z'^2)^{3/2}/|z''| \tag{4.14}$$

in which z' and z'' are the first-order and the second-order derivative at the valley of surface profile. Thus, for an ideal sinusoidal surface profile $z=a\cdot\cos(x/l)$ as shown in Figure 4.3, its equivalent root radius at the valley is:

$$\rho_{val} = 1/K_{val} = (1+z'^2_{val})^{3/2}/|z''_{val}| = 1/|z''_{val}| = l^2/a \tag{4.15}$$

in which $z'|_{val} = 0$.

For a machined surface with random micro geometrical features, the equivalent root radius $\overline{\rho}$ of this surface is defined as the average of the root radii for the three deepest valleys, that is, $\overline{\rho} = (\rho_1 + \rho_2 + \rho_3)/3$.

The equivalent root radius of valleys could be measured and calculated by using optical interferometry Veeco NT1100. Firstly, the 3D surface texture was measured as shown in

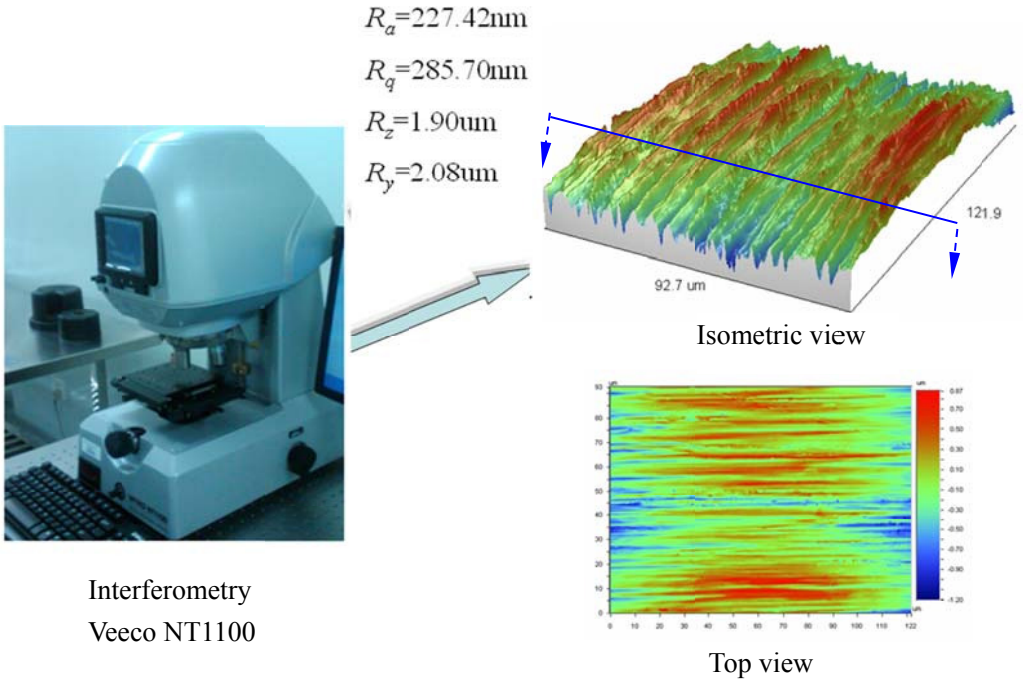

(a) Optical interferometry and the measured 3D surface texture of a ground part

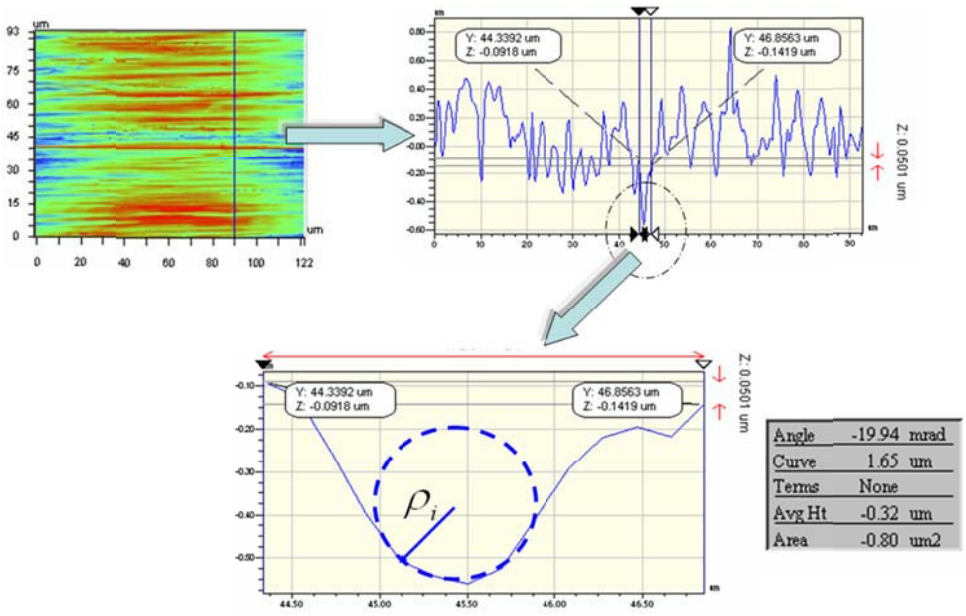

(b) Measurement of the root radius of a valley on surface profile

Figure 4.5 The measuring process of the root radius of a valley on the surface

Figure 4.5(a). Then, certain a cross-section vertical to the grinding marks is extracted from the 3D surface texture and the corresponding 2D surface profile is derived as shown in Figure 4.5(b). The root radii of the 3 lowest valleys are measured separately from different scanning areas. Finally, the equivalent root radius of this surface profile is calculated using the average of the 3 measured root radii.

4.2.3.2 Evaluation of SCFs based on orthogonally-designed external-grinding experiment

In order to validate the feasibility of the proposed empirical equation for evaluating stress concentration factor, the surface texture characteristics for an array of orthogonally-designed externally-ground GH4169 specimens are machined and measured (refers to Chapter 5 for detailed experimental design and arrangement). Their surface roughness parameters, such as R_a, R_t, R_z, R_{Sm} and $\overline{\rho}$, are also acquired. The detailed measuring specifications for the Veeco

NT1100 are as follows: measuring domain 736×480, sampling interval 165.2μm, cut-off frequency 0.8mm.

According to Eqs. (4.10) and (4.11), the stress concentration factor K_{st} which is caused by machining-induced micro surface texture and the effective fatigue stress concentration factor K_{EF_NS} which also considers the effect of material sensitivity, are calculated based on the measured surface roughness parameters for this series of ground specimens. These results are compared with those calculated by the empirical equation proposed by Arola [16]. The final results are as shown in Table 4.1. By taking into account the material property, the values of effective fatigue stress concentration factor K_{EF_NS} are lower than those of the stress concentration factor K_{st} caused by machining-induced micro surface texture. The relative errors for the estimated K_{st} compared with the K_t from the Arola empirical equation are all smaller than 11.74%.

Table 4.1 The orthogonally-designed external-grinding experiment and the SCFs evaluation for the ground GH4169 cylindrical specimens

	Grinding parameters			**Surface geometrical characteristic parameters measurement**									**SCFs evaluation**			
Sample No.	v_w (m/min)	a_p (mm)	v_s (m/s)	R_a (μm)	R_q (μm)	R_z (μm)	R_t (μm)	R_{Sm} (μm)	ρ_1 (μm)	ρ_2 (μm)	ρ_3 (μm)	$\overline{\rho}$ (μm)	K_t (Arola)	K_{st}	e_1 (%)	K_{EF_NS}*
CG1	8	0.005	15	0.2589	0.259	2.13	2.4	2.535	1.34	1.73	1.78	1.617	1.372	1.394	1.57	1.383
CG2	8	0.01	20	0.2977	0.298	2.54	2.94	3.091	1.53	1.26	1.33	1.373	1.455	1.554	6.77	1.536
CG3	8	0.015	25	0.2214	0.260	2.3	2.55	2.812	2.08	2.4	2.37	2.283	1.293	1.238	4.30	1.233
CG4	8	0.02	30	0.3132	0.299	2.87	3.35	2.996	2.49	1.92	1.26	1.890	1.277	1.395	9.29	1.386
CG5	12	0.005	20	0.2103	0.210	1.77	1.9	2.911	1.43	1.74	1.56	1.577	1.211	1.367	12.9	1.357
CG6	12	0.01	15	0.2601	0.268	2.14	2.35	2.761	1.7	1.62	4.91	2.743	1.209	1.236	2.28	1.233
CG7	12	0.015	30	0.3191	0.289	2.54	2.71	3.022	1.65	1.26	1.71	1.540	1.409	1.482	5.22	1.469
CG8	12	0.02	25	0.2345	0.2423	2.35	2.73	3.131	1.7	1.53	2.59	1.940	1.222	1.324	8.40	1.317
CG9	16	0.005	25	0.2546	0.268	2.04	2.2	3.121	1.42	1.93	1.28	1.543	1.289	1.440	11.69	1.428
CG10	16	0.01	30	0.2372	0.232	2.03	2.21	3.181	1.58	1.78	2.59	1.983	1.187	1.326	11.74	1.319
CG11	16	0.015	15	0.2165	0.293	2.01	2.2	3.299	1.43	1.26	1.75	1.480	1.288	1.410	9.45	1.398
CG12	16	0.02	20	0.2195	0.296	2.1	2.32	3.235	1.86	2.05	3.89	2.60	1.168	1.231	5.41	1.228
CG13	22	0.005	30	0.2349	0.247	2.19	2.32	3.126	3.98	1.7	2.1	2.593	1.146	1.229	7.24	1.225
CG14	22	0.01	25	0.2204	0.285	1.99	2.06	2.868	1.36	1.77	1.3	1.477	1.296	1.371	5.8	1.360
CG15	22	0.015	20	0.2400	0.257	2.04	2.21	2.04	2.21	2.47	1.83	2.170	1.218	1.277	4.91	1.272
CG16	22	0.02	15	0.2576	0.324	2.07	2.2	2.07	2.2	2.08	1.96	2.08	1.237	1.297	4.83	1.291

*Material constant α for GH4169 is calculated in terms of Eq. (4.17) and α=0.0446mm. The ultimate tensile strength for GH4169 is about 1500Mpa.

4.3 STRESS CONCENTRATION EFFECT BASED ON SURFACE AND SUBSURFACE CHARACTERISTICS

Section 4.2 discussed the establishment of evaluation of stress concentration factors based on surface geometrical topography or texture. These SCFs mainly depend on the surface roughness parameters and the equivalent root radius of the valleys which are derived from surface micro geometrical measurement. Therefore, the evaluation of these SCFs principally reflects the effect of surface micro geometrical features on practical fatigue properties. During the machining processes, in addition to the micro surface geometrical features/texture produced on the surface, there are also accompanying phenomena such as material work hardening, microstructure transformation and residual stress change happened within the subsurface layer of material. These factors will also affect the ultimate fatigue strength of machined parts just as does surface roughness. An integrated model, which considers the effects of primary surface integrity characteristics (including surface roughness, microhardness and residual stress) on the stress concentration and consequent fatigue performance of machined parts, is becoming essential for the design and prediction of the fatigue properties of the key parts used in the fields of automotive, aircraft and aerospace industry.

For some widely-used aero-engine materials such as titanium alloys or superalloys, the influencing weight factors of the surface roughness, surface microhardness and residual stress on the stress concentration and resultant fatigue strength could be empirically determined according to collecting and analysing a large number of existing experimental

data. For example, in a high temperature environment, each characteristic of surface integrity for a ground part will have a different influencing weight on the fatigue strength of superalloys. The extents of the reduction of the fatigue strength for superalloys caused by surface roughness, surface hardening and surface residual stress are separately given as shown in Figure 4.6, under the working conditions: loading frequency 5000Hz, working environment temperature 800~900°C and stress cycle 10^6~10^8 [21-23]. It is shown that the extents of influence from surface roughness, surface hardening and residual stress account for around 50%, 40%~45% and 5%~10% respectively. Some researchers have indicated that, if the surface roughness R_a of the machined parts could be kept in the range of 0.16μm ~ 5μm, then the above-mentioned influencing weight factors will remain stable in most of situations, no matter how the physical or mechanical statuses change within the ground surface and subsurface [21-23]. However, it should be noted that this kind of proportional relationship is obtained experimentally and empirically from some types of materials under specific testing environments. For many materials, most of the machining-induced residual stress will be released and the microhardness of surface layer will also correspondingly decrease when the working environment temperature is high (e.g. above 800°C). In this situation, the effect of surface roughness on the actual stress concentration and resultant fatigue performance will dominate and take a main role. If the fatigue testing is carried out at room temperature, the extent of the effect from the residual stress and work-hardening layer on the fatigue strength will be higher than those for the high temperature situation as shown in Figure 4.6 [21-23]..

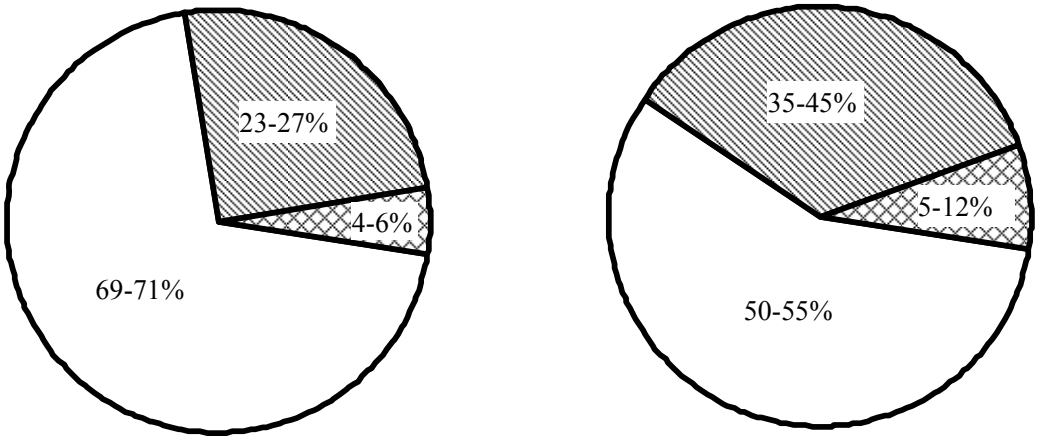

(a) low/medium-cycle (<10^6) (b) high-cycle (10^8)

Figure 4.6 The influencing proportions of surface integrity characteristics on fatigue strength degradation for ground superalloy part above 800°C)
(surface roughness: blank; surface hardening: shade line; residual stress: crosshatch)

As is well known, it is insufficient to determine the fatigue performance of a superalloy only according to a certain surface integrity characteristic. The characteristic parameters from surface micro geometry and subsurface material alterations should be considered as a whole. This means the surface integrity characteristics, such as surface roughness, surface microhardness and residual stress, will act together and contribute a combined effect on the actual stress concentration and the fatigue strength of parts. For convenience in engineering practice, it is assumed that each surface integrity characteristics will have a linear superposition effect on the ultimate fatigue strength of machined parts. Combined with the experimental data shown in Figure 4.6, an integrated equivalent fatigue stress concentration factor, K_{IEF}, which comprehensively considers the effect of surface geometric texture and subsurface material alterations for a machined part suffering fatigue alternating load, is proposed and represented as follows:

$$K_{IEF} = \beta_1 \cdot K_{st} + \beta_2 \cdot K_{HV} + \beta_3 \cdot K_{\sigma R} \tag{4.16}$$

in which K_{st} is the stress concentration factor caused by the machining-induced surface geometrical texture variation; K_{HV} is the stress concentration factor caused by the surface microhardness variation; $K_{\sigma R}$ is the stress concentration factor caused by the surface residual stress variation; β_1, β_2 and β_3 are corresponding weight coefficients. For low or medium-cycle fatigue testing (e.g. $N_f <= 10^6$) with high temperature, it is suggested that β_1=0.7, β_2=0.25, β_3=0.05; while for the high-cycle fatigue testing (e.g. $N_f >= 10^8$) with high temperature, it is suggested that β_1=0.5, β_2=0.4, β_3=0.1 [21-23].

For the stress concentration factor caused by cyclic or work hardening, Reference [24] suggested K_{HV} could be expressed as follows:

$$K_{HV} = K_{st}^{\frac{1}{1+n_H}} \quad \text{(for materials of high notch sensitivity)} \tag{4.17}$$

$$\text{or} \quad K_{HV} = K_{st}^{\frac{2}{3+n_H}} \quad \text{(for materials of low notch sensitivity)} \tag{4.18}$$

Eqs. (4.17) and (4.18) reflect the extent of equivalent stress concentration caused by cyclic work hardening along with micro-geometrical texture. n_H is the cyclic hardening exponent and $n_H = 1 - \sqrt{\sigma_s / \sigma_b}$.

For the stress concentration effect caused by surface residual stress, $K_{\sigma R}$ is proposed as:

$$K_{\sigma R} = \frac{\sigma_{R0}}{\sigma_s} \cdot K_{st} \tag{4.19}$$

in which σ_{R0} is the measured value of surface residual stress, σ_s is the yield limit of the material. If the surface residual stress σ_{R0} is tensile stress and larger than the ultimate tensile strength σ_b of the material, the excessive tensile stress will cause the surface of the part to produce a crack and results in an abrupt drop of fatigue strength. If the surface residual stress σ_{R0} is tensile stress and $\sigma_s < \sigma_{R0} < \sigma_b$, the tensile stress will cause the material near to the local

surface to yield and lower the actual fatigue strength. If the surface residual stress σ_{R0} is tensile and $0<\sigma_{R0}<\sigma_s$, the residual stress will overlap with the applied alternating load and make the nominal fatigue strength reduced and the extent of stress concentration increased. If the surface residual stress σ_{R0} is compressive and $\sigma_{R0}<0$, the compressive stress will in fact counteract a partial effect of the applied alternating load and make the nominal fatigue strength improved and the actual effective stress concentration factor to further decrease.

4.4 MULTIPLE STRESS CONCENTRATION EFFECT

For a part or specimen that does not contain a pre-designated macro notch, its theoretical stress concentration K_{st} caused by the micro surface texture characteristics (such as machined marks, lays or roughness) is usually slightly greater than 1. For a part or specimen with macro structural size change, such as a fatigue testing sample with pre-designated geometrical notches, its stress concentration caused by the macro structural notches is usually an integer and larger than 1, e.g. K_{t1} =2, 3, or 5. If the fatigue performance of a specimen with macro notches is to be accurately assessed, the stress concentration caused by the macro notches and the superposed micro surface texture both need to be taken into account. When there are two or more stress raisers within the structural parts, they actually constitute a problem called multiple stress concentration.

In engineering practice, multiple stress concentration is quite common considering the geometric complexity of the machine parts or structures. For an infinite plane with a central circular hole and subjected to uniaxial tensile load, as shown in Figure 4.7, if there is also a small notch on the edge of the circular hole, then it forms a situation of multiple stress

concentration. Due to the presence of the small notch, the SCF at the local point A will be higher than that when it only has a central hole. These two different stress raisers will actually influence each other and generate a new stress distribution state.

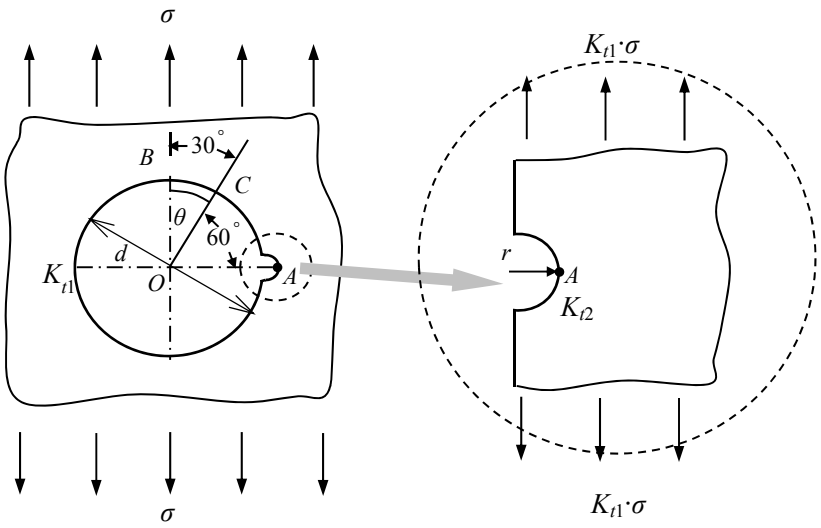

Figure 4.7 Multiple stress concentration when a small notch overlapped on a central hole

If the SCF of the infinite plate with a central hole is assumed to be K_{t1} and if the SCF of a plate with a smaller semi-circular notch on its edge is assumed to be K_{t2}, there is normally no general rule that could define the relationship between K_{t1} and K_{t2}. However, for some simple loading situations with regular-shaped notches in engineering applications, finding an approximate solution to multiple stress concentration is possible. For example, for the situation when the geometrical size of one stress raiser is far smaller than another (as shown in Figure 4.7, $d/2 >> r$, and r is the radius of curvature of the small semi-circular notch), then it can be considered that the tiny notch won't affect the global stress distribution of the infinite plane with a circular hole but only contribute its stress concentration to the local stress field near the notch itself. According to the geometric stress concentration theory proposed by Peterson [13-14], the SFC for the infinitely plate with a central hole is K_{t1}=3.0;

while the SFC for a semi-circular notch is K_{t2} = 3.06. Considering that small semi-circular notch will not strongly affect the global stress field distribution caused by the large central hole but only contribute at the local position near the notch area, the stress status near the location of the central hole can be hence taken as a tensile plate subjected to stress loading of $K_{t1}\cdot\sigma$. Therefore, the peak stress of the small semi-circular notch at the point A could be expressed to be $K_{t2}\cdot(K_{t1}\cdot\sigma)$. Finally, the stress concentration factor at A is equal to the product of K_{t2} and K_{t1}, i.e. $K_{t12}|_A = K_{t2}\cdot K_{t1}$ = 9.18, for tensile loading.

If the small semi-circular notch moves from A to B, the value of double stress concentration factor for this structure element will be different. According to the geometric stress concentration theory proposed by Peterson [13-14], the single theoretical stress concentration factor at point B caused by the central hole under this loading situation is -1.0; and the overall stress concentration factor at point B caused by both the central hole and the small semi-circular notch is $K_{t12}|_B = K_{t2}\cdot K_{t1}$ = -1.0×3.06 = -3.06.

If the small semi-circular notch moves from point A to point C (the angle from point C to the direction of external load is θ = 30°), then the stress concentration aroused from the central hole structure under this kind of loading situation is 0. Consequently, the overall stress concentration factor for point C is $K_{t12}|_C = K_{t2}\cdot K_{t1}$= 0×3.06 = 0. Thus, once the loading mode is determined, the small notches at different positions of the central hole will produce distinct degrees of stress concentration [13-14]. For the infinite plate with a central hole subjected to uniaxial tensile or bending load, if there is a small semi-circular notch overlapped on the circumference with an inclined angle θ to the direction of the external load, then the stress

concentration factor at that point can be expressed as:

$$K_{t12}(\theta)=K_{t2}\cdot K_{t1}=K_{t2}\cdot[1-2\cdot\cos(2\theta)] \tag{4.20}$$

in which $K_{t1}=[1-2\cdot\cos(2\theta)]$ is the stress concentration factor for a point located on the circumference of a central hole with an angle θ away from the direction of external load.

If the geometrical size of the small semi-circular notch is downsized to the order of magnitude of the micro surface texture height, and it is assumed to be substituted by a surface profile of micro asperities and with its deepest valley at point A, as shown in Figure 4.8, then the overall stress concentration factor at point A can be expressed as:

$$K_{t12}|_{A}=K_{t2}\cdot K_{t1}=K_{st}\cdot[1-2\cdot\cos(2\times90°)]=3K_{st} \tag{4.21}$$

in which K_{st} is the stress concentration factor that is mainly caused by the machining-induced surface texture.

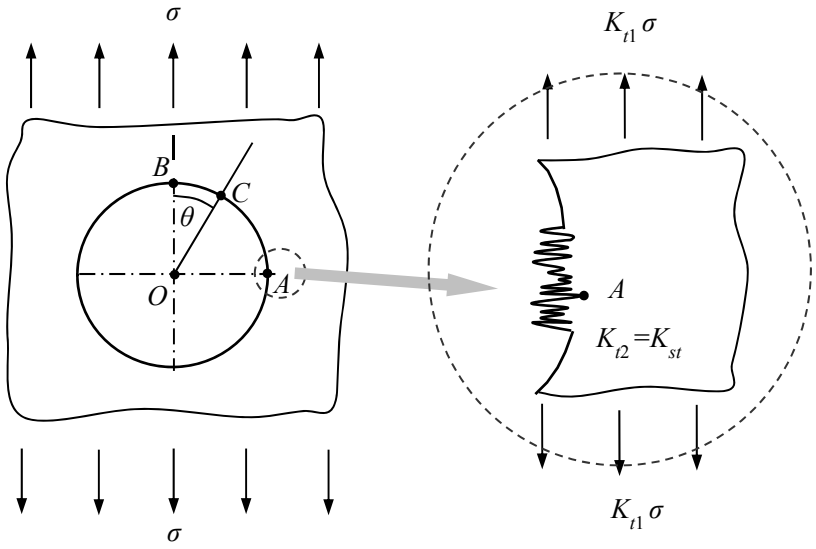

Figure 4.8 Multiple stress concentration when micro texture overlapped on a macro hole

If a plate (or a rod) with a regular macroscopic-sized fatigue notch, such as a U-notch or V-notch, and if the angle between the direction of machining-induced lays/texture and the

direction of the fatigue load is φ (as shown in Figure 4.9 below), then the overall maximum stress concentration factor for this part at its most dangerous position A is expressed as

$$K_{tMG} = K_{t2} \cdot K_{t1} = K_{st} \cdot K_{t1} = [1 + A_K \cdot (\frac{R_a}{\overline{\rho}})(\frac{R_t}{R_z})] \cdot K_{t1}$$
$$\approx [1 + n \cdot (\frac{R_{Sm}}{R_z})^{0.5} (\frac{R_a}{\overline{\rho}})(\frac{R_t}{R_z})] \cdot K_{t1} \quad (4.22)$$

Eq. (4.22) gives a method to estimate the overall SCF for a structure of a macro notch on which the machining-induced surface texture is overlapped. n is a coefficient which counts in the effect of load type and direction.

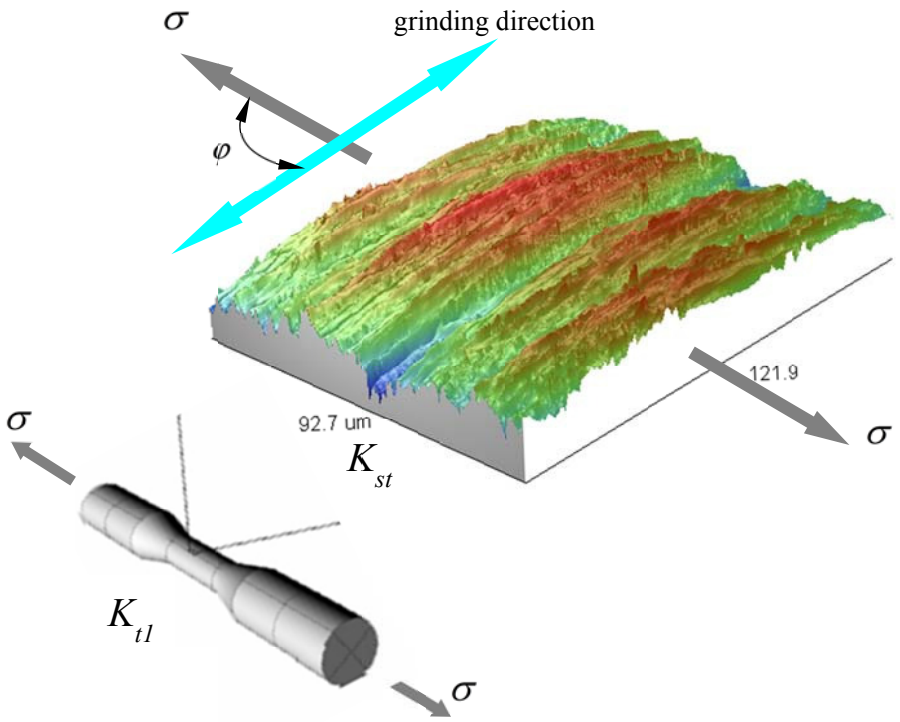

Figure 4.9 Multiple stress concentration situation for the grinding-induced micro surface texture overlapped on the macro geometrical structure of a fatigue testing specimen

As shown in Figure 4.9, if the angle between the load direction and the machining-induced

lays or texture is φ, then it could be assumed that n=1+sin(φ); When the load direction is perpendicular to the direction of machining-induced lays or texture (i.e. φ=90°), then n=2 and it will bring the most dangerous situation for this structure with the max value of SCF.

Finally, a comprehensive empirical model for evaluating the SCFs of a ground part subjected to uniaxial fatigue loading is proposed and presented in Table 4.2, which considers the effects from the machining-induced surface texture, work hardening and residual stresses on the surface and within subsurface layer, as well as the effect from the abrupt change of macro structural size of the machined parts.

Table 4.2 The SCFs models for machined parts under various conditions

<table>
<tr><td></td><td colspan="2">Effective SCFs evaluation for machined fatigue specimen (considering the effect of macro notches and overlapped micro surface texture, K_{t1} >1)</td></tr>
<tr><td></td><td>Empirical evaluation model</td><td>Remarks</td></tr>
<tr><td>(1)

SCF caused by machining -induced micro surface texture (and pre-designated macro structure)</td><td>(a) Surface theoretical SCF caused by machining-induced micro surface texture
$$K_{st} = 1 + A_K(\frac{R_a}{\overline{\rho}})(\frac{R_t}{R_z})$$
in which $A_K = n\sqrt{\lambda}$.
(b) SFC considering material sensitivity
$$K_{EF\_NS} = 1 + q \cdot (K_{st} - 1) = 1 + \frac{K_{st} - 1}{1 + \alpha/\overline{\rho}}$$
(c) Multiple SCF caused by machining-induced micro surface texture overlapped on a macro geometrical structure
$$K_{tMG} = K_{st} \cdot K_{t1} = [1 + A_K \cdot (\frac{R_a}{\overline{\rho}}) \cdot (\frac{R_y}{R_z})] \cdot K_{t1}$$
in which K_{t1} is the SCF of the pre-designed macro geometrical structure, such as a fatigue notch.</td><td>For the multiple stress concentration K_{tMG}, it is necessary that the size of one stress raiser is far smaller than another and it is better if the surface only subjected to simple tensile loading.

Material constant α could be related to the ultimate tensile strength or be derived by checking a chart. For steel (σ_b>550Mpa),
$$\alpha = 0.025 \cdot \left(\frac{2070}{\sigma_b}\right)^{1.8} (mm);$$
For Al, α = 0.51 mm.</td></tr>
</table>

(2) The effective fatigue SCF which considers surface hardening and residual stress, as well as surface geometry	**The integrated effective fatigue SCF which also considers the effects from surface hardening and residual stress as well as surface geometry** $K_{IEF} = \beta_1 \cdot K_{tMG} + \beta_2 \cdot K_{HV} + \beta_3 \cdot K_{\sigma R}$ β_1, β_2, β_3 are influencing coefficients. K_{HV} reflects the effect from surface hardening: $K_{HV} = K_{tMG}^{2/(3+n_H)}$ (for notch insensitive material) or $K_{HV} = K_{tMG}^{1/(1+n_H)}$ (for notch sensitive material) $K_{\sigma R}$ reflects the effect from residual stress: $K_{\sigma R} = \frac{\sigma_{R0}}{\sigma_s} \cdot K_{tG}$	For the high temperature (650ºC) and fatigue cycle less than 10^6: β_1=0.7, β_2=0.25, β_3=0.05; For the fatigue cycle of 10^8: β_1=0.5, β_2=0.4, β_3=0.1. n_H is hardening index and for plastic material, $n_H = 1 - \sqrt{\sigma_s / \sigma_b}$; For notch sensitive material, $n_H = 1 - \sqrt{\sigma_{0.2} / \sigma_b}$. σ_{R0} is the measured surface residual stress; σ_s is the yield strength.

4.5 SUMMARY

This chapter introduced the definitions and concepts of the various stress concentration factors including theoretical stress concentration, effective stress concentration and multiple stress concentration. An example of measuring and evaluating SCFs for superalloy GH4169 specimens from an array of orthogonally-designed externally-grinding experiment are given. Considering the effect of micro surface geometrical texture on the surface and SI characteristics within the subsurface layer of machined parts, an integrated empirical model for evaluation of effective fatigue stress concentration factor K_{IEF} is proposed and developed based on existing fatigue experimental data for a superalloy working at high temperature environment. This model comprehensively takes account into the effects of SI characteristic parameters, such as surface roughness, microhardness and residual stress. This chapter also

proposed a multiple stress concentration evaluation model which includes the machining-induced surface texture effect overlapped on the macro pre-designated stress raisers. Finally, a table which includes the proposed SCF empirical estimation models are listed and summarized. The feasibility and accuracy of the empirical estimation models are validated by using the external grinding experiment for GH4169 superalloy specimens, which provides an analytical basis for specific engineering applications, such as manufacturing of precise engine-used parts and machining of ultra-finished mirror surface.

REFERENCES

[1] Johnson, K.L. Contact Mechanics. Cambridge, UK: Cambridge University Press, 1985

[2] Zhang, G. et. al. Effect of Roughness on Surface Stress Concentration Factor and Fatigue Life. Journal of Mechanical Strength, 2010, **32**(1), pp.110-115.

[3] Xiu, S.C. et. al. Modification for Theoretical Model of Ground Surface Roughness. Journal of Northeastern University, 2005, **28**(8), pp.770-773.

[4] Hu, B.R. et. al. Relationship Between Fatigue Notch Factor K_f and Stress Concentration Factor K_t. Journal of Material Engineering, 2007, **7**, pp.70-73.

[5] Li, L. et. al. Research and Application of Fatigue Notch Factor of Machined Surface, Modular Machine Tool & Automatic Manufacturing Technique, 2009, **2**, pp.1-7.

[6] As, S.K. et. al. Surface Roughness Characterization for Fatigue Life Predictions using Finite Element Analysis. International Journal of Fatigue, 2008, **30**(12), pp.2200-2209

[7] Schijve, J. Fatigue and Structures and Materials (2nd Edition). London: Springer-Verlag, 2009

[8] Yao, W.X. Structural Fatigue Life Analysis. Beijing: National Defense Industry Press, 2003

[9] Huang, Q. and Ren, J.X. Surface Integrity and Its Effects on the Fatigue Life of the Nickel-based Superalloy GH33A. International Journal of Fatigue, 1991, **13**(4), pp.322-326.

[10] Brinksmeier, E. Increase of Fatigue Life of Components by High-pressure Water Jet Surface Peening. Annals of the CIRP, 1992, **41**(1), pp.737-749.

[11] Mercer, C. et. al. Micro mechanisms of Fatigue Crack Growth in a Forged Inconel 718 Nickel-based Superalloy. Materials Science and Engineering: A, 1999, **270**(2), pp.308-322.

[12] Collins, J.A. Failure of Materials in Mechanical Design: Analysis, Prediction, Prevention (2nd Edition). New York: Johns Wiley & Sons, 1993 (ISBN: 978-0-471-55891-0)

[13] Pilkey, W.D. Peterson's Stress Concentration Factors (2nd Edition). New York: John Wiley & Sons, 1997

[14] Pilkey, W.D. and Pilkey, D.F. Peterson's Stress Concentration Factors (3rd Edition). New York: John Wiley and Sons, 2008

[15] Neuber, H. Kerbspannungsleshre. Berlin: Springer, 1958

[16] Arola, D. and McCain, M.L. Surface Texture and the Stress Concentration Factor for FRP Components with Holes. Journal of Composite Materials, 2003, **37**(16), pp.1439-1460.

[17] Arola, D. and McCain, M.L. An Examination of the Effects from Surface Texture on the Strength of Fiber Reinforce Plastics, Journal of Composite Materials, 1999, **33**(2), pp.102-123.

[18] Arola, D. and Williams, C.L. Surface Texture, Fatigue, and the Reduction in Stiffness of Fiber Reinforced Plastics. ASME Journal of Engineering Materials and Technology, 2002, **124** (2), pp.160-166.

[19] Arola, D. and Williams, C.L. Estimating the Fatigue Stress Concentration Factor of Machined Surfaces,. International Journal of Fatigue, 2002, **24**(9), pp. 923-930.

[20] Arola, D. and McCain, M.L. et. al. Waterjet and Abrasive Waterjet Surface Treatment of Titanium: A Comparison of Surface Texture and Residual Stress, Wear, 2002, **249**(1), pp.943-950.

[21] Ai, X. High-speed Machining Technology. Beijing: National Defense Press, 2003.

[22] Ren, J.X. and Hua, D.A. The Principle of Grinding. Beijing: Publishing House of Electronics Industry, 2010

[23] Ren, J.X., Kang R.K. and Wang, X.B. Grinding Technology for the Difficult-to-machine Materials. Beijing: Publishing House of Electronics Industry, 2010

[24] Hu, Z.Z. and Cao, S.Z.. Prediction of Effective Stress Concentration Factors for Metals. Science in China (Series A), 1993, **23**(1), pp.83-91.

CHAPTER 5 GRINDING INFLUENCES ON SURFACE INTEGRITY FOR GH4169 SUPERALLOY

5.1 INTRODUCTION

Superalloy, also known as heat-resistant alloy or high-temperature alloy, usually has outstanding high-temperature strength, excellent thermal stability, good corrosion and wear resistance. Superalloy can withstand complex stress and work reliably under an oxidation and gas corrosion environment even at 600°C-1100°C. Consequently, it is widely employed for the hot sections in aero-engines and in the automobile industry [1]. GH4169, a representative Ni-based superalloy, has been widely used as turbine discs, monoblock rotors, drive shafts, blisk and vane components in the aerospace industry because of it superior properties [2-4]. It has a similar composition and mechanical properties with Inconel 718 (U.S. trademark) and NC19FeNb (France trademark). When machining GH4169 superalloy, its combination of properties like high-temperature strength, low thermal conductivity and strong work-hardening contributes to its undesirable and poor machinability. Further, its surface integrity characteristics and service performance are susceptible to the variation of the machining parameters and conditions, which leads to GH4169 superalloy being considered as typical difficult-to-machine material.

Surface integrity provides an effective means of characterizing and assessing the surface and subsurface features and related functionality. Different cutting parameters and conditions usually will cause variations of the surface integrity characteristics and corresponding

mechanical properties of the machined components, especially for some materials which are hard to cut. Poor surface integrity will deteriorate the surface state, form adverse stress concentration, initiate surface cracks, speed up fatigue fracture and even constitute a potential danger for the machined components in service. For quite some time, many researches have focused on the machinability and surface integrity of difficult-to-machine materials for the aerospace industry and other fields of applications [3-7]. Ezugwu summarized the machinability of difficult-to-machine materials such as aeroengine alloys, hardened steel and structural ceramics. These materials provide a serious challenge for cutting tool materials and usually result in the concentration of high temperatures at the tool–workpiece interface during machining which strongly affect the surface quality of the machined components [8]. Novovic compared the effects of surface topography and integrity on fatigue performance for conventionally and non-conventionally machined titanium alloy and steel [9]. Ulutan and Ozel reviewed the machining induced surface integrity in titanium and nickel alloys for both the aerospace and biometrical industry and they concluded that further modelling studies are needed to create predictive physical-based models that are in good agreement with the results of reliable experiments [10]. Considering that the surface integrity of a machined component will be mainly affected and could be controlled by its machining operational parameters when other machining conditions are settled down, many researches have been carried out to find their relationship for different manufacturing processes and materials. For instance, Jawahir analysed and reviewed works concerning the surface texture effect on the surface integrity and related functional performance during

material removal processes carried out in recent years [11]. Xu investigated the influence of machining-induced high temperatures on the workpiece surface integrity in the surface grinding of a cast Ni-base superalloy K417 using different machining parameters to achieve the change of temperature [12]. Zhao studied the variation of surface and subsurface integrity characteristics for diamond-ground optical glasses material by the ultra-precision machining of fused silica and fused quartz assisted with electrolytic in-process dressing [13]. Bushlya researched how the turning parameters and conditions will influence the machinability of Inconel 718 components with coated and uncoated PCBN tools [14]. Ding investigated the effect of the creep feed grinding process on the grindability and surface integrity of Ni-based alloy when using CBN wheels [15]. Further, researches have also been concerned with thermally induced machining damage, especially for the high speed machining or grinding of superalloy [16-20].

As compared with other difficult-to-machine superalloys or ceramic materials, GH4169 is comparatively new aerospace superalloy used for turbine blisk and shaft components. Studies on the machinability of GH4169 superalloy, especially the related surface integrity characteristics such as the 3D surface topography, residual stress and microhardness as well as the microstructure beneath the surface, are still relatively few. Kong researched the broaching performance and formation of saw-tooth chips during the high speed machining of GH1469 using an FEM simulation technique [21]. Xue experimentally investigated the performance and the wear mechanisms of a PVD-TiAlN coated carbide tool in turning of GH4169 [22]. Grinding is normally used as the final finishing process for the critical

components and it has been widely employed for the machining of superalloy used in the aerospace industry. When it comes to the machining-induced surface integrity aspects in the grinding of GH4169 superalloy, comprehensive studies focusing on both the grindability and related grinding-induced surface integrity characteristics effects are seldom found. During grinding with abrasive wheels, the excellent physical properties of GH4169 superalloy together with its poor thermal conductivity make it extremely difficult to be machined and usually lead to large grinding force and extra-high temperature at the grinding zone and consequently potential changes of the surface integrity characteristics within the machined surface layer. At present, it is still more difficult to ensure the surface quality and integrity of ground components of GH4169 superalloy than it is for normal metal components during mass production. In view of this, a systematic study of the grindability and the relationship between the machining parameters and the formation mechanism of the surface integrity characteristics for grinding of GH4169 superalloy is of practical engineering significance and urgency.

5.2 GRINDING MATERIAL AND EXPERIMENT ARRANGEMENT

5.2.1 Material Properties and Geometry

GH4169 superalloy composition is usually characterized by containing around 5% of Nb, around 21% of Cr, a small amount of Al and Ti to form its strengthening phases γ' ($Ni_3(AlTi)$) and γ'' (Ni_3Nb) which can enhance the alloy's strength and ensure favorable combination properties within the operating temperature range of from 20°C to 750°C. After

direct aging treatment, the microstructure of GH4169 superalloy is usually comprised of its matrix material, γ' and γ'' strengthening phases dispersed in the matrix and fine particle δ phase mainly consolidating the grain boundaries. The nominal composition and physical properties of the workpiece material are given in Table 5.1 and Table 5.2, respectively [1].

Table 5.1 The nominal composition of GH4169 superalloy (wt. %) [1]

C	Cr	Ni	Co	Mo	Al	Ti	Nb	Fe
≤0.08	17-21	50-55	≤1	2.8-3.3	0.2-0.6	0.65-1.25	4.75-5.5	Balance
Mn	B	Mg	Si	P	S	Cu	Ca	Pb
<0.35	<0.006	<0.01	<0.35	<0.015	<0.015	<0.30	<0.01	0.0005

Table 5.2 The physical and mechanical properties of GH4169 [1]

T (°C)	Yield strength $\sigma_{0.2}$ (MPa)	Tensile strength σ_b (MPa)	Elongation δ_5(%)	thermal conductivity (W/m, °C)	modulus of elasticity E (GPa)	melting point (°C)	Hardness (HV)	Density (g/cm^3)
20	1240	1450	>10	13.4	205	1310	376-480	8.24
650	1000	1170	>12	22.1	205	—	—	—
750	740	950	25	23.5	—	—	—	—

The actual measured value of the microhardness of the workpiece material for the grinding experiments is around 480HV. This workpiece for grinding experiments is supplied in two forms. One is a bar of size φ30×100mm (30mm diameter and 100mm length) for orthogonally designed experiments of external grinding, whilst the second is a rectangular block of size 30×25×10mm for single-factorial experiments of plane grinding. Direct aging treatment is applied to the specimen. The heat treatment process is: heat the raw material to 720°C ± 5°C and hold for around 8 hours; then cool the material with a velocity of -50°C/h in the furnace to 620°C ± 5°C and hold this temperature for another 8 hours; finally wait until the material cools to room temperature in free open air.

5.2.2 Machining and Measurement Equipment

A single alundum grinding wheel with Al_2O_3 abrasive grit was employed for the grinding experiments, having an abrasive grit size of 80#. The cutting fluid used was a normal 5% emulsion. The 3D surface texture and roughness were measured using a Veeco NT 1100 3D white light interferometer with a resolution of 2 nm on the optical Z-axis. The measurement of surface residual stress and the residual stress profile (the variation of residual stress with depth below the surface) were made using the XA-350 x-ray stress analysis system. The measurement of surface microhardness and microhardness profile (the variation of microhardness with depth below the surface) were conducted using EverOne MH-50 microhardness tester with a load of 25g and a hold time of 10s. Subsurface microstructures were also revealed and analyzed with the metallographic microscope technique.

5.2.3 Experimental Design and Procedure

5.2.3.1 Grinding arrangement

Orthogonal experimental design is a scientific method that can investigate the effects of multiple factors on the researched objective function [23]. The orthogonal table can reduce the total number of trials and increase the amount of information of the tested points. Compared to the trial number of factorial design experiments, only a few representative tests are needed to determine the most significant factor that may affect the researched objective function. For the external grinding of GH4169 superalloy, the processing parameters are the main factors affecting the surface integrity characteristics once the wheel properties and

lubrication conditions are established. A three-factors four-levels orthogonal experiment ($L_{16}(4^5)$) for external grinding was designed, as shown in Table 5.3. The three factors investigated here are wheel speed $v_{s,}$ workpiece speed v_w and depth of cut a_p. They are taken as independent variables for the orthogonal design. The levels for each factor are: wheel speed v_s=15, 20, 25, 30m/s; workpiece speed v_w=8, 12, 16, 22m/min; depth of cut a_p=0.005, 0.01, 0.015, 0.02mm. The workpiece sample size φ30×100mm.

Table 5.3 Orthogonally-designed external grinding tests & SI characteristics measurement

Samples No.	Grinding parameters			SI characteristics measurement		
	v_w (m/min)	a_p (mm)	v_s (m/s)	R_a (μm)	σ_{R0} (MPa)	HV_1 (kgf/mm^2)
EG1	8	0.005	15	0.259	-241.8	512.38
EG2	8	0.01	20	0.298	-383.1	539.71
EG3	8	0.015	25	0.260	-161.1	501.33
EG4	8	0.02	30	0.299	-467.3	508.59
EG5	12	0.005	20	0.210	-438.9	539.91
EG6	12	0.01	15	0.268	-210.1	478.76
EG7	12	0.015	30	0.289	-83.4	473.76
EG8	12	0.02	25	0.2423	-554.6	494.21
EG9	16	0.005	25	0.268	-354.2	531.77
EG10	16	0.01	30	0.232	-460.2	494.21
EG11	16	0.015	15	0.293	-550.3	487.25
EG12	16	0.02	20	0.296	-334.2	504.85
EG13	22	0.005	30	0.247	-493.2	487.08
EG14	22	0.01	25	0.285	-453.3	508.78
EG15	22	0.015	20	0.257	-190.4	508.59
EG16	22	0.02	15	0.324	-215.3	556.13

The linear regression analysis method is then employed to help to establish the empirical correlation between the grinding parameters and surface roughness characteristic. Accurately establishing and analyzing the empirical relationships can help to find the most influencing factors and guide the selection of a reasonable range of operational parameters for the actual

grinding process and will certainly decrease the trial-producing time and machining cost as well as attaining acceptable surface quality when grinding GH4169 superalloy.

Further, single-factorial plane grinding tests were designed and listed in Table 5.4, in which the effect of depth of cut a_p on the surface integrity characteristics such as surface roughness, residual stress and microhardness distribution and microstructure beneath the machined surface are quantitatively compared and analyzed in detail. The wheel speed and workpiece speed are specified as v_s=25m/s and v_w=10m/min respectively; while the depth of cut a_p monotonically increases from 0.005mm to 0.04mm. A reasonable value of depth of cut will give good surface quality and integrity characteristics on the ground surface.

Table 5.4 Single-factorial test of plane grinding & SI characteristics measurement

Sample No.	v_w (m/min)	v_s (m/s)	a_p (mm)	Residual stress vs. depth below surface	Microhardness vs. depth below surface	Microstructure vs. depth below surface
PG1	10	25	0.005	σ_R=$\sigma_R(h)$ *	HV=$HV(h)$ **	***
PG2			0.015	σ_R=$\sigma_R(h)$ *	——	——
PG3			0.025	σ_R=$\sigma_R(h)$ *	HV=$HV(h)$ **	***
PG4			0.035	σ_R=$\sigma_R(h)$ *	——	——
PG5			0.04	σ_R=$\sigma_R(h)$ *	HV=$HV(h)$ **	***

*: refer to Figure 5.3&5.4; **: refer to Figure 5.7; ***: refer to Figure 5.9;

5.2.3.2 Measurement and characterization

This research combines different techniques to measure and characterize the cutting performance and surface integrity characteristics of the ground surface. The surface topography and roughness of the machined surface were observed and analyzed with the 3D white light interferometric microscopy technique and scanning electron microscopy. The surface roughness was measured at 3 different positions on a machined sample using an

optical interferometer and taking the average as the final surface roughness value R_a.

The X-ray stress analysis technique and local layer-peeling method were used to measure surface residual stress and subsurface residual stress distribution for external and plane ground samples. The surface and subsurface residual stresses were attained using X-350A x-ray stress analysis system with a Cr-anticathode, piping current I=8mA, piping voltage U=25kV. The subsurface residual stresses were measured layer by layer with the help of an electrolytic corrosion device for local layer peeling.

The microhardness of the machined surface was measured using a microhardness tester with the beveling plane method. With this method, a small plane with around 3° inclination to the ground surface was beveled and polished. Microhardness measurements were carried out at the different location of the bevel plane which actually gave the microhardness with different depths below the ground surface. The polished bevel plane also makes the boundary of the diamond indentation more clearly discerned and helps to accurately calculate the value of microhardness (See Figure 5.6).

The subsurface microstructure and grain morphology of the workpiece material were observed using a scanning electron microscope. Detailed metallurgical variation of the microstructure of the samples that were ground with three different depth of cut a_p were compared with the results obtained using the metallographic microscope technique.

5.3 EFFECTS OF GRINDING PROCESS ON SURFACE INTEGRITY

5.3.1 Surface Roughness and Effects

5.3.1.1 Orthogonally designed experiment for external grinding

The 3D surface topography for some of the machined samples are visually presented in Figure 5.1. With the specified external grinding parameter range, the ground surfaces are of comparatively lower roughness value and the maximum surface roughness is R_a=0.324μm; there are prominent grinding marks and lays along the machining direction on the workpiece surface.

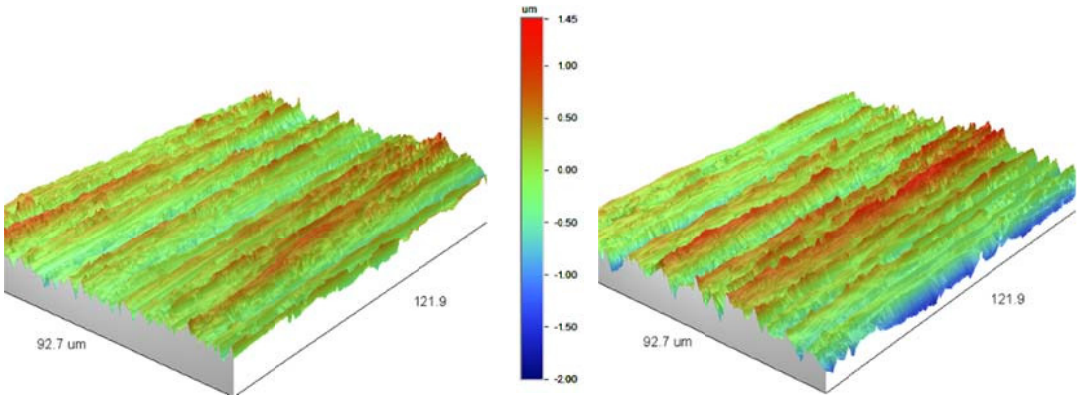

(a) EG1: R_a=0.259μm (b) EG2: R_a=0.298μm

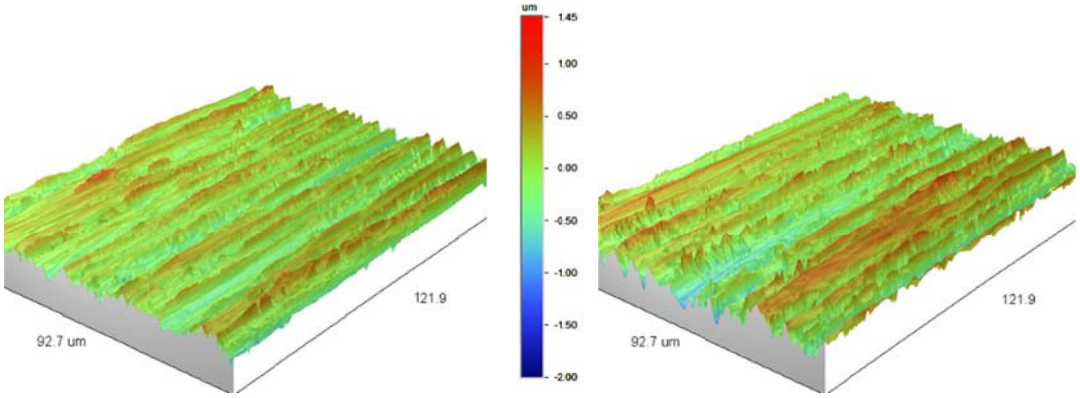

(c) EG5: R_a=0.210μm (c) EG6: R_a=0.268μm

Figure 5.1 3D surface texture of externally ground components for orthogonal experiments

Seen in Figure 5.1, samples EG2 and EG6 were ground with a comparatively higher value of depth of cut, and their ground 3D surfaces obviously contain deeper grooves and higher peaks when compared with those of samples EG1 and EG5. Correspondingly, the surface roughness values of samples EG2 and EG6 are larger than those of samples EG1 and EG5 respectively.

According to the arrangement of grinding parameters and the measured values of surface integrity characteristics in Table 5.3, an empirical equation which expresses the correlation between the measured surface roughness R_a and the 3 main grinding parameters within the range researched is derived from linear regression analysis as follows:

$$R_a = 10^{-0.228} \cdot v_w^{0.01} \cdot a_p^{0.112} \cdot v_s^{-0.101} \tag{5.1}$$

Although the correlative coefficient (R=0.86) and the significance level are not desirable, this mpirical equation still offers some helpful information. Within the grinding parameter range researched, the depth of cut a_p is of the maximum power-law index among 3 main grinding parameters and is the most important factor that affects the surface roughness R_a. From the empirical equation, the depth of cut a_p is positively correlated to the surface roughness, which means that R_a will decrease with the decrease of a_p; the workpiece speed v_w is comparatively less correlative to the surface roughness R_a; while the wheel speed v_s is negatively correlated to the surface roughness, which means that R_a will reduce if the wheel speed v_s increases. Within the grinding parameter range researched, the surface quality and roughness could correspondingly be improved by reasonably increasing the wheel speed v_s, or by reducing the depth of cut a_p.

5.3.1.2 Single-factorial experiment for plane grinding

A single-factorial grinding test, which focuses on investigation of the effect of depth of cut a_p on the surface integrity characteristics such as surface roughness, residual stress and microhardness distribution and microstructure beneath the surface, was designed, as shown in Table 5.4. The 3D surface topography of these plane-ground samples are visually displayed in Figure 5.2. As can be seen, the effect of depth of cut a_p on surface roughness and topography is very apparent and intensive. When the wheel speed and workpiece speed are specified, surface roughness will monotonically soar with increase of the depth of cut a_p. For the sample PG1 ground with a_p=0.005mm, the surface roughness is low and R_a=0.284μm. For the sample PG3 ground with a_p=0.025mm, the surface has obvious grooves and peaks with R_a=0.421μm. For the sample PG5 ground with a_p=0.04mm, the grooves are much deeper and the peaks more widely dispersed over the ground surface with a roughness value of R_a=0.896μm which is much larger than those of sample PG1 and PG3.

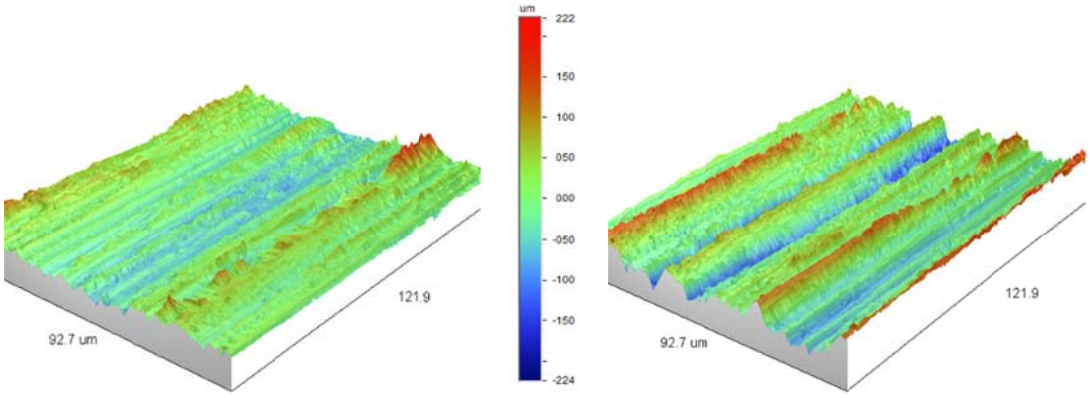

(a) PG1: R_a=0.284μm (b) PG3: R_a=0.421μm

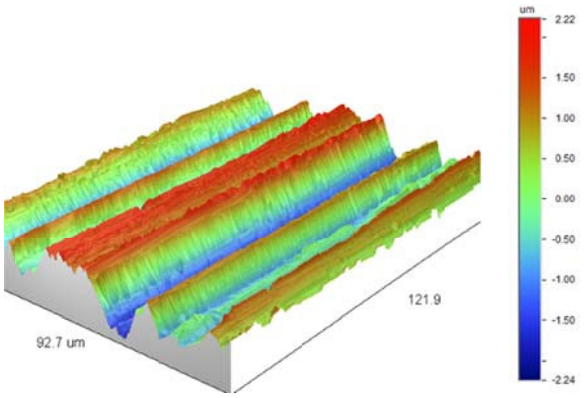

(c) PG5: R_a=0.896μm

Figure 5.2 3D surface texture of plane ground components for single-factorial experiments

5.3.2 Surface and Subsurface Residual Stress and Effects

Generally, the formation mechanism and influencing factors of residual stress for machined surfaces mainly originate from two aspects [24-28]. One is from the machining-induced thermal effect and it usually has much more in-depth influence on a material of low thermal conductivity with worse machining conditions; another is from the machining-induced mechanical action or plastic deformation. During the cutting process, massive cutting heat will be produced on the interface between the tool and the workpiece. The heat energy is then transferred to the subsurface layer and even to the core of the workpiece; therefore the local high temperature will make the volume of the surface and subsurface material swell and firstly produce a kind of compressive stress. Considering the low thermal conductivity of GH4169 material, the grinding heat will mainly accumulate in a thin layer near the surface while the core and bulk material of the workpiece will keep at a comparatively low temperature or even at ambient temperature during the limited machining process. After the cutting tool has left the workpiece surface, the heated and swelled subsurface layer is then

gradually cooled and tends to contract, but the bulk material will prevent the surface and subsurface layer from contracting or shrinking at that time, so residual tension is likely to be present on the newly machined surface and subsurface layer. Consequently, the thermal effect is finally prone to produce tensile residual stress on the machined surface of the workpiece. The mechanically-induced (or deformation-led) residual stress during the grinding process can be explained by a combination of plastic deformation in the superficial surface layer and elastic deformation in the underlying surface. When the mechanical-cutting action stops, the elastic deformation below the subsurface layer tends to restore while the plastically-deformed thin superficial layer is inclined to counteract its springing back. To achieve force equilibrium and geometric compatibility after the grinding process, elastic rebalancing and existing plastic deformation will place the surface and superficial layer in the state of residual compressive stress.

GH4169 superalloy has excellent mechanical properties and usually exhibits severe work-hardening. It also combines poor thermal conductivity with tough and strengthened phases in its matrix material. Generally, its machinability is not as good as its mechanical properties. During grinding, grinding heat is built up easily in the cutting zone, which deteriorates the cutting condition and degrades the tool life. As a result, high cutting forces with high localized temperatures are produced around the grinding wheel surface and the workpiece surface, thus leading to high values of surface roughness and tensile residual stress.

5.3.2.1 Analysis of residual stress distribution below surface

The residual stress distribution of the samples that have been plane-ground with different machining parameters are measured and compared. As shown in Figure 5.3, the residual stresses distribution over the depth below the surface h of the workpiece, are presented in terms of two directions: σ_{Rx}, parallel to the grinding direction and σ_{Ry}, perpendicular to the grinding direction.

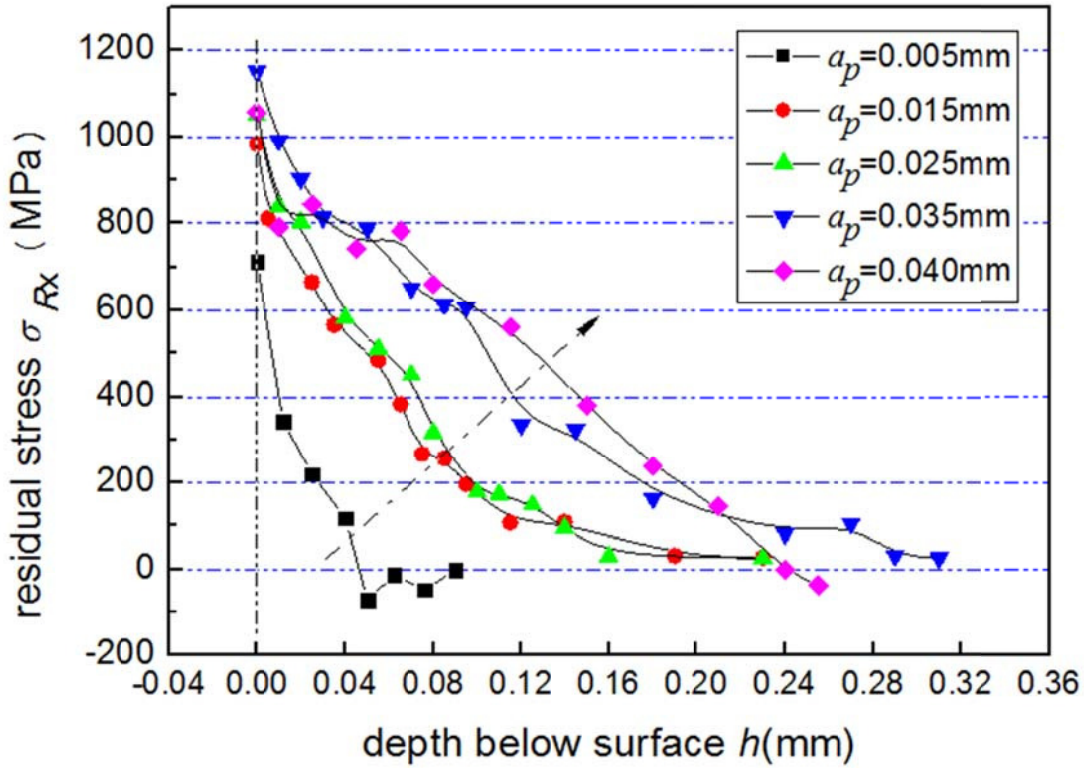

Figure 5.3 σ_{Rx} distributions over the depth below surface for different plane-ground samples

From the residual stress distribution profiles shown in Figure 5.3 and Figure 5.4, some findings and analyses are listed as follow: (1) the plane ground surfaces are mainly of adverse tensile residual stresses when compared to external grinding. This is caused by the low thermal conductivity of GH4169 superalloy and the adverse cutting conditions around the interface of the workpiece and the grinding wheel. The thermally diffusive condition of

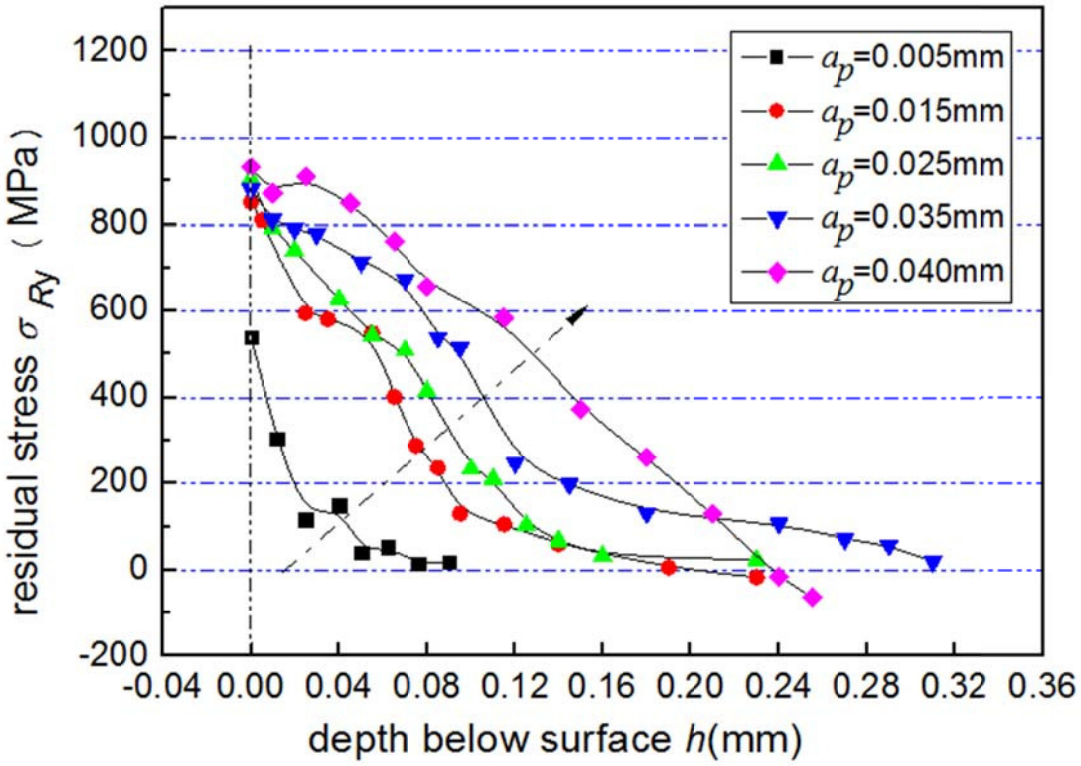

Figure 5.4 σ_{Ry} distributions over the depth below surface for different plane-ground samples

plane grinding is usually worse than that of external grinding, and massive grinding heat is accumulated at the outermost part of the ground surface producing higher grinding temperature at this location. At this moment, the thermal effect is more significant and the ground surface will take on tensile residual stress according to the thermal-mechanical coupling action. (2) the magnitude of the tensile residual stress closely depends on the grinding parameters like depth of cut a_p for this single-factorial plane grinding test. The residual stress σ_{Rx}, which is parallel to the grinding direction and σ_{Ry}, which is perpendicular to the grinding direction, are generally of the same order of magnitude, although σ_{Rx} at the surface is around 250Mpa larger that σ_{Ry} at the sample surface when a_p=0.035mm. With the value of the depth below the surface, h, increases, the tensile stresses σ_{Rx} and σ_{Ry} both will monotonically decrease no matter what the value of a_p is. For the residual stress σ_{Rx}, it

decreases rapidly when the depth below the surface, h, is smaller than 40μm. The residual stress decreases more gradually when the depth below the surface, h, is larger than 200μm. When the value of depth of cut a_p increases, the tensile stresses σ_{Rx} and σ_{Ry} both will rise; and the thickness of the subsurface zone where residual stress prevails will also obviously increase with the increase of depth of cut a_p. Usually, the increase of depth of cut a_p will intensify the plastic deformation, improve the grinding energy input and lead to a fast rise of the grinding temperature at the machined interface. Finally, high tensile residual stress on the plane-ground surface and subsurface will develop due to the more significant thermal effect. When the depth of cut, a_p, increases from 0.005mm to 0.04mm, the thickness of the subsurface zone where residual stress effects are present will increase from around 100μm to 310μm.

5.3.3 Surface and Subsurface Microhardness and Effects

During machining process like grinding, the workpiece surface will usually experience severe plastic deformation and its grain structure and lattices in the vicinity of machined surfaces will be distorted or elongated and appear to be a kind of high-level fibrous structure. This kind of mechanical action usually will make the surface microhardness much higher than that of the bulk material. At the same time, most of the plastic deformation energy is converted into heat energy during the grinding of a GH4169 workpiece. Although the ground chips will take away quite a substantial part of the heat energy, there is still a large portion of grinding heat that will build up at the thin superficial layer of the workpiece which could not be quickly passed into the core and bulk material in time due to the intensive frictional

interaction at the interface and low thermal conductivity of GH4169 superalloy. Thus, the surface and subsurface layer of the workpiece will be experiencing the equivalent to a high-temperature surface annealing or recrystallization process along with the work-hardening mechanical action. As is known, annealing is a process of heat treatment and will usually increase the toughness of alloys and reduce some of the excess hardness. That is to say, the surface annealing process essentially will eliminate the unbalanced microstructure and physical properties of the machined surface with grain growth or recrystallization, which finally softens the surface and subsurface material. Generally speaking, the workpiece material will mostly maintain its work-hardening effect when the temperature is below 0.4-0.5 times the material's melting point. However, if the temperature further increases, both the material flow stress and material strength will decrease. Thereby, the extent of work hardening caused by the plastic deformation will be weakened when the surface annealing occurs at high temperature during grinding [24].

Considering the interaction of the work-hardening effect and the possible surface annealing caused by local high-temperature during the grinding of GH4169, there are likely to be 3 kinds of scenarios of the variation of microhardness within the subsurface layer [29-30]:

(1) If the abrasive grits of the grinding wheel are sharp and the lubrication condition is good, and if the grinding material removal rate is well controlled, then the machined surface will not experience surface annealing or grinding burn and will mainly be work-hardened: its microhardness profile will usually have a peak value at the machined surface as is shown in Figure 5.5(a).

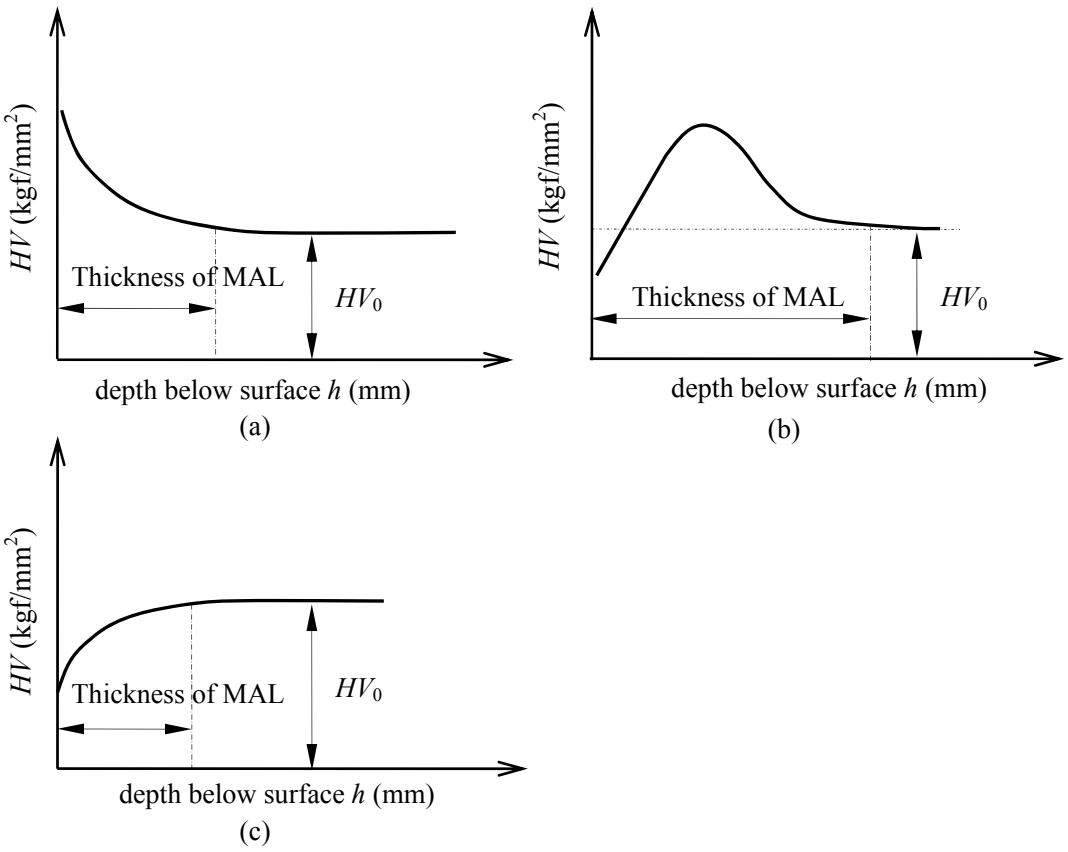

Figure 5.5 The mechanism for formation of microhardness of ground surface[29-30]

(2) If the abrasive grits are dull and if the grinding material removal rate is unreasonably high, massive grinding heat will gather around the machined surface and produce local high temperature at the outermost thin superficial layer of the machined surface. Once this temperature is above the annealing temperature or the transformation temperature of the superalloy, the microstructure near this area will gradually change to equiaxed grains, the strengthening phase in the alloy may be resolved and the microhardness of this area will drop rapidly. However, its underlying layer near the core will keep the effect of cold deformation strengthening due to the large grinding force and inaccessibility of grinding heat. With the depth below the surface, h, increases, the microhardness value at the surface and subsurface will firstly go below that of the bulk material HV_0, then increase to a peak and finally

approach the hardness of the bulk material, as shown in Figure 5.5(b) (3) if the lubrication is insufficient or with dry grinding, the grinding state around the interface will rapidly deteriorate and the grinding temperature will exceed the recrystallization or annealing temperature. Then the whole surface and material-altered-layer (MAL) will experience severer thermal action and sometimes even grinding burn may occur. As a result, the microhardness of the surface and subsurface will all be below that of the bulk material HV_0, as shown in Figure 5.5(c).

5.3.3.1 Effect of grinding parameters on microhardness

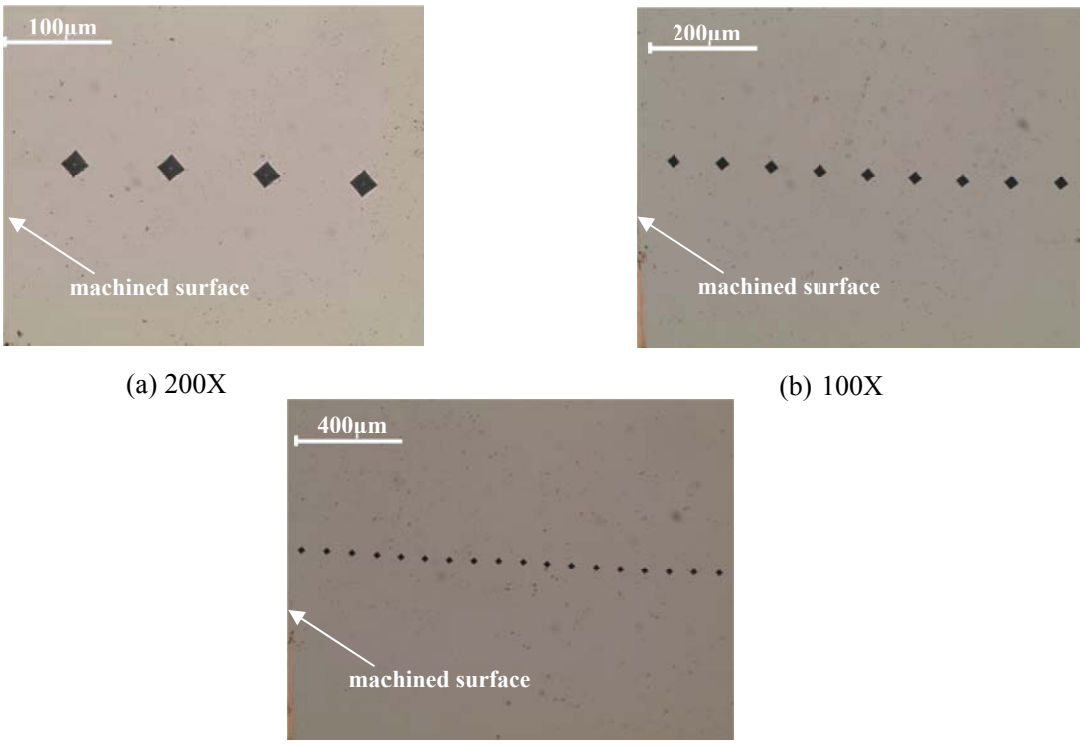

(a) 200X (b) 100X

(c) 50X

Figure 5.6 Microhardness measurement process

Figure 5.6 shows the measurement process of microhardness and the indentation marks on a polished bevel plane. The actual variation of microhardness values with the depth below the surface from the single-factorial test are shown in Figure 5.7. The surface microhardness

values of the samples PG1, PG3 and PG5 are respectively HV_1=440, 435 and 417. They are obviously lower than the value of the bulk material (HV_0≈480). The effect of work-hardening does not show up in this case; the surface and subsurface are actually softened. This is mainly because the thermal conductivity of GH4169 is comparatively low and a mass of thermal energy could not be quickly passed into the core, but congregates only at the superficial layer of the ground surface. This will cause extremely high temperature at the ground surface layer and once the temperature exceeds the annealing temperature or is higher than the solution temperature of the strengthening phase γ' or γ'', the material microstructure of the surface layer will change, the grains structure will grow and the strengthening phases may be dissolved. Then the mircohardness of the surface and whole material-altered layer will fall to a low value.

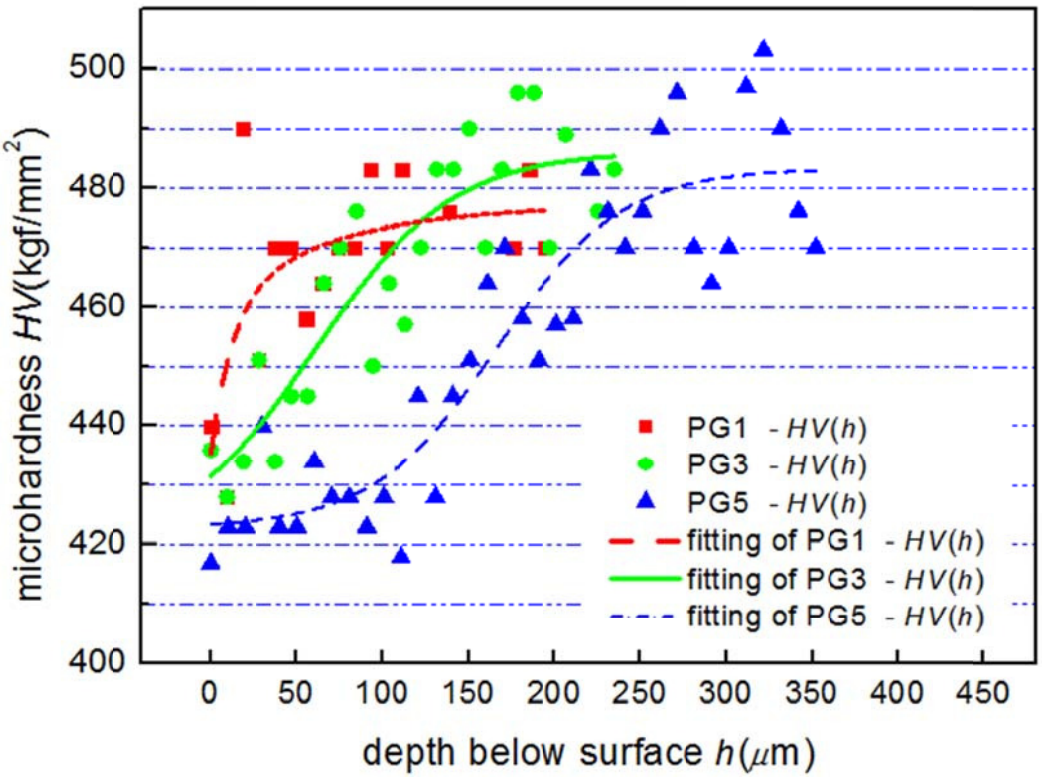

Figure 5.7 Microhardness profile varies with depth below surface for plane grinding test

As the depth of cut a_p increases (from sample PG1 to PG5), the related plastic deformation

will increase and more mechanical energy will transfer to thermal energy. Therefore, the temperature at the interface of the workpiece and grinding wheel periphery will soar to a value which exceeds the annealing temperature of the GH4169 material and make the measured values of microhardness have a rapid drop. As shown in Figure 5.7, the outermost surface microhardness of sample PG1(with a_p=0.005mm) does not drop too much and is around HV_1=440; while for the sample PG5(with a_p=0.04mm), its surface and subsurface endure much greater thermal effects due to the large grinding parameter and the value of microhardness drops to the lowest of around HV_1=417. With the increase of the depth below the surface, h, the microhardness value will gradually approach that of the bulk material. The thickness of the material-altered layer where the microhardness varies will increase with the increase of depth of cut a_p. When a_p increases from 0.005mm to 0.04mm, the thickness of the region of microhardness variation will increase from 200μm to 360μm.

5.3.4 Subsurface Microstructure and Effects

GH4169 superalloy usually needs to experience aging treatment to attain saturated Ni austenite to secure its better mechanical properties. The microstructure of the GH4169 superalloy is shown in Figure 5.8(a) and the grains are distributed homogenously within the field of view. The grain size is well-proportioned and the grain boundary is clear to discern. When further magnified, the inhomogeneous structure δ phase can be clearly observed as shown in in Figure 5.8(b). The δ phase structures are granular or like a short bar and are mainly dispersed in the grain boundary or within grains which will help to strengthen the matrix.

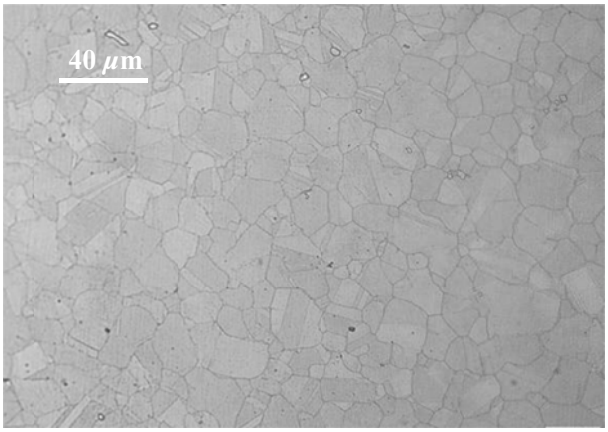

(a) Grain size and morphology of GH4169 superalloy

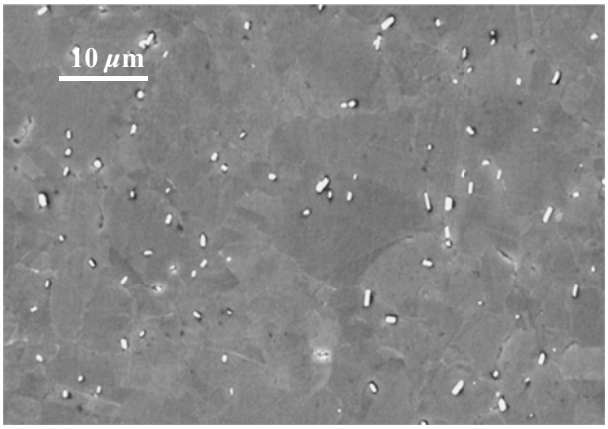

(b) Grain morphology with granular δ phase of GH4169 superalloy

Figure 5.8 Microstructure of GH4169 superalloy

5.3.4.1 Effect of the grinding parameters on microstructure

In Figure 5.9, the microsections parallel to the grinding direction for the ground GH4169 samples are given. Samples PG1, PG3 and PG5 correspond to grinding parameters with different depths of cut a_p=0.005mm, 0.025mm and 0.04mm. The grinding direction is from left to right. Compared with the metallograph of the unprocessed original state of the bulk material in Figure 5.9(a), the microstructure of the ground PG1 sample (with a_p=0.005mm) does not have obvious shape or size changes in metallurgy; the degree of deformation of

grains within the subsurface layer is also not obvious; the plastic deformation shown by lattice distortion or skewness is not remarkable and the visible and discernable depth that plastic deformation may reach to (the thickness of the plastically-deformable layer) is only about 3μm.

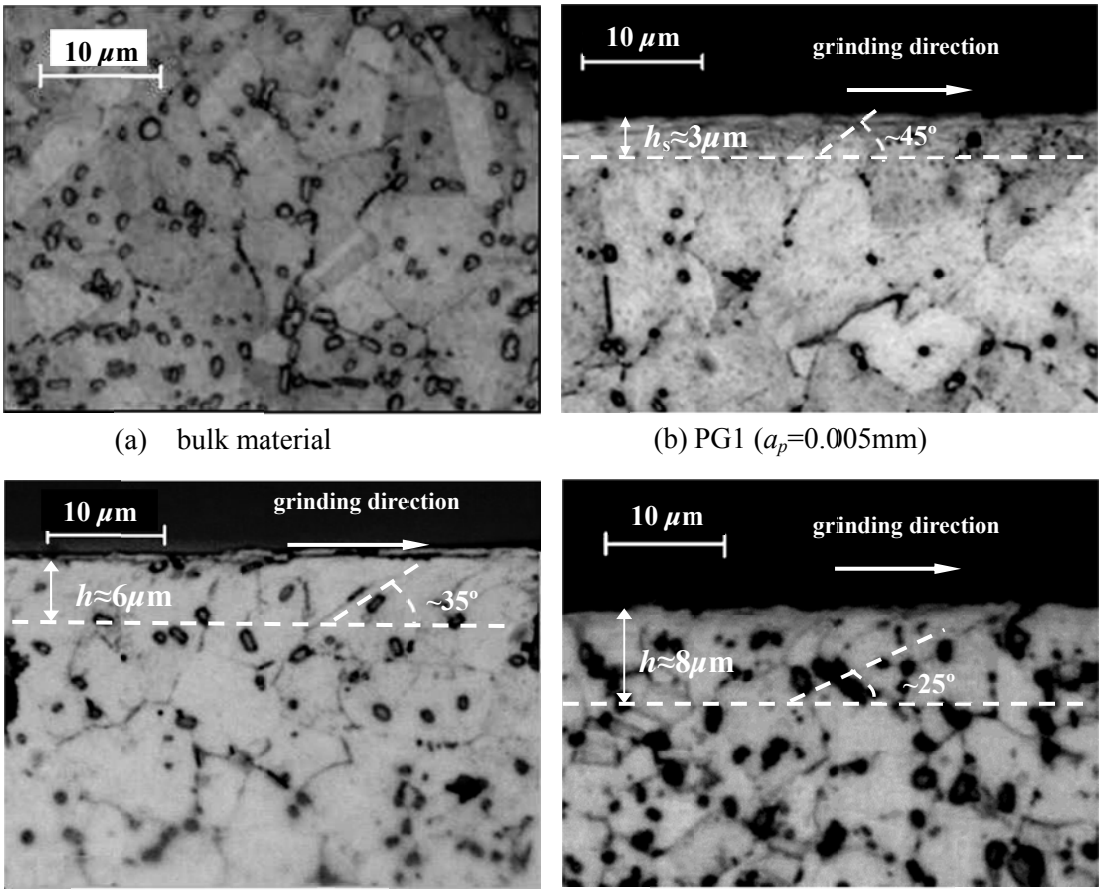

(a) bulk material (b) PG1 (a_p=0.005mm)

(c) PG3 (a_p=0.025mm) (d) PG5 (a_p=0.04mm)

Figure 5.9 Microstructure metallograph of GH4169 after plane grinding with different a_p

In Figure 5.9(c) and (d), when the depth of cut a_p increases to 0.025mm and 0.04mm, the grains in the vicinity of the ground surface are apparently stretched and distorted along with the grinding direction. In view of the larger grinding parameter values of a_p, the thickness that the plastic deformation can reach to correspondingly increases to about 6~8μm; the skewness angle of grain flow lines reduces from around 45° to around 25° which means the

degree of grain skew and elongation towards the grinding direction has been enhanced; the grain aspect ratio also consequently increases.

On the other hand, seen from the top view, as shown in Figure 5.10, no visible cracks or defects could be found on the ground surfaces of sample PG1 considering its a_p and material removal rate are small. Only clear scratches engraved by the abrasive grits are seen along the

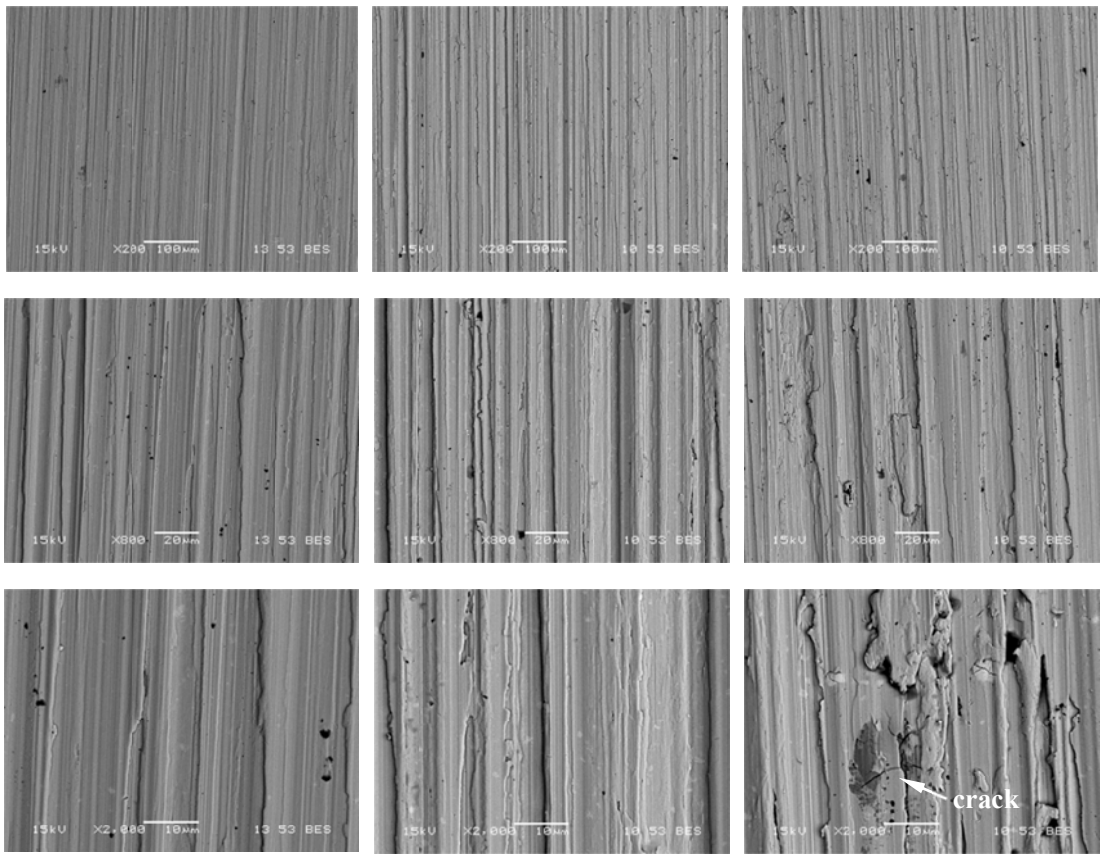

(a) PG1 (b) PG3 (c) PG5

Figure 5.10 SEM micrographs of the GH4169 samples by plane grinding with different a_p

grinding direction even when the maginfication is 2000X. When the a_p increases to 0.025mm, side flow and smeared material are observed in the area of the feed marks for sample PG3; however, when a_p further increases to 0.04mm, the surface of sample PG5 has cracks perpendicualr to the grinding direction; some material broken off from the workpiece also

overlaps on the machined surfaces. Its surface behavior is apparently deteriorated and worse than that of samples PG1and PG3.

5.4 SUMMARY

Based on the experiment study and detailed analyses of the grinding of GH4169 superalloy, some conclusions related to its grindability and surface integrity may be drawn as follows:

(1) Depth of cut a_p and wheel speed v_s are the main influencing factors on the surface roughness R_a for external grinding. Within the investigated grinding parameters range, the surface roughness R_a will reduce as the depth of cut a_p reduces or the wheel speed v_s increases. The depth of cut a_p shows a more profound and remarkable effect on the surface roughness R_a for plane grinding, When the depth of cut a_p increase from 0.005mm to 0.04mm, the corresponding magnitudes of surface roughness are nearly tripled, rising from 0.284μm to 0.896μm. Thus, reasonable choice and control of the wheel speed v_s and depth of cut a_p will effectively improve the ground surface quality.

(2) External grinding is advantageous in securing compressive residual stress on the machined surface; while plane grinding is prone to producing adverse tensile residual stress on the machined surface. For plane grinding, all residual stress profiles within the thin subsurface layer exhibit tensile residual stresses with their maximum tensile stress at the surface. Once the excessive tensile residual stress exceeds the material strength of GH4169, adverse perpendicular cracks will appear which will largely degrade the performance of machined parts. When the value of depth of cut a_p increases, the tensile stresses σ_{Rx} and σ_{Ry} both will rise; at the same time, the thickness of the subsurface layer

where the residual stress prevails will also obviously increase as the depth of cut a_p increases. Usually, adopting a high value of depth of cut a_p will intensify the plastic deformation, improve the grinding energy input and lead to a fast rise of the grinding temperature at the machined interface. Finally, high tensile residual stress will be generated on the plane-ground surface and within the subsurface due to the high and intensive thermal effect. When the of depth of cut a_p increases from 0.005mm to 0.04mm, the thickness of the subsurface layer in which residual stress exists will increase from around 100μm to 310μm.

(3) The magnitude of microhardness for externally-ground surfaces are slightly larger than that of the original bulk material (HV_0≈480) and the ground surfaces are work-hardened to some extent; while for plane grinding, all the measured values of surface mircohardness are smaller than that of the bulk material. With the increase of the depth below the surface, h, the value of microhardness will gradually approach that of the bulk material. The thickness of the material-altered layer in which the microhardness varies will also increase with the increase of depth of cut a_p. When a_p increases from 0.005mm to 0.04mm, the thickness of the microhardness-varied layer will increase from 200μm to 360μm.

(4) The microstructure of the material on and below the plane-ground surface will be stretched and distorted along the grinding direction. The degree of deformation of the grain lattices is dependent on the depth of cut a_p, which produces different grinding forces and friction forces on the interface between the wheel and the machined surface.

The PG5 specimen's surface, which was ground by the depth of cut a_p=0.04mm, has the most remarkable change of microstructure; with the grain skewness angle around 25° and the thickness of the plastic deformation layer about 6~8μm. This large magnitude of depth of cut should be undoubtedly avoided during the practical grinding of GH4169 because it is likely to initiate fatal intergranular cracks on the machined surface.

REFERENCES

[1] Gu, M. Aeronautical Materials Handbook (2nd Edition). Beijing: China Standard Press, 2001.

[2] Yu, R.L. et. al. Notch Sensitivity of GH4169 Superalloy. Aerospace Material & Technology, 1998, **3**, pp.19-21

[3] Ezugwu, E.O. et. al. The Machinability of Nickel-based Alloys: A Review. *Journal of Materials Processing Technology*, 1999, **86**(1-3), pp.1-16.

[4] Rahman, M. et. al. The Machinability of Inconel 718. *Journal of Materials Processing Technology*, 1997, **63**(1-3), pp.199-204.

[5] Liu, J.K. et. al. Microstructure and Mechanical Properties of Diffusion Bonded Single Crystal to Polycrystalline Ni-based Superalloys Joint, Materials & Design, 2013, **49**, pp.622-626.

[6] Guo, Y.B., Li, W. and Jawahir, I.S. Surface Integrity Characterization and Prediction in Machining of Hardened and Difficult-to-machine Alloys: A State-of-Art Research Review and Analysis, Machining Science and Technology, 2009, **13** (4), pp.437-470.

[7] Griffiths, B.J. Manufacturing Surface Technology-Surface Integrity and Functional Performance. London: Penton Press, 2001(ISBN 1-8571-8029-1).

[8] Ezugwu, E.O., Bonney, J. and Yamane, Y. An Overview of the Machinability of Aeroengine Alloys. Journal of Materials Processing Technology, 2003, **134**(2), pp.233-253.

[9] Novovic, D. et. al. The Effect of Machined Topography and Integrity on Fatigue Life. International Journal of Machine Tools and Manufacture, 2004, **44**(2-3), pp.125-134.

[10] Ulutan, D. and Ozel, T. Machining Induced Surface Integrity in Titanium and Nickel Alloys: A review. International Journal of Machine Tools and Manufacture, 2011, **51**(3), pp.250-280.

[11] Jawahir, I.S. et. al. Surface Integrity in Material Removal Processes: Recent advances. CIRP Annals-Manufacturing Technology, 2011, **60**(2), pp. 603-626.

[12] Xu, X.P. et. al. Effect of Grinding Temperatures on the Surface Integrity of a Nickel-based Superalloy. Journal of Materials Processing Technology, 2002, **129**(1-3), pp.359-363.

[13] Zhao, Q. et. al. Surface and Subsurface Integrity in Diamond Grinding of Optical Glasses on Tetraform 'C'. International Journal of Machine Tools and Manufacture, 2007, 47(14), pp.2091-2097.

[14] Bushlya, V. et. al. Effect of Cutting Conditions on Machinability of Superalloy Inconel 718 During High Speed Turning with Coated and Uncoated PCBN Tools, Procedia CIRP, 2012, **3**, pp.370-375.

[15] Ding, W.F. et. al. Grindability and Surface Integrity of Cast Nickel-based Superalloy in Creep Feed Grinding with Brazed CBN Abrasive Wheels. Chinese Journal of Aeronautics, 2010, 23(4), pp.501-510.

[16] Abukhshim, N.A. et. al. Heat Generation and Temperature Prediction in Metal Cutting: A Review and Implications for High Speed Machining. International Journal of Machine Tools and Manufacture, 2006, **46**(7-8), pp.782-800.

[17] Malkin, S. and Guo, C. Thermal Analysis of Grinding. CIRP Annals - Manufacturing Technology, 2007, **56** (2), pp.760-782.

[18] Chang, C.C. and Szeri, A.Z. A Thermal Analysis of Grinding. Wear, 1998, **216**(1), pp.77-86

[19] Hou, Z.B. and Komanduri, R. On the Mechanics of the Grinding Process, Part II-

Thermal Analysis of Fine Grinding. International Journal of Machine Tools and Manufacture, 2004, **44**(2-3), pp.247-270.

[20] Lu, X.D. et. al. High Temperature Structure Stability of GH4169 Superalloy. Materials Science and Engineering: A, 2013, **559**, pp.623-628.

[21] Kong, X.W. et. al. Broaching Performance of Superalloy GH4169 Based on FEM. Journal of Materials Science & Technology, 2011, **27**(12), pp.1178-1184.

[22] Xue, C. and Chen, W.Y. Adhering Layer Formation and Its Effect on the Wear of Coated Carbide Tools during Turning of a Nickel-based Alloy. Wear, 2011, **270**(11-12), pp.895-902.

[23] Montgomery, D.C. Design and Analysis of Experiments (6th Editon). New York: John Wiley & Sons, 2005.

[24] Chen, X. and Rowe, B.W. Analysis and Simulation of the Grinding Process. Part II: Mechanics of Grinding. International Journal of Machine Tools and Manufacture, 1996, **36**(8), pp.883-896.

[25] Outeiro, J.C. et. al. Machining Residual Stresses in AISI 316L Steel and Their Correlation with the Cutting Parameters. Machining Science and Technology, 2002, **6**(2), pp. 251-270

[26] Outeiro, J.C. et. al. Analysis of Residual Stresses Induced by Dry Turning of Difficult-to-machine Materials. CIRP Annals-Manufacturing Technology, 2008, **57**(1), pp.77-80.

[27] Gunnberg, F. et. al. The Influence of Cutting Parameters on Residual Stresses and Surface Topography during Hard Turning of 18MnCr5 Case Carburised Steel. Journal of Materials Processing Technology, 2006, **174**(1-3), pp. 82-90.

[28] Sharman, A.R. et .al. An Analysis of the Residual Stresses Generated in Inconel 718 When Turning. Journal of Materials Processing Technology, 2006, **173**(3), pp.359-367.

[29] Metcut Research Associates, Machining Data Handbook (3rd Edition). Institute of

Advanced Manufacturing Sciences, Inc., Cincinnati, USA.

[30] Davim, J. P. Surface Integrity in Machining. London:Springer-Verlag, 2010

CHAPTER 6 MACHINING-INDUCED SURFACE INTEGRITY AND ITS EFFECT ON FATIGUE PERFORMANCE FOR GH4169 SUPERALLOY

6.1 INTRODUCTION

With the further development of modern manufacturing technology in the fields of automobile and aerospace industry, the requirements of reliability and long service life for the precision-machined surfaces and parts are becoming increasingly more stringent and demanding. The fatigue property is one of the most important functionalities of machined parts. It is considered as the principal mode of failure for critical machined parts and may lead to unexpected accident during service.

The fatigue property and performance of a machined part are closely related to its machined surface geometrical texture and subsurface SI characteristics. According to existing statistics researches on the malfunction and failure of engineering parts, fatigue fracture caused 60%~90% of the final failure of the key mechanical structures and parts used in the industrial field. This number could reach 80%, especially in the field of aero-engine manufacturing. There have already been many catastrophic accidents in history, which showed the potential danger of surface irregularities and subsurface metallurgical transformations caused by inappropriate machining parameters or cooling condition during the manufacturing process. In fact, these machining-induced changes in surface geometry and subsurface characteristics are of vital importance to ensure the surface integrity and functional performance of the machined parts.

As above-mentioned, most engineering failures are caused by accumulating fatigue damage when an alternating or cyclic loading is applied on structures and parts, such as suspended bridges, railways, airplane wings and rotary vanes in aero-engines. Although the magnitude of alternating load is normally less than the yield strength of the materials, its persistent action will gradually result in crack initiation and sudden fracture of parts, which is considered usually unexpected and more severe than the failure caused by static loading.

As is well known, the fatigue damage and crack initiation usually originates from a machined surface or locations near to the surface of a machined part. This is because the machined surface is the boundary of the material and machining process will destroy the integrity of grains on the surface which deteriorates the mechanical properties of the whole machined part; at the same time, the nominal stresses are often higher (e.g., for bending loading) at the surface and the abrupt change of micro geometrical shapes near the machined surface (such as machining marks, micro notches or grooves) are easy to form the potential geometrical stress raisers which will cause adverse stress concentration and initiate micro cracks on the machined surface. If the machined part mainly works under a corrosive environment and is subjected to alternating load, the poor machined surface integrity will rapid deteriorate the surface state and result in final fatigue failure. Although many researchers have already tried to improve the machined surface integrity and consequent fatigue performance of machined parts by optimizing the manufacturing processes and related machining parameters, there are still realistic difficulties in mass production for accurately measuring and controlling the status of surface integrity for machined parts. In

this chapter, the relationship between machining-induced surface integrity characteristics (such as surface roughness, surface microhardness and residual stress) and fatigue performance (especially fatigue life) for ground GH4169 specimens are investigated. The effect of the machining parameters (grinding speed v_s, workpiece rotational speed v_w and depth of cut a_p) and the consequent effect of the surface integrity characteristics on fatigue life of the ground parts, are studied based on orthogonally-designed grinding experiments and fatigue tests followed by corresponding fractographic analyses. These research results offer guidance to effectively control and ensure the surface integrity and ultimately improve the fatigue performance of the machined GH4169 parts in service.

6.2 SURFACE INTEGRITY AND ITS EFFECT ON FATIGUE LIFE FOR GROUND GH1469 PARTS

Many researchers have studied the impact of surface texture and subsurface characteristics on the fatigue performance of machined parts [1-5]. There were also different views in assessing the degree of influence of the primary surface integrity characteristics (surface roughness R_a, surface microhardness HV_1 and residual stress σ_{R0}) on the fatigue properties. Some researchers believed that the surface residual stress is the most influential factor that determines fatigue properties [1-3]; while some other researchers considered surface roughness and surface microhardness as the principal influencing factors [4-6]. In fact, the effects from distinctive surface integrity characteristics are concurrent and interactive in a typical working environment, and the surface integrity characteristics are not completely independent and may correlate and interact with each other to some extent. Considering the

differences in the material properties, manufacturing process, loading conditions and working environment, the influencing degree of each surface integrity characteristic on the fatigue properties of the machined part are different. According to the surface integrity model framework proposed in Chapter 3, which describes the relationships between processing parameters, surface integrity characteristics and final fatigue properties, any surface integrity characteristic may be the dominant factor affecting the fatigue properties of the machined part in its specific application. Hence, it is better to elaborately investigate the effect of certain typical surface integrity characteristic parameters on the fatigue properties for a selected material and under actual working conditions.

6.2.1 Rotating Bending Fatigue Test for GH4169 Specimens

Based on practical observation and experience in various applications, the real causes that affect the fatigue life of a machined part are actually the combination or integration of the 5 primary surface integrity characteristics, especially the integrated effects from surface roughness R_a, surface microhardness HV_1 and residual stress σ_{R0}. A series of orthogonally-designed grinding experiments with different machining parameters were carried out and the corresponding rotary bending fatigue tests for these ground specimens are implemented at room temperature to investigate the overall effects of surface integrity characteristic parameters on the fatigue life of these GH4169 specimens. The detailed requirements of the heat treatment for specimen material, grinding process parameters and operating condition of fatigue test are as follows:

(1) Direct aging treatment is applied to the specimen material [7], GH4169 superalloy. The

detailed process is: heat the raw material to 720°C ± 5°C and hold for around 8 hours; then cool the material with a velocity of -50°C/h in the furnace to 620°C ± 5°C and hold this

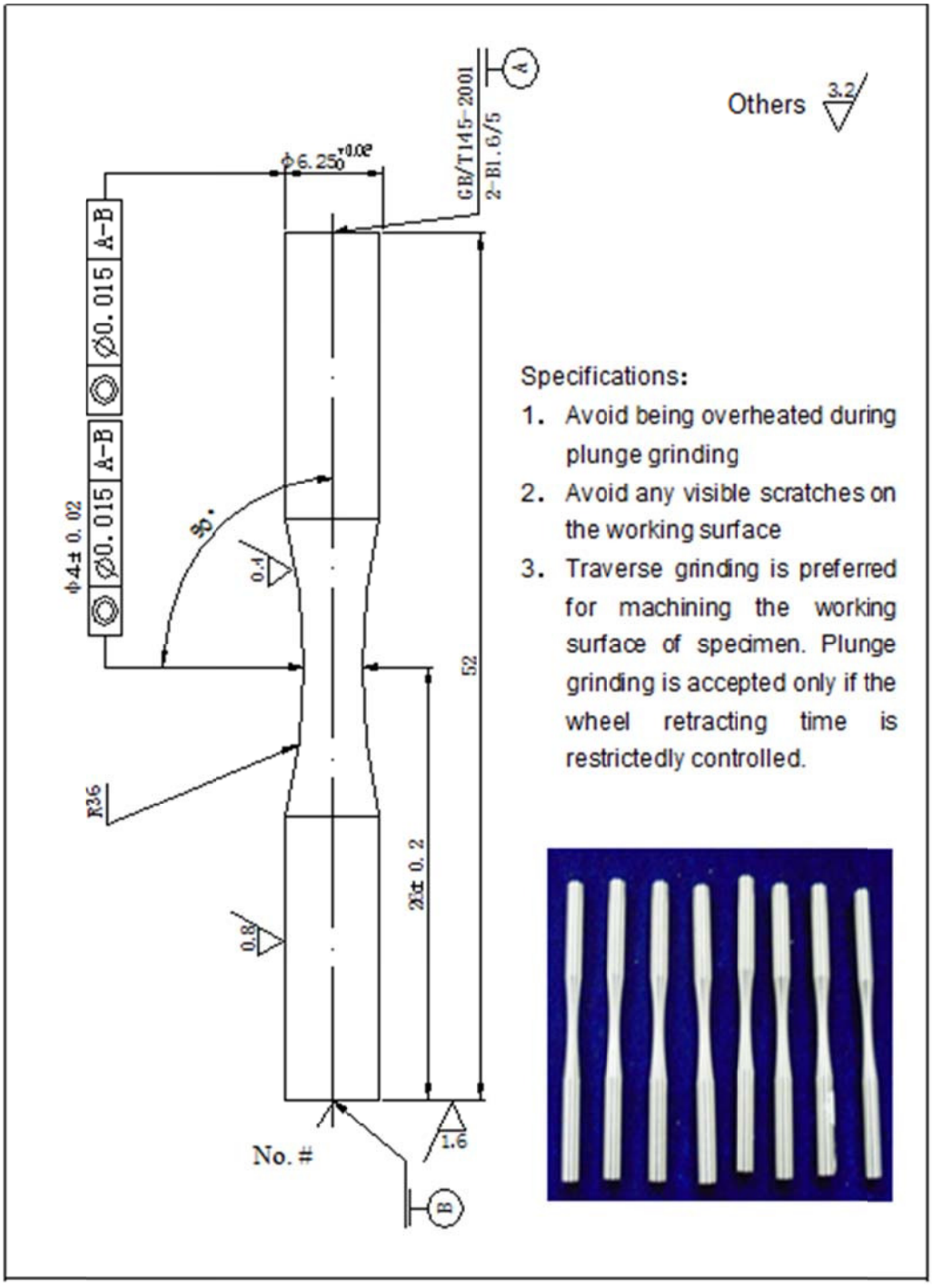

Figure 6.1 Machining specifications for GH4169 rotary bending fatigue specimens

temperature for another 8 hours; finally wait until the material cools to room temperature in free open air. After this treatment, the amount of δ phase in the material will reduce, and the

strength and impact performance are correspondingly improved. The mechanical properties of GH4169 superalloy can be found in Table 5.2.

(2) The geometrical size and machining requirement of specimen for the rotary bending fatigue test are shown in Figure 6.1. The specimens will firstly experience rough turning and then semi-finished turning until the diameter of the working surface on the specimen approaches 4.1+0.1mm. The final processing for the working surface of the fatigue specimens is external plunge grinding, using the grinding parameters designed in Table 6.1. It is noted that the specimen preparation is especially important and an undamaged surface is essential for further accurate analysis.

(3) The specimens are tested on the standard rotating bending fatigue testing machine and high alternating tensile load are applied. This type of fatigue testing can be useful for determining the mechanical properties of material and the effect of machining-induced surface micro geometry change (e.g. surface texture) on stress concentration and fatigue properties. The fatigue test is carried out under room temperature; the stress level is 800MPa and the loading frequency is 83.3Hz (5000 rpm).

Considering the difficulty of machining the surface of a specimen with very small diameter (only 4 mm) and the limitations of the practical grinding machine tool, the external plunge grinding is arranged for the fatigue specimens as Table 6.1 and the workpiece rotational speed for specimens is fixed at v_w=2.56m/min. For each group of grinding parameters, 6 fatigue specimens are ground; the final fatigue life measured being the average for a group of specimens.

Table 6.1 Orthogonally-designed external plunge-grinding experiments for GH4169 fatigue tests (Grinding parameters ↔ SI ↔ SCF ↔ Fatigue)

Test No.	SI grinding parameters		SI characteristic parameters measurement										SCF and error calculation					Fatigue life
	a_p (mm)	v_s (m/s)	R_a (μm)	R_z (μm)	R_t (μm)	R_{Sm} (μm)	ρ_1 (μm)	ρ_2 (μm)	ρ_3 (μm)	$\overline{\rho}$ (μm)	HV_1 (kgf/mm^2)	σ_{R0} (MPa)	K_t (Arola)*	K_{st} (or K_{tG})	e_1 (%)	K_{IEF}	e_2 (%)	N_f ($\times 10^5$)
1	0.002	15	0.3073	2.365	2.53	2.914	3.36	3.26	1.30	2.64	561.23	-70.7	1.249	1.276	2.2	1.204	3.61	1.70
2	0.002	20	0.2895	2.365	2.63	2.399	2.48	2.35	2.68	2.50	508.75	-31.2	1.257	1.259	0.15	1.190	5.31	1.830
3	0.002	25	0.3372	3.09	3.545	2.713	1.19	1.61	1.34	1.38	521.88	-108.8	1.561	1.525	2.3	1.433	8.21	1.363
4	0.006	15	0.3057	2.725	3.085	2.507	1.21	2.73	1.41	1.78	552.65	-60	1.388	1.372	1.1	1.294	6.79	1.388
5	0.006	20	0.2519	2.315	2.53	2.207	2.3	1.75	1.56	1.87	552.28	-100.3	1.294	1.287	0.54	1.212	6.34	1.488
6	0.006	25	0.2494	1.855	2.035	2.852	3.37	2.01	3.55	2.98	530.20	-36.4	1.184	1.228	3.73	1.161	1.91	1.368
7	0.01	15	0.2429	2.18	2.345	2.568	2.23	1.91	1.89	2.01	492.88	-19.4	1.259	1.282	1.76	1.213	3.76	1.333
8	0.01	20	0.2641	2.31	2.485	2.198	1.71	1.7	1.52	1.64	529.23	-55.8	1.345	1.337	0.63	1.262	6.25	1.317
9	0.01	25	0.2631	2.3267	2.633	3.045	2.02	2.37	1.36	1.92	558.68	-66	1.310	1.355	3.41	1.278	2.52	1.525

*Within the grinding parameter range researched, compared with the calculation results from Arola's proposed equation for K_t, the calculated results for the micro geometrical surface texture caused SCF K_{st} is only of the maximum relative error of 3.73%. Compared with the calculation results from Arola's proposed equation for K_t, the calculation results for the proposed overall effective SCF K_{IEF}, which considers the integrated effect of micro surface texture, surface microhardness and residual stress, is of the maximum relative error of 8.21%。

6.2.2 Correlation between Surface Roughness and Fatigue Life

The surface roughness is usually taken as the measurement standard that ensures the surface accuracy and quality, and it is one of the most important factors that influence the fatigue performance of machined parts. Viewed from the requirements of surface integrity, surface roughness is actually a generalized concept which not only includes the surface roughness standard parameters (such as R_a, R_z, R_q) but also involves some parameters relating to geometrical features such as the depth of micro notch, root radius of surface profile valley defined in Chapter 3. All of these geometrical features may cause excessive stress concentration when the machined part is subjected to alternating loading and can finally lead to premature fatigue fracture.

Surface texture and the corresponding surface roughness values R_a (or S_a) of the ground specimens processed by different grinding parameters are measured as shown in Figure 6.2. According to the measured surface roughness and the corresponding grinding parameters, an empirical relationship between the grinding parameters and the value of surface roughness for these externally-ground GH4169 specimens is established by using linear regression analysis as follows:

$$R_a = 0.158 \cdot a_p^{-0.1218} \cdot v_s^{-0.0284} \tag{6.1}$$

Although the correlative coefficient and the significance level of the regression analysis are not perfect, this empirical equation still offers some helpful and general information. Within the investigated grinding parameters range, the depth of cut a_p is of the maximum power-law index and is taken as the most important factor that affects the surface roughness R_a. From

the empirical equation, the wheel speed v_s is negatively correlated to the surface roughness, which means that R_a will reduce if the wheel speed v_s increases; while the depth of cut a_p is negatively correlated to the surface roughness, which means that R_a will increase with the decrease of a_p. This conclusion seems contradictive with the conventional trend between surface roughness and the wheel cutting speed. The reason for this inference is likely to be that the time for the specimens' plunge-grinding was slightly long when compared to the small diameter of the fatigue specimen and the machined surface experienced excessive buffing. As a result, the values of surface roughness no longer reflect their original correlation to the pre-designated grinding parameters (wheel speed v_s or depth of cut a_p), but to the process of excessive buffing, which latter is normally an uncontrollable process. To overcome this weakness, traverse-grinding may be a better alternative to control the expected surface/subsurface roughness behavior of the specimens.

Based on the measured values of fatigue life and surface roughness in Table 6.1, the empirical equation which describes the relationship between the surface roughness R_a and the fatigue life N_f for externally-ground GH4169 specimen is established by linear regression analysis as follows:

$$N_f = 2.058 \cdot R_a^{\,0.2626} \tag{6.2}$$

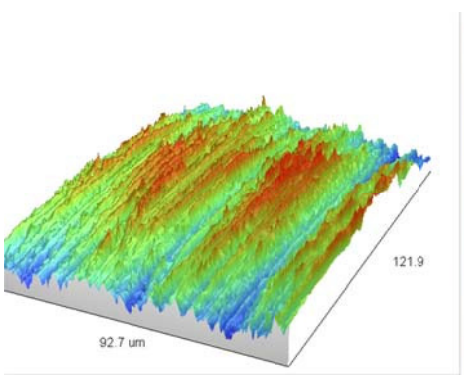

(a) 1#: R_a=0.3073; R_z=2.365; R_t=2.53

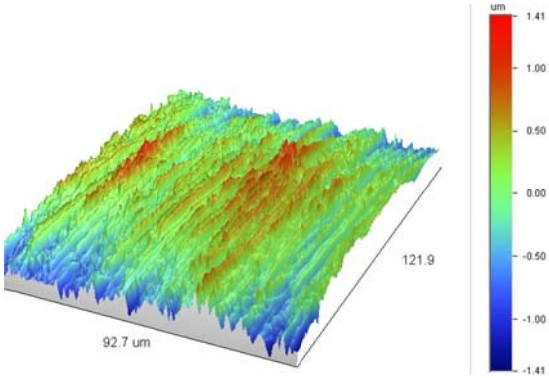

(b) 2#: R_a=0.2895; R_z=2.365; R_t=2.63

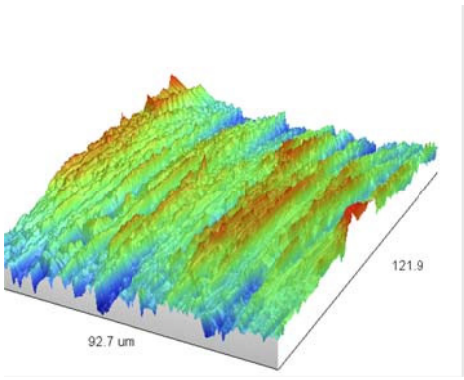

(c) 3#: R_a=0.3372; R_z=3.090; R_t=3.545

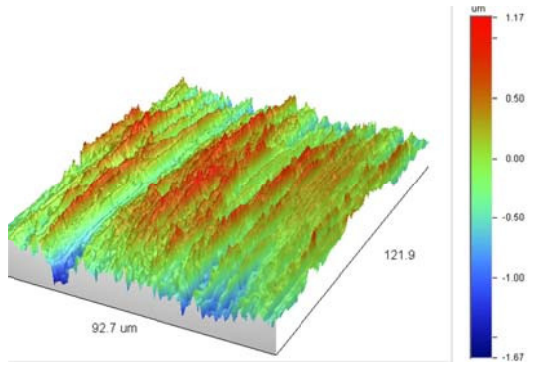

(d) 4#: R_a=0.3057; R_z=2.725; R_t=3.085

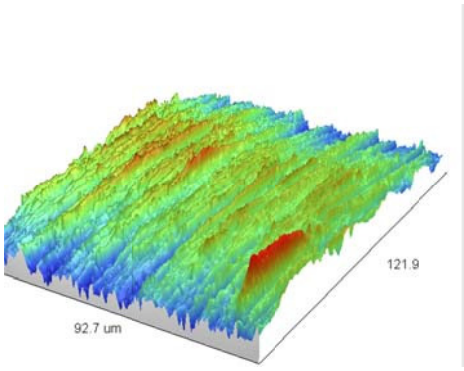

(e) 5#: R_a=0.2519; R_z=2.315; R_t=2.53

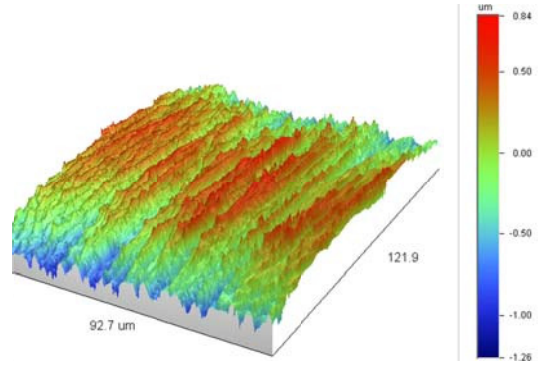

(f) 6#: R_a=0.2494; R_z=1.855; R_t=2.035

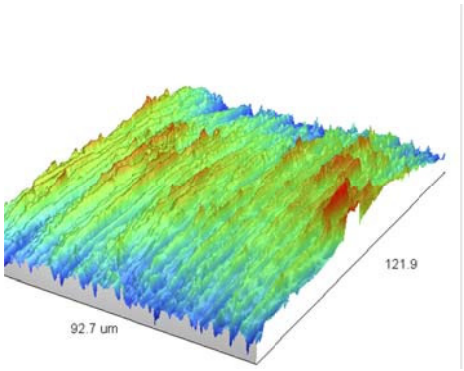

(g) 7#: R_a=0.2429; R_z=2.180; R_t=2.345

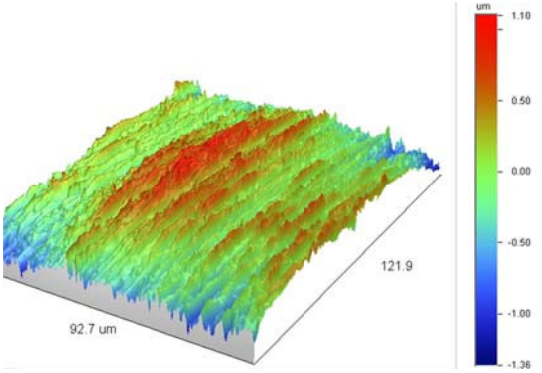

(h) 8#: R_a=0.2641; R_z=2.310; R_t=2.485

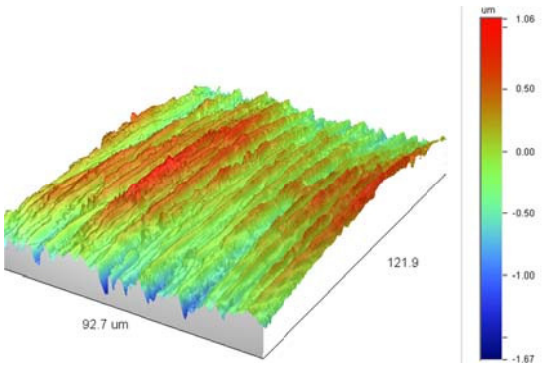

(i) 9#: R_a=0.2631; R_z=2.327; R_t=2.633

Figure 6.2 3D surface textures of the rotary bending fatigue specimens

According to orthogonally-designed grinding experiments and measurements of the final fatigue life listed in Table 6.1, the empirical equation which expresses the variation of the fatigue life of the GH4169 ground specimens with the grinding parameters was established by linear regression analysis as follow:

$$N_f = 1.028 \cdot a_p^{-0.10} \cdot v_s^{0.0582} \tag{6.3}$$

The depth of cut a_p has the more obvious effect on the fatigue life than the wheel speed v_s does. Within the grinding parameter range researched, the fatigue life N_f will increase as the depth of cut a_p decreases. This is because the extent of plastic deformation and possibility of material phase transformation below the machined surface will normally decrease with the decrease of a_p. Hence, the possibility of the formation of potential stress raisers on the surface and within the subsurface will decrease, and the fatigue life will correspondingly increase. The wheel speed v_s is positively correlated to the fatigue life N_f, which means that N_f will increase if the wheel speed v_s increases. This is because a reasonable increase of wheel speed v_s will reduce the surface roughness and the amount of potential stress concentration raisers; the fatigue life will correspondingly increase.

Although surface roughness parameters are the most commonly-used standard for evaluation

of the surface quality, it is not the only index adopted to assess the fatigue properties of a machined part which is working within a complex environment. Numerous researches have shown that the integrated effect of different surface integrity characteristics (surface microhardness, surface residual stress as well as surface roughness) is actually the main cause that determines the final fatigue performance of machined parts.

6.2.3 Correlation between Surface Microhardness and Fatigue Life

Hardness is a measure of the resistance to deformation, indentation or penetration of a material by means of indenting, abrasion or scratching with a hardness tester based on different hardness standard such as Brinell, Knoop, Rockwell or Vickers hardness. The lack of a uniform definition indicates that the hardness might not be an essential material property, but an integrated material behavior with contributions from the elastic modulus, yield strength, work hardening, and ultimate strength and so on. Hardness measurement can be carried out within the macroscopic or microscopic range according to the indentation force applied and the corresponding displacement obtained, and the Vickers hardness is often used for evaluating the microhardness of a machined surface.

During the grinding process, the abrasive grits will scratch, plough and finally cut off the material from the surface of a part. These actions will firstly cause plastic deformation and then dislocation motion among the material lattices within the subsurface. The interaction between different slip systems and defected lattices will cause the pile-up of dislocation which finally hinders the further increase of plastic deformation and results in work-hardening. The microhardness and material strength at the surface layer of the

work-hardened part will be correspondingly improved although its ductility will be weakened. GH4169 is a kind of superalloy which is prone to work-hardening. During the grinding process of GH4169, the crystal lattices of material are seriously distorted within the plastic deformation zone and work-hardening occurs easily. Work-hardening normally causes excessive distortion and even fibrosis of the crystal lattices, which eventually strengthens the yield limit and increases the microhardness of the material near to the machined surface layer. If there are already inclusions or internal cracks below the work-hardened surface layer, a larger number of loading cycles will make these internal defects grow rapidly or eventually propagate within the material. However, the work-hardened surface layer will actually restrain the dislocation formation and the macro crack propagation from further growing to the outermost surface. According to the Taylor dislocation relation [8], the relationship between the critical plastic flow stress (or resolved shear stress) τ and the dislocation density ρ_d can be expressed as follows:

$$\tau = \tau_0 + \alpha \cdot G \cdot b \cdot \sqrt{\rho_d} \tag{6.4}$$

where τ_0 is the critical resolved shear stress in the absence of interfering dislocations, called the intrinsic strength of a material of low dislocation density; and α is a numerical constant dependent on the material (~ 0.4); G is shear modulus and b is Burger's vector which represents the magnitude and direction of dislocation in a crystal lattice; ρ_d is dislocation density indicating the number of dislocations per unit volume (or per unit area for 2D measurement).

According to the measured surface microhardness and the corresponding grinding

parameters, an empirical relationship between the grinding parameters and the value of surface microhardness for externally ground GH4169 specimens is established using linear regression analysis, as follows:

$$HV_1 = 525.48 \cdot a_p^{0.00011} \cdot v_s^{0.00542} \tag{6.5}$$

As seen from Eq. (6-5), the power-law indexes for the depth of cut a_p and the wheel speed v_s are quite small which indicates that both of the grinding parameters are of limited influence on the machined surface microhardess within the investigated grinding parameters range. Based on experience and further analysis, it is likely to be found to be caused by the dispersiveness of the measured surface microhardness values. According to the measured values of the microhardness and the fatigue life in Table 6.1, an empirical regression model which interprets the relationship between surface microhardness and fatigue life based on externally plunge-ground GH4169 specimens could be expressed as follows:

$$N_f = 0.0725 \cdot HV_1^{0.4792} \tag{6.6}$$

From Eq.(6.6), the fatigue life of specimens will benefit from the increase of the surface microhardness within the grinding parameters range employed.

6.2.4 Correlation between Surface Residual Stress and Fatigue Life

The formation of residual stress on the machined surface and within the subsurface layer is a complicated procedure. The causes are usually attributed to 2 aspects: the nonuniform plastic deformation effect caused by machining-induced mechanical stress; and the thermal stress effect caused by local high-temperature near the interface between the machining tool and the machined surface. During the machining process, the zone or material layer near to the

surface will produce severe plastic deformation because of the cutting force and local high temperature. As the temperature near to the machined surface cools down after the cutting process, the residual stress will be left on the machined surface and within the subsurface layer.

The residual stress on the machined surface could be generally categorized as tensile residual stress and compressive residual stress according to its directionality. Generally, residual compressive stress is beneficial to the fatigue life of machined parts; while tensile residual stress is adverse and will reduce the fatigue life of machined parts. It is noted that the influencing factors for the fatigue life of a machined part are actually more than just the residual stress. They are actually not only involved in the magnitude and distribution of the residual stress, but also relate to elastic properties, external stress conditions and the working environment of machined parts. The magnitude of working stress that affects the fatigue life of machined parts is actually the sum of the nominal applied stress and the final residual stress obtained after machining. When evaluating the residual stress effect on fatigue performance, the stability and variation of the residual stress with the working stress cycle should also be taken into account. Stephens and Fuchs proposed a criterion to determine if material yield or residual stress relaxation will occur within the machined surface layer under an alternating loading [9]:

$$\sigma_m + \sigma_a + \sigma_r > \sigma_s \tag{6.7}$$

in which σ_m is the mean stress and $\sigma_m=(\sigma_{max}+\sigma_{min})/2$; σ_a is the stress amplitude of alternating stress and $\sigma_a=(\sigma_{max}-\sigma_{min})/2$; σ_s is the yield limit; σ_r is the residual stress. When there is a

residual stress on the surface, it will combine with the external applied alternating load; the real mean working stress σ_{rm} is the yield stress that the machined part subjected to:

$$\sigma_{rm} = (\sigma_r + \sigma_m) \tag{6.8}$$

The real maximum and minimum working stress then could be expressed as:

$$\sigma_{\max}^{real} = (\sigma_r + \sigma_m) + \sigma_a \tag{6.9a}$$

$$\sigma_{\min}^{real} = (\sigma_r + \sigma_m) - \sigma_a \tag{6.9b}$$

Considering that a fatigue crack usually initiates from the weakest point on the surface, fatigue failure is likely to happen at the extreme values of real working stress but not at the average value. When $(\sigma_r+\sigma_m)+\sigma_a>\sigma_s$, the real stress applied on the machined surface exceeds the yield strength of the material, and the surface of the machined part will yield which results in plastic flow and a redistribution of the initial residual stress field and finally the relaxation of elastic residual stress during service. Hence, the residual stress won't affect the fatigue property of the machined specimen in this case. When $(\sigma_r+\sigma_m)+\sigma_a < \sigma_s$, there will be no relaxation of residual stress, and its effect on the fatigue property will depend on its direction and magnitude. If the residual stress is tensile and its magnitude is high, the fatigue life of machined specimen will drop dramatically even if the surface roughness is low; for a brittle material, once the maximum working stress at any point on the surface exceeds the tensile ultimate strength of the material σ_b, which is $(\sigma_r+\sigma_m)+\sigma_a>\sigma_b$, an adverse surface crack will initiate and fatigue fracture will rapidly occur. If the machined surface is of compressive residual stress, it will be beneficial to the fatigue life of the machined parts because it will help to defer the potential crack's initiation and its propagation from the surface.

From Table 6.1, the residual stresses of ground GH4169 specimens before fatigue testing are compressive (with minus sign). Within the orthogonally-designed grinding parameters range, an empirical model between the absolute value of surface residual stress and the grinding parameters are established using multiple linear regressive analysis as follows:

$$\left|\sigma_{R0}\right| = 1.79 \cdot a_p^{-0.215} \cdot v_s^{0.760} \tag{6.10}$$

It can be seen that the wheel cutting speed v_s has the most profound effect on the absolute value of surface residual stress within the investigated grinding parameters range. As the wheel cutting speed v_s increase, the interfacial friction thermal energy produced and the mechanically energy consumed will both increase, and the local temperature at the surface or within the subsurface layer of machined parts will rapidly rise because of the poor thermal conductivity of superalloy GH4169. After grinding, the magnitude of the surface tensile residual stress at the ground surface and subsurface will increase.

According to the fatigue testing result listed in Table 6.1, an empirical model between the absolute value of surface residual stress and the fatigue life is established using single linear regressive analysis as follows:

$$N_f = 1.468 \cdot \left|\sigma_{R0}\right|^{0.000264} \tag{6.11}$$

Within the studied range of the grinding parameters for GH4169, the power-law index for the absolute value of residual stress is small and has a very weak correlation with the fatigue life of the machined specimens. This is because the magnitude of the residual stress may change during the fatigue loading test. Further, the local high temperature and working environment will also influence the actual fatigue life.

6.2.5 Integrated Effect of Surface Integrity Characteristics on Fatigue Life

When a machined part is in service, its surface is usually subjected to maximum loading and is vulnerable to an external stress status and a corrosion environment, both of which make the cracks easy to initiate and develop from the surface. During the machining process, the subsurface material will experience work-hardening and produce an internal residual stress distribution within the subsurface layer, as well as the machining-induced micro surface texture left on the surface. These changes from surface geometry and subsurface layer will cause different extents of stress concentration, which constitutes a danger to and deteriorates the fatigue performance of the machined part. For the ground GH4169 specimens, their fatigue properties actually depend on the integration of all primary surface integrity characteristics; that is to say, the surface roughness, surface and subsurface microhardness and residual stress distribution will jointly influence the fatigue properties of the machined parts.

In order to determine the relationship between the fatigue life and the primary surface integrity characteristic parameters, an empirical model correlating the fatigue life N_f to surface roughness parameters R_a, surface microhardness HV_1 and surface residual stress σ_{R0} is established with linear regression analysis based on the measured surface integrity characteristic results in Table 6.1:

$$N_f = 10^{-2.9406} \cdot R_a^{0.4625} \cdot HV_1^{1.3111} \cdot \left|\sigma_{R0}\right|^{-0.1216} \tag{6.12}$$

Within the investigated range of grinding parameter, the surface microhardness HV_1 has a maximum power-law index and is taken as the most important factor to affect the fatigue life

N_f. From the empirical equation, the surface microhardness HV_1 is positively correlated to the fatigue life N_f, which means that N_f will increase with the increase of HV_1; while the absolute of the surface residual stress is negatively correlated with the fatigue life N_f, which means that fatigue life N_f will reduce if the tensile residual stress σ_{R0} increases. The surface roughness R_a is positively correlated with the fatigue life N_f, which means that the fatigue life N_f will increase as R_a increases within the researched range of grinding parameters. This conclusion seems contradictive with the conventional trend between surface roughness and the fatigue life. The reason for this inference is likely to be that the time for the specimens' plunge-grinding was slightly long when compared to the small diameter of the fatigue specimen and the machined surface experienced excessive buffing. As a result, the values of surface roughness no longer reflect their original correlation to the pre-designated grinding parameters but to the process of unwanted excessive buffing, which latter is normally an uncontrollable process. To overcome this weakness, traverse-grinding may be a better alternative to control the expected surface/subsurface integrity behavior of specimens.

According to the measured average spacing between irregularities R_{sm} and the equivalent root radius of the dominant valleys for the surface profile $\bar{\rho}$ in Table 6.1, the grinding-induced micro geometric stress concentration factor K_{st} for the fatigue test specimens is calculated. The variation trend between the machining-induced geometric stress concentration factor K_{st} and the measured equivalent root radius $\bar{\rho}$, as well as the variation trend between K_{st} and the arithmetic average roughness R_a for the ground GH4169 specimens, are shown in Figure 6.3 and Figure 6.4 respectively. The relationship between the

machining-induced geometric stress concentration factor K_{st} and fatigue life N_f is also fitted and shown in Figure 6.5.

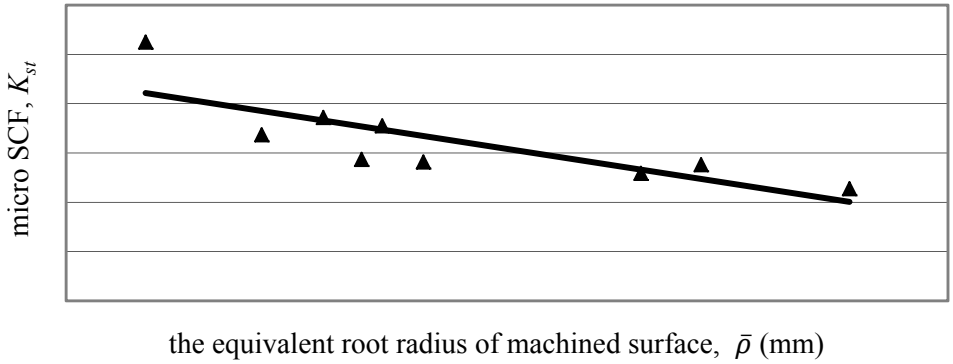

Figure 6.3 The correlation between the micro SCF K_{st} and the equivalent root radius $\bar{\rho}$

From Figure 6.3, as the equivalent root radius $\bar{\rho}$ increases, the degree of sharpness for the micro valleys within the surface profile and the consequent stress concentration will both reduce; as a result, the magnitude of the calculated stress concentration factor will correspondingly reduce. As can be seen from Figure 6.3, the equivalent root radius and the calculated stress concentration factor are of a good linear degree of fitting.

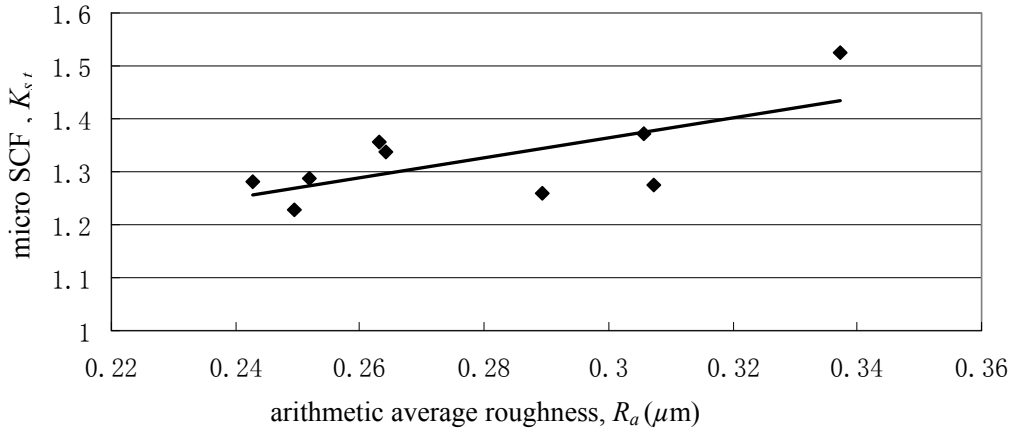

Figure 6.4 The correlation between the micro SCF K_{st} and the surface roughness R_a

As can be seen from Figure 6.4, with the increase of surface roughness R_a, the surface becomes much rougher and the number of deep valleys on the machined surface may also

increase. This will lead to higher possibility of the presence of surface defects and stress raisers. Thus, the corresponding calculated stress concentration factor will increase.

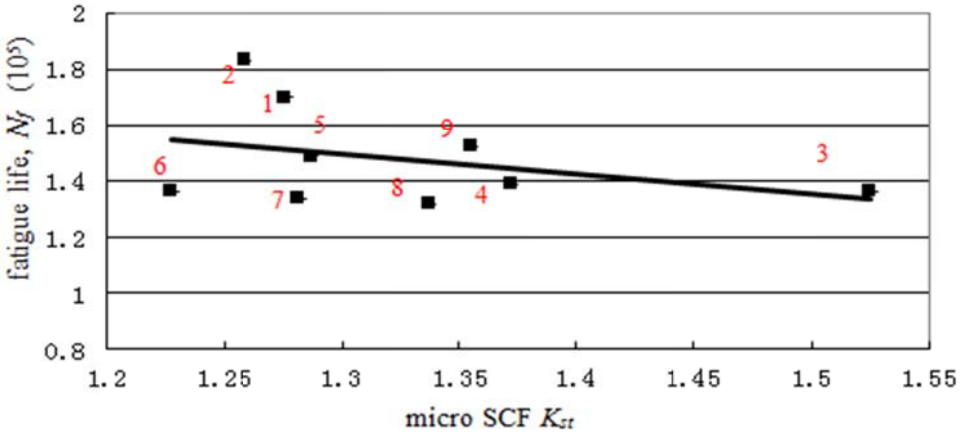

Figure 6.5 The correlation between the micro SCF K_{st} and the fatigue life N_f

Although the calculation of the micro geometric stress concentration factor K_{st} has only considered the effect from machining-induced geometrical surface texture change (mainly surface roughness parameters but not including the effects of the surface micro-hardness, residual stress and other factors on the fatigue properties), the fatigue life N_f and calculated stress concentration factor K_{st} are still assume a good linear trend in Figure 6.5. The overall trend is that the fatigue life N_f decreases with the increase of the machining-induced geometric stress concentration factor K_{st}.

6.3 Fractographic Analysis for Ground GH4169 Fatigue Specimens

Fractographic analysis, also called fracture surface analysis, is an essential means by which to judge the fracture failure mode, determine failure reasons and mechanism and finally to propose some improvement and preventive measures for machined parts in their design and

manufacturing stages [10]. The procedure of fatigue fracture usually includes 3 stages: fatigue crack initiation, fatigue crack propagation and abrupt rupture of the fatigue specimen.

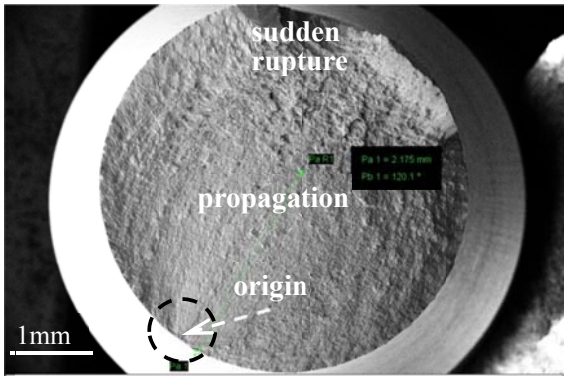

(a) fracture surface morphology (7#)

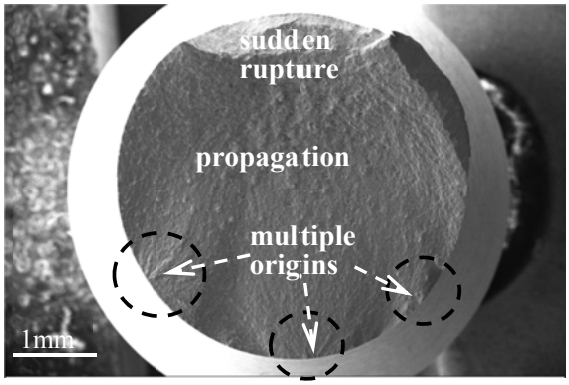

(b) fracture surface morphology (1#)

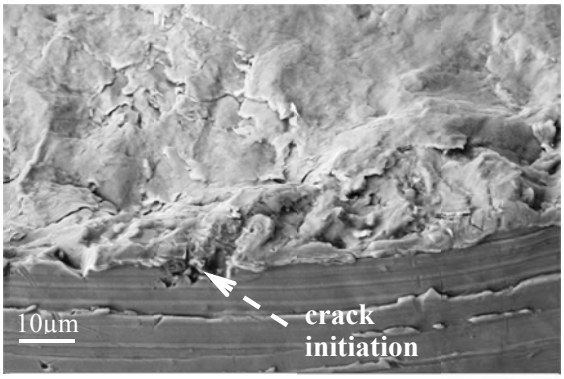

(c) magnification of origin (7#)

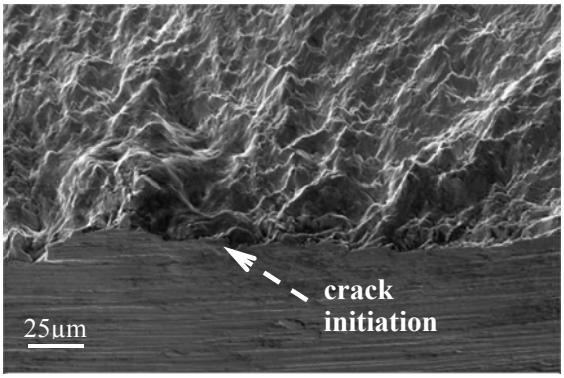

(d) magnification of origin (1#)

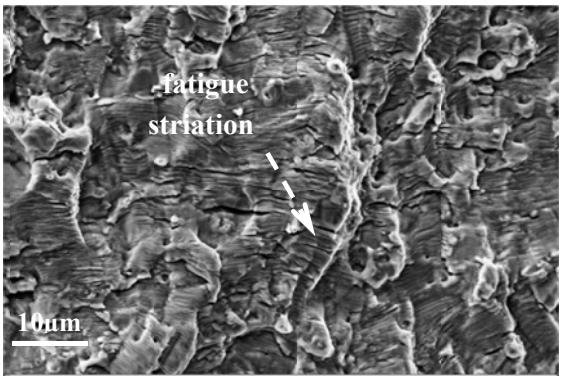

(e) striation in growth zone (7#)

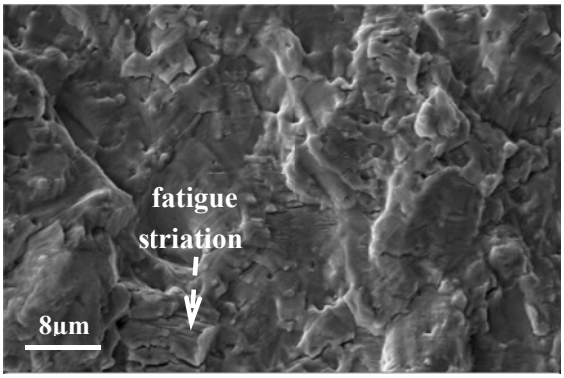

(f) striation near growth zone (1#)

Figure 6.6 morphology of the fractured areas of GH4169 fatigue specimens 1# and 7#

During each stage, the surface and subsurface behavior is complicated and involves in

different physical and chemical changes. At the same time, distinct marks and features are left on the fractured surfaces of specimens which actually made a record and reflected different information during the whole fatigue fracture procedure. As shown in Figure 6.6(a), a typical fatigue fracture surface will contain 3 different zones corresponding to its 3 fracture stages: the fatigue crack initiation/origin zone (normally with radial marks), the fatigue crack propagation zone (normally with smooth beach-pattern marks), and the sudden rupture zone (normally with a rough appearance).

From the point of view of fracture mechanics, the fatigue fracture surface actually includes the information of material properties and surface integrity characteristics generated during the machining processes. For example, fatigue striations are microscopic features on a fatigue fracture surface that identify one propagation cycle of a fatigue crack. These are not always present and can only be seen under a scanning electron microscope. By doing the fractographic analysis, the failure reasons and the maintenance cycle could be determined for the fatigue fractured parts inspected, which actually provides guidance for the effective maintenance and reliable use of some critical parts in industry.

The fatigue fracture areas of specimen 7# and 1# from the rotary bending fatigue test are shown in Figures 6.6(a) and (b). There is obviously a crack origin and sudden fracture zone on the fracture surface of specimen 7#. Radial marks are starting off from the crack origin. Multiple crack origins are found on the fracture surface of specimen 1#. This is because the external load level is high and the grinding surface roughness of ground specimen 1# is also higher than that of specimen 7#, so there are likely to have been stress raisers on the

machined surface of specimen 1#.

Fatigue cracks usually originate from the machined surface of parts. This is not only because the surface of parts is subject to the maximum external load, but also because there are machining-induced surface texture or defects which will cause adverse stress concentration. From Figures 6.6(c) and (d), potential fatigue cracks initiated at the root of the machining marks or scratches for the ground GH4169 specimens 1# and 7#. That is to say, the fatigue life of a machined part depends closely on the manufacturing technology and related machining parameters, which produce different surface texture or scratches.

Near the fatigue propagation zone, there are relatively clear, slightly curved and wave-like stripes (also called fatigue striations) parallel to each other, seen in Figures 6.6(e) and (f). Fatigue striations are the microscopic features left on the fatigue fracture surface after local fatigue crack propagation. The normal direction of the striations roughly points to the fatigue crack propagation direction and its presence is usually taken as responsible for the occurrence of fatigue fracture. Typically, each stripe or striation corresponds to a propagation cycle under the fatigue loading which is large enough to produce slip dislocation within the material. It is also can be inferred that the fatigue life of a specimen (especially at the crack propagation stage) will be significantly dependent on the amplitude and frequency of fatigue loading.

6.4 SUMMARY

Multiple-factor orthogonal grinding experiments and related rotating bending fatigue tests are carried out to investigate the correlations among the machining parameters, surface

integrity characteristics and fatigue properties for the ground GH4169 superalloy. The rotary bending fatigue test specimens are machined according to the designed grinding parameters under steady grinding conditions with a sharp Al_2O_3 sand wheel and emulsified lubricant. The effects of surface integrity characteristics on the fatigue life of the specimens are analysed both individually and integrally. By fractographic analysis of the fractured specimens, the fracture reasons and mechanism caused by the machining-induced surface integrity characteristics and fatigue loading condition, are studies and discussed. At the same time, the relationship between the micro surface stress concentration factor K_{st} (caused by microscopic geometrical surface texture) and the fatigue life N_f, is derived based on the results from orthogonally-designed grinding experiments and rotary bending fatigue tests. Actually, it can also be said that the relationship between surface integrity characteristics and parts' final fatigue properties could be bridged and analyzed through the effective surface concentration factor. The variation of fatigue life generally showed a consistently and monotonically descending trend with the increase of the stress concentration factor. The calculated results from the proposed empirical equation for estimating the effective fatigue SFC are of small relative error when compared with those calculated from the Arola equation [11], which actually demonstrated the accuracy and practicability of the proposed estimating model for stress concentration.

REFERENCES

[1] Meng, B. et. al. Effect of Surface Topography on Micro-Mechanical Behavior for

Different Metallic Materials. Journal of Aeronautical Materials, 2006, **26**(4), pp.56-60.

[2] Meng, B. and Guo, W.L. Quantitative Analysis of the Effect of Surface Topography on Fatigue Strength. Materials for Mechanical Engineering, 2006, **30**(5), pp.26-29.

[3] Yang, M.K. et. al. Surface Roughness and Its Effect on Fatigue Life of Superalloy GH4169. Aeronautical Manufacturing Technology, 1997, **6**, pp.11-13.

[4] Yang, M.K. and Ren J.X. The Effect of Machining Surface Integrity on Fatigue Life of Superalloy GH4169. Aviation Precision Manufacturing Technology, 1996, 32(6), pp.28-31.

[5] Hu, Z.H. and Yuan, Z.J. The Generating Mechanism of Residual Stress during Grinding. Transaction of Harbin Institute of Technology, 1989, **6**, pp.51-59

[6] Mercer, C. et. al. Micromechanisms of Fatigue Crack Growth in a Forged Inconel 718 Nickel-based Superalloy, Materials Science and Engineering: A, 1999, **270**(2), pp.308-322.

[7] Gu, M. Aeronautical Materials Handbook (2nd Edition). Beijing: China Standard Press, 2001.

[8] Mitchell, B.S. An Introduction to Materials Engineering and Science-for Chemical and Material Engineering. New York: John Wiley & Sons, 2004

[9] Stephens, R.I. et. al. Metal Fatigue in Engineering (2nd Edition). New York: John Wiley & Sons, 2000

[10] Liu, X.L. et. al. Quantitative Fractographic Analysis for Fatigue. Beijing: National Defense Industry Press, 2010

[11] Arola, D. and Williams, C.L. Estimating the Fatigue Stress Concentration Factor of Machined Surfaces. International Journal of Fatigue, 2002, **24**(9), pp.923-930.

CHAPTER 7 CONCLUSIONS AND FUTURE WORK

7.1 CONCLUSIONS

7.1.1 Overall Research Results

To bridge the gap between industry and academia, this research manages to establish a surface integrity descriptive model which could digitally and quantitatively define the primary surface integrity characteristic parameters for comprehensively characterizing their influence on functionality in practice. Surface and subsurface integrity characteristics interact with each other and jointly determine the functionality of machined surfaces or parts. Further, the framework of a surface integrity model is also proposed to offer a chance for better understanding the interactions among the machining processes, surface integrity characteristic parameters and service performance. The correlation of manufacturing processes, surface integrity characteristics and final functionality are well illustrated in the proposed framework of the surface integrity model. In order to accurately evaluate the surface integrity and the consequent functionalities, especially fatigue-related performance, different empirical equations for estimating the effective stress concentration factors of certain machined surface are proposed and summarized according to geometrical inference and grinding experimental analysis. The impact of multiple stress concentration is emphasized and taken into account for the ground samples, which considers the situation when the machining-induced microscopic surface texture superimposes on its macroscopic pre-designated structural notches or other macro stress raisers. The accuracy and feasibility

of those empirical equations are validated by calculating and comparing the SCFs for the externally-ground GH4169 cylindrical samples. The surface integrity characteristics for a difficult-to-machine high-temperature alloy GH4169, which is widely used in the aerospace industry, are systematically studied. Based on the orthogonally-designed grinding experiments for GH4169 samples, the effects of machining process parameters on the surface integrity characteristics of the machined parts are quantitatively investigated; the formation mechanism and laws for different primary surface integrity characteristics, such as surface roughness, microhardness and residual stress, are also analyzed. According to the measured SI characteristics from the grinding experiments and corresponding fatigue tests, the correlations between the grinding process parameters and the surface integrity characteristics, between the grinding process parameters and the fatigue life, and between the surface integrity characteristics and the fatigue life, are analyzed and discussed.

7.1.2 Discussion and Limitations

However, the surface integrity of machined parts is actually affected by a variety of external factors and operational conditions in the cutting system besides the 5 primary SI characteristics mainly investigated. For the research in this thesis, only the factors such as workpiece material properties, grinding wheel properties and grinding process parameters are involved. The grinding processing experiments are assumed to be carried out under steady cutting conditions. These assumptions and constraints make the proposed empirical equations is not a perfect model which does not completely reflect all the factors that affect the relationships between the grinding process parameters, surface integrity characteristics

and fatigue properties. In addition, the empirical model is established based on the linear regression analysis within the specific grinding parameters range. The application of this empirical model might be more suitable for the processes of close cutting situations and materials of similar mechanical properties.

7.2 CONTRIBUTION TO KNOWLEDGE AND PRACTICE

(1) A surface integrity descriptive model, which took the surface roughness, macro and microstructure, surface microhardness and residual stress as the primary characteristics for investigation into surface integrity and corresponding fatigue performance of machined parts, is established. In this model, most of the SI characteristic parameters/variables are digitally and quantitatively defined; the relevant measurement methods and data representation format for SI requirement are also included. This model provides SI assessment with a better possibility for data extension when different workpiece materials, machining processes and corresponding SI characteristic variables need to be accumulated for further analysis.

(2) An estimation model for microscopic geometrical stress concentration factor K_{st}, which considers the effect of machining-induced surface texture on the extent of stress concentration, are proposed and derived. This model not only includes the traditional surface roughness height parameters such as R_a, R_z and R_t (along the Z axis), but also includes the possible influences from the root radius of profile $\overline{\rho}$ and average spacing of profile peaks R_{Sm}, both of which contain the geometrical information in the horizontal direction (along the X axis). This equation reflects the effect of micro surface geometrical parameters on the degree of stress concentration for a machined surface. At the same time, an estimation model,

which associates both SI characteristics and macro pre-designated fatigue notches with the effective stress concentration factor of the machined parts, is established. This model takes account of the integrated effects of the macro/micro surface geometry, residual stress and microhardness characteristics from the machined surface or within the subsurface layer on the eventual stress concentration. It is really convenient and comprehensive method by means of which to estimate the stress concentration degree and assess fatigue performance in engineering practice.

(3) For nickel-based GH4169 superalloy, the effect of grinding parameters on the formation of surface integrity characteristics (such as surface roughness, surface residual stress and surface microhardness) is systematically studied. Based on specific grinding experiments, the formation mechanism for each surface integrity characteristic on the machined surface or within the machined subsurface layer are analyzed and revealed. Considering the correlations between the processing parameters, the surface integrity characteristics and the fatigue properties (shown in Figure 3.5), the effects of the grinding parameters on surface integrity characteristics and the effect of surface integrity characteristics on fatigue life are studied using an orthogonally-designed fatigue test and relating fractographic analysis for the ground and the fractured GH4169 specimens. This research offers a specific guidance to effectively control processing parameters, ensure surface integrity and ultimately improve the fatigue performance (such as fatigue life) for machined parts in service.

7.3 FUTURE WORK

Considering that the empirical model is established based on the linear regression analysis

within the specific grinding parameters range, it will be more desirable to develop an analytical model in the future, which could accurately describe the correlations between the surface integrity characteristics and a wider process parameter range for specific material properties, and therefore could more quantitatively control and accurately predict the surface integrity characteristics of machined parts. Considering that the modelling work involved is very complex and that there is no existing theory to resort to, more powerful analytical methods and tools need to be developed for further research.

Material heterogeneities, such as inclusions, particles or voids, could also act as the stress raisers when the machined part is sustaining external load. The developed stress concentrations will lead to local permanent plastic deformation and initiate microcrack even when the magnitude of stress is far below the yield strength/limit of material. In fact, this research also attempts to establish a surface integrity descriptive and assessing model which takes the fatigue life as an evaluation target and the generalized effective stress concentration factor as the key indicator to associate the surface integrity characteristics with fatigue properties. Generally, the stress concentration mentioned in this thesis includes two aspects of meaning corresponding to the implication of surface integrity: the first is the surface geometrical-aspect stress concentration which consider both pre-designated macro structural change caused stress concentration factor K_{t1} and machining-induced micro surface texture caused stress concentration factor K_{st}; the second is the mechanical-aspect stress concentration K_{ut} which is caused by discontinuity of material properties, or nonuniformity residual stress and microhardness distribution within the subsurface layer.

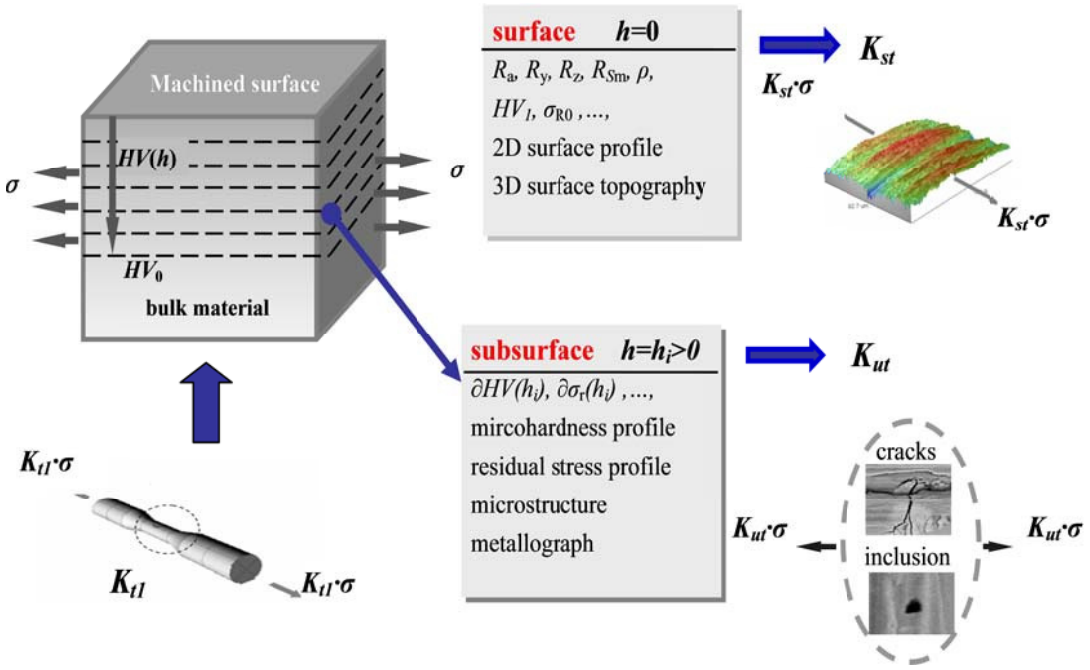

Figure 7.1 Schematic diagram of possible stress concentration from the surface and subsurface of a machined part

As shown in Figure 7.1, the stress concentration effect may originate from both surface and subsurface factors. The surface geometrical-aspect stress concentration has been systematically investigated in this research. Some of the subsurface factors, such as microhardness and residual stress distribution, have also been included in this thesis although it does not cover all of the possibilities or influencing factors such as inclusions and microcracks. It is desirable to take into account both the surface geometrical stress concentration (e.g. K_{st} and K_{tG}) and the subsurface mechanical/physical stress concentration (e.g. K_{ut}) together for a more comprehensive SI and fatigue functionality evaluation in the future.

REFERENCES

[1] Field, M. and Kahles, J.F. Review of Surface Integrity of Machined Components. CIRP Annals-Manufacturing Technology, 1971, **20**(2), pp.153-162.

[2] Field, M., Kahles, J.F. and Cammett, J.T. A Review of Measuring Methods for Surface Integrity. CIRP Annals-Manufacturing Technology, 1972, **21**(2), pp.219-238.

[3] Field, M. Surface Integrity-A New Requirement for Improving Reliability of Aerospace Hardware. Proceedings of 18th Annual National SAMPE Symposium, April 3-5, 1973, Los Angeles, California, USA.

[4] ANSI B211.1, American National Standards on Surface Integrity. Society of Manufacturing Engineers (SME),1986